OPTIMIZING INTERATOMIC POTENTIALS FOR PHONON PROPERTIES

A Dissertation
Presented to
The Academic Faculty

by

Andrew Rohskopf

In Partial Fulfillment
of the Requirements for the Degree
Master of Science in Mechanical Engineering in the
George W. Woodruff School of Mechanical Engineering

Georgia Institute of Technology
May 2018

OPTIMIZING INTERATOMIC POTENTIALS FOR PHONON PROPERTIES

Approved by:

Dr. Asegun Henry, Advisor
Woodruff School of Mechanical Engineering
Georgia Institute of Technology

Dr. Samuel Graham
Woodruff School of Mechanical Engineering
Georgia Institute of Technology

Dr. Shannon Yee
Woodruff School of Mechanical Engineering
Georgia Institute of Technology

Date Approved: January 6, 2018

ACKNOWLEDGEMENTS

First, I would like to thank my family. I would like to thank my parents for their love and patience in raising me, and always supporting my endeavors. They have provided me with the opportunity to succeed in whatever path I choose in life. I would like to thank them for teaching me, through example, the value of working hard to achieve goals. I would also like to thank my sister for her continued love and support.

I would like to express my sincere gratitude to my advisor, Dr. Asegun Henry. His boundless stream of knowledgeable advice has propelled me further to achieving my academic and professional goals. He has provided many golden opportunities and advices, for which I am forever grateful. I benefited greatly from his thoughtful guidance, patient mentoring, and extreme expertise. Dr. Henry shows that he cares about his students through his actions, and I could not ask for a better advisor.

My appreciation also goes to other members of the Atomistic Simulation & Energy (ASE) group. I must thank Wei Lv, Kiarash Gordiz, Hamid Seyf and Freddy Deangelis for their kind help and discussions, along with teaching me the necessary research tools to become a contributing member of the group.

Finally, I would like to thank Intel corporation and the National Science Foundation Graduate Research Fellowship for financial support.

TABLE OF CONTENTS

LIST OF TABLES

LIST OF FIGURES

LIST OF SYMBOLS AND ABBREVIATIONS

E	Total energy
f	Bose-Einstein distribution
$\mathbf{F}$	Force vector
H	Hamiltonian
ijk	General indices
k_B	Boltzmann constant
M	Number of configurations
n	Electron density
N	Number of atoms
N_e	Number of electrons
O	Big O notation
P	Number of parameters
T	Temperature
$\mathbf{q}$	Reciprocal lattice vector
Q	Heat flux vector component
$\mathbf{Q}$	Heat flux vector
r	Radial distance
$\mathbf{r}$	Position vector for a single electron
r_c	Cutoff value
$\mathbf{R}$	Position vector for a single atom
$\overline{\mathbf{R}}$	Positions of all atoms
s	Polarization index

σ	Stress tensor component
u	Displacement in a single direction
U	Potential energy
v	Phonon group velocity component
$\mathbf{v}$	Phonon group velocity vector
V	Volume
w	Weighting factor
z	Objective function component
Z	Objective function value
Å	Angstroms
$\alpha\beta\gamma$	General Cartesian directions
$\boldsymbol{\lambda}$	Vector of fitting parameters
κ	Thermal conductivity
Λ	Phonon mean free path
θ	Angle
Φ, Ψ	2^{nd} and 3^{rd} order force constants
ψ	Wave function
ω	Angular frequency (THz)
$\hbar$	Reduced Planck's constant
$\arg\min$	Arguments of the minima
c-Si	Crystalline silicon
c-Ge	Crystalline germanium
DDM	Direct displacement method
DFT	Density functional theory

EMD	Equilibrium molecular dynamics
GA	Genetic algorithm
GK	Green-Kubo
GKMA	Green-Kubo modal analysis
IFC	Interatomic force constant
LAMMPS	Large-scale Atomic/Molecular Massively Parallel Simulator software
LD	Lattice dynamics
M3BC	Morse – 3-body – Born – Coulomb
MD	Molecular dynamics
MPE	Mean percent error
MPI	Message Passaging Interface
NEMD	Non-equilibrium molecular dynamics
NN	Nearest neighbor
NVE	Constant number of atoms, volume and energy
PBE	Perdew-Burke-Ernzerhof
PES	Potential energy surface
PGM	Phonon gas model
POPs	Phonon optimized potentials
SWBC	Stillinger-Weber-Born-Coulomb
TBC	Tersoff-Buckingham-Coulomb
TEP	Taylor expansion potential

SUMMARY

Molecular dynamics (MD) simulations calculate the trajectory of atoms as a function of time. Material properties that depend on the dynamics of atoms can be predicted in terms of these atomic motions, yielding insight into atomic-level behaviors that ultimately dictate these properties. Such insight is crucial for developing a low-level understanding of material behavior, and MD simulations have been used to successfully predict properties for decades. Thermal transport properties in solids are largely dictated by collective atomic vibrations known as phonons, which can be understood and probed deeply through analysis of MD trajectories. The heart of MD simulations is the mathematical representation of potential energy between atoms, termed the interatomic potential, from which the forces and dynamics are calculated. The use of MD simulations to generally predict and describe thermal transport has not been fully realized due to the lack of accurate interatomic potentials for a variety of systems and obtaining accurate interatomic potentials is not a trivial task. Furthermore, it is not known how to create potentials that are guaranteed to accurately predict phonon properties, and this thesis seeks to answer this question. The goal is to create potentials that accurately predict phonon properties, which are thereby termed phonon optimized potentials (POPs).

CHAPTER 1. INTRODUCTION

This introductory chapter reviews the concept of phonons; what phonons are and how they are modeled. Existing theories for modeling phonons are explained along with their shortcomings, as well as more general theories based on molecular dynamics (MD) simulations. Atomistic thermal transport involves the study of phonons using these computational techniques, and it forms one of the key approaches for theoretical and computational research in nanoscale heat conduction. This chapter introduces the biggest problem that hinders the progress of atomistic thermal transport modeling, namely the problem of accurately describing interactions between atoms in a computationally cheap manner.

1.1 Phonons

Heat transfer occurs through a variety of thermal energy carriers; electromagnetic radiation transfers heat via photons [1], fluids can transport heat via the diffusion of molecules and their interactions [2], and electrically conducting solids transport heat via electrons [3]. However, all phases of matter transport heat via atomic motions, and this is the main method of heat conduction in semiconductors, insulators, and covalently bonded solids [4]. The idea that atomic motions influence thermal properties was first introduced by Einstein, where he used Planck's radiation theory to show that quantization of atomic vibrations can explain the temperature dependent heat capacity of solids [5]. Atomic motions in well-ordered crystalline materials consist of vibrations around an equilibrium site [6]. These lattice vibrations then form sinusoidal waves in the crystal [7]. Such lattice vibrations have quantized amplitudes due to quantum mechanics, and each quanta of energy is called

a phonon [8]. Phonons in crystalline materials possess well-defined wave characteristics and can therefore be ascribed distinct wave vectors and wavelengths [7]. Lattice dynamics (LD) is a formalism for solving the equations of motion for atoms, and was first formulated in 1912 by Born and von Karman to describe phonons [9]. However, it wasn't until the 1950s that experimental advancements in the form of neutron scattering enabled measurements of these vibrational frequencies, thus confirming their existence and the validity of the LD theoretical treatment[10-12].

Although phonons are largely responsible for thermal energy transfer in many solids and their behavior can be modeled via LD, there are also classical theories applicable to macroscopic systems [13]. The classical theory of heat conduction is based on Fourier's law, which states that the heat flux Q through a system is proportional the negative gradient of the temperature field with respect to position ∇T, given by Equation 1.

$$Q = -\kappa \nabla T \tag{1}$$

The constant of proportionality, κ, is the thermal conductivity of the material. Thermal conductivity in solids possesses contributions from electrons and phonons [14]. The contributions to thermal conductivity in many technologically relevant materials, such as semiconductors and insulators, are dominated by phonons [4], since the number of conducting electrons is negligible. Fourier's law in Equation 1 accurately predicts thermal behavior in solids until the characteristic length reaches the mean free path of phonons [13]. Many important modern devices, such as transistors for example, are reaching length scales smaller than the mean free paths of many phonons [15,16] and as a result, modified or revised/new models must be developed to understand the behavior of such systems.

One example of the breakdown of Fourier's law stems from an inability to treat thermal conductivity as a material specific, yet size/geometry independent parameter [17,18]. As one shrinks the size of a material, one can account for deviations from Fourier's law by simply modifying the associated thermal conductivity, where the modification occurs because some phonons begin to interact with boundaries more frequently than other phonons [19-21]. Quantifying such size effects and phonon behavior has become a major undertaking in the nanoscale phonon transport community and it has been largely successful [22-24]. A thorough understanding of phonons and how to predict/model their behavior, will lead to better understanding of thermal transport properties in terms of the underlying phonon contributions to such properties [25]. Here, it is useful to note that the traditional definition of phonons as wave-like vibrational modes in crystals evolved out of formulations from LD to describe the frequencies, group velocities and wave-vectors of these modes in crystals [26]. Some of these quantities, such as velocity, also led to a corpuscle theory of phonons by treating phonons as quasi-particles that can scatter with each other and other particles, which is more formally described in the next section [8].

1.2 Phonon Gas Model

Phonons were originally modelled as gas particles colliding in a closed vessel in a model known as the phonon gas model (PGM), in which case kinetic theory can be used to calculate gas transport properties [8]. Peierls introduced the PGM in 1929 to describe the random thermal transport from phonons in solid materials[27]. In this sense, the PGM treats the vibrational modes in a crystalline solid (i.e., phonons) as quasi-particles with well-defined velocities, that can scatter with each other [8]. Kinetic theory, which is normally applied to predict transport properties of gases of molecules, can then be used to describe

transport properties in a gas of phonons [28]. The PGM states that each phonon with a wave-vector $\mathbf{q}$ and polarization index s carries a quanta of harmonic oscillator energy $\hbar\omega$ [8,27]. In the PGM, a phonon identified by $\mathbf{q}s$ can then travel with group velocity $v_{\mathbf{q}s}$ and can scatter with other phonons, boundaries, or crystal imperfections [8]. Kinetic theory applied to a gas allows one to calculate the gas thermal conductivity, which depends on the specific heat, velocities and mean free paths of the particles [29]. The thermal conductivity of a phonon gas is therefore written as a sum over all contributions from individual phonons with wave-vector $\mathbf{q}$ and polarization index s, normalized by the crystal volume V, as [30-32]

$$\kappa^{\alpha\beta} = \frac{1}{V}\sum_{q,s} c_{\mathbf{q}s} v^{\alpha}_{\mathbf{q}s} \Lambda^{\beta}_{\mathbf{q}s} \tag{2}$$

where $c_{\mathbf{q}s} = \hbar\omega_{\mathbf{q}s}\partial f_{\mathbf{q}s}/\partial T$ is the specific heat of mode $\mathbf{q}s$ in terms of the Bose-Einstein distribution $f_{\mathbf{q}s}$. The group velocity and mean free path of mode $\mathbf{q}s$ in general α and β Cartesian directions are given by $v^{\alpha}_{\mathbf{q}s}$ and $\Lambda^{\beta}_{\mathbf{q}s}$, respectively. Here, the mean free path represents the product of the group velocity and the average amount of time between collisions.

It is important to express Equation 2 here since it illustrates some key aspects of the PGM, which assumes vibrational modes possess particle quantities such as velocities and mean free paths. The PGM results in accurate thermal conductivity predictions for pure crystals, where the vibrational modes are wave-like and can be assigned quantities such as group velocities and wave-vectors [33,34]. Conversely, one could state that the PGM requires

that the modes of vibration can be described with wave-vectors and group velocities, since every mode is envisioned to carry heat like a particle and thus it must have an associated speed. Many normal modes, however, have been shown to lack well-defined wave vectors and velocities, when some form of disorder is present or some form of symmetry is lost[35-37]. The PGM therefore breaks down when disorder is added to the system, since many modes in disordered systems lack well-defined group velocities and wave-vectors, as long range periodicity is lost [38,39]. The PGM is therefore not a general method to predict thermal conductivity since many systems contain some level of disorder such as defects, grain boundaries or deviations from a perfect crystalline lattice. The PGM provides accurate thermal property predictions for pure crystals, but it cannot be generally applied to other types of solid with some level of disorder and this limitation stems from the intrinsic requirement of wave-like quantities for every mode [7,34,40].

Although the PGM is somewhat limited in application, more modern approaches utilizing molecular dynamics (MD) simulations possess much more generality [41,42]. MD simulations provide a computational foundation to study the dynamics of any atomic system in any phase of matter [43]. Linear response theory in statistical mechanics provides a framework for relating material properties to the atomistic level dynamics obtained from MD in a general way, regardless of the phase of matter or any level of disorder in the system [44]. Thermal property prediction using MD is therefore general in applicability to a variety of materials, unlike the traditional approaches that rely on the validity of the PGM [42].

1.3 Molecular Dynamics (MD)

MD simulations involve numerical simulation of the motions of atoms as a function of time. Dynamics are determined by solving Newton's equations of motions numerically for a system of interacting particles, where the interactions between particles are approximated as mathematical functions known as interatomic potentials, force fields, or are often just referred to as "potentials". Obtaining the dynamics first involves calculating the force for every atom. In classical MD the force $\mathbf{F}_i$ on an atom i is given by the classical mechanical definition as the gradient of the system potential energy via

$$\mathbf{F}_i = -\frac{\partial U\left(\overline{\mathbf{R}}, \boldsymbol{\lambda}\right)}{\partial \mathbf{R}_i} \tag{3}$$

where $\mathbf{R}_i$ is the position of atom i and U is the interatomic potential, which is represented as an analytical function of all atomic positions $\overline{\mathbf{R}}$ and a set of parameters $\boldsymbol{\lambda}$ that are used/fit to describe a specific material/chemistry [43]. A typical simulation starts with random initial velocities for every atom corresponding to a specific temperature. By knowing the forces on each atom from Equation 3, Newton's 2nd law yields an acceleration for each atom, and a finite timestep is used to numerically integrate the acceleration and solve for velocities and positions at the next timestep. A popular choice of integration algorithm that is also used in this thesis is the Verlet algorithm [45].

A single MD simulation can be thought of as a member of a statistical ensemble; a single simulation will sample microstates associated with a system that corresponds to macroscopic constraints/observables [46]. How the equations of motion are integrated then depends on constraints associated with or imposed by the ensemble; constraints can include temperature in the form of thermostats, barostats for pressure constraints, or imposing total

energy conservation. Imposing constant composition (number of atoms), volume and total energy results in a microcanonical ensemble, often abbreviated NVE[47]. Constant number of atoms, volume and temperature simulations generate configurations belonging to the canonical or NVT ensemble by utilizing thermostats [46]. Barostats are applied to integrate the equations of motion in a constant number of atoms, pressure and temperature NPT ensemble [48,49]. Each ensemble provides an approach to sample the phase space (positions and velocities) resulting from dynamics with the different macroscopic constraints. For an equilibrium MD simulation to study thermal conductivity, the atomistic dynamic quantities, e.g., positions, velocities and forces at a given timestep, can then be used as inputs to calculate the heat flux through a material, based on Hardy's general energy-flux operator [50]. Hardy's expression for the volume averaged instantaneous heat flux vector $\mathbf{Q}$ is given by [50]

$$\mathbf{Q} = \frac{1}{V}\sum_i \left[E_i \mathbf{v}_i + \sum_j \left(-\frac{\partial U_j}{\partial \mathbf{R}_i} \cdot \mathbf{v}_i \right) r_{ij} \right] \tag{4}$$

where the indices i and j run over all atoms, and $\frac{\partial U_j}{\partial \mathbf{R}_i}$ is the gradient of the potential energy of atom j with respect to the position $\mathbf{R}_i$ of atom i. Other quantities obtained from the MD simulation are the per-atom total energies E_i, velocities $\mathbf{v}_i$, and pairwise distances r_{ij}. Equation 4 assumes that the per-atom energy E_i and potential U_j are well-defined quantities, which is the case for analytical interatomic potentials that define the total energy as a sum of all per-atom contributions [51]. During a MD simulation the heat flux in Equation 4 can be calculated as a function of time. Time correlation functions of the heat flux can

then be used to calculate thermal conductivity tensor $\kappa^{\alpha\beta}$ [52], utilizing the Green-Kubo relation [53]

$$\kappa^{\alpha\beta} = \frac{V}{k_B T^2} \int_0^\infty \left\langle Q^\alpha(t+t') \cdot Q^\beta(t) \right\rangle dt' \tag{5}$$

where k_B is the Boltzmann constant, T is the system temperature, and the integrand is the heat flux autocorrelation.

The power of the MD method, utilizing GK theory, lies in its generality; it is applicable to any phase of matter, unlike the PGM [50]. The generality allows one to declare any atomic structure at the beginning of the simulation, and this structure may contain varied composition, defects, boundaries, etc. MD simulations also generally sample the phase space according to the ensemble, i.e., every atom experiences dynamics and motion at finite temperatures [50]. The motion of every atom also naturally includes anharmonicity to full order, which offers a great advantage to MD for studying phonon transport, over many other methods that start from the harmonic approximation and introduce complexity as they attempt to incorporate anharmonicity [34]. Furthermore, recent advances in techniques such as Green-Kubo modal analysis [35]decompose the motions and GK thermal conductivity calculated in MD simulations into contributions from individual vibrational modes. This supplies further insight into how different vibrational modes contribute to thermal transport and thermal conductivity. Modal analysis can also be applied to interfaces via interface conductance modal analysis (ICMA), which provides insight into how vibrational modes contribute to thermal transport across interfaces [54].

MD simulations and modal analysis provide general methods to study thermal transport properties in any material or phase of matter. The generality of these methods lies in the fact that the inputs are basic atomistic quantities that exist in every system such as atomic velocities, positions and forces, as there are no assumptions about the nature of vibrational modes in the system nor any requirements to ascribe group velocities to such modes [50,52,54]. While MD simulations and modal analysis provide general methods to study and predict thermal transport in any atomic system, the real power of these methods has yet to be realized, as accurate MD simulations of thermal transport in many systems, including pure crystals, are still challenging [55,56]. This is due to the lack of a wide variety of accurate interatomic potentials, which are at the heart of the MD method [56,57].

1.4 The Lack of Potentials

In a MD simulation, the forces on each atom depend on the gradient of the system potential energy via Equation 3 at each timestep; these forces dictate the dynamics for the next timestep, and therefore dictate the heat flux and final bulk properties calculated via linear response theory [52]. Accurate forces are required for accurate dynamics, which in turn determine bulk properties. Thus, property prediction when the force and potential are inaccurate still yields results, but they may not be physically meaningful. Much worse, for such an inaccurate simulation, there would be no faith in any predictions or explanations of experimental data. This issue is particularly important because one of the most important roles modelling and simulation play in science is to provide detailed insight and understanding. Thus, if the simulations are not of high fidelity, they provide little to no new trustworthy insight. Furthermore, when many existing potentials are applied to thermal property prediction, they often yield inaccurate thermal properties [23,57]. This discrepancy

between existing potentials and thermal property prediction arises from the fact that most of these potentials were not made with the thought of thermal transport or phonons in mind [57]. This issue is better appreciated by considering the century-long history of potential development, especially as it pertains to phonons and thermal transport.

1.4.1 History of Potentials for Phonons

Commonly used potentials in the heat transfer community today were inspired by original works on potentials in the early 1900s [58]. Analytical representations of interaction potentials began in 1924, when John Lennard-Jones determined an analytical expression to represent the van der Waals energy and forces between ideal gas molecules, and later extended his potential to describe bulk compression properties of simple ideal gas crystals [59,60]. A few years later, Morse crafted a potential that described anharmonic bonds between diatomic gas molecules [61]. Early work involving potentials, in the 1920s and 1930s, involved studying compressional and thermodynamic properties of gases and simple ideal gas crystals [62]. In the 1950s and 1960s, a surge in experimental methods to measure elastic constants, mechanical properties, and crystal structure led researchers to parameterize the original potentials made for gases (Morse, Lennard-Jones, etc.)[59,61] to cubic structured metals [63,64]. All the potentials up to this point described 2-body interactions between pairs of atoms and Born noted that being restricted to 2-body interactions would not properly describe elastic properties in more complex crystal structures containing more than one basis atom (e.g., diamond, wurtzite, etc.), as seen in many covalently bonded solids where phonon transport is dominant [65]. Stable classical MD simulations of more complex structures such as semiconductors and covalent solids, where phonon transport is a

dominant mode of heat conduction, were not possible until the development of potentials containing 3-body terms by Tersoff in 1985 [58].

The Tersoff potential incorporated short-range angular interatomic interactions into a Morse-like functional form to successfully describe the cohesive energy, bond energy and bulk elastic properties of diamond structured silicon [58]. That same year, Stillinger and Weber created a 3-body potential for silicon that was more adept at describing melting [66]. Even today, the Tersoff and Stillinger-Weber potentials are still the most commonly used functional forms for MD simulations of thermal transport in simple semiconductors, such as silicon [67]. Many more analytical potentials inspired by the 3-body Tersoff and Stillinger-Weber formulations arose in the 1990s to study other phenomena. These formulations, for example, included functional forms that could describe transitions from covalent to metallic bonding [68], phase transitions such as melting [69], and energetics associated with clusters, surfaces and defects [70]. Potentials up to this point in time were still parameterized against experimental quantities, similar to the creation of cubic metal potentials in the 1950s, although the more flexible 3-body forms allowed for these parameterizations to be successful at stabilizing covalent solids [58,71,72]. Brenner noted, in response to the rise of many analytical potentials in the 1990s and their different parameterizations, that analytical potentials lacked transferability; once parameterized for one situation they may not properly describe another atomic scenario, and many analytical forms were shown to be unable to describe multiple phenomena simultaneously [51]. This problem of transferability is especially true for phonons; many traditional analytical potentials for covalent solids were shown to yield poor agreement to experimental phonon properties and thermal conductivity since they were optimized for other purposes [57,73-77]. In response to the lack

of parameterizations of analytical potentials that described phonons and thermal transport accurately, some attempts in the late 1990s and early 2000s involved parameterizing potentials against experimental phonon frequencies [56,78-80].

Creation or re-parameterization of potentials to describe phonons and thermal transport in semiconductor and insulator systems was a largely attempted by trial and error, and still yielded inaccurate phonon and thermal property prediction [76,78,79,81]. Broido *et. al* even abandoned the use of analytical potentials in favor of using the Boltzmann transport equation (BTE), which is similar in concept to kinetic theory, to calculate thermal conductivity directly from first principles. Here they used LD, where the 2nd order force constants were determined directly from density functional theory (DFT) [34], and they used 3rd order force constants as inputs to Fermi's golden rule, to determine the phonon-phonon scattering rates [34]. This breakthrough approach requires no adjustable parameters and exhibits excellent agreement with experiments and can be predictive [34]. However, it is not a complete solution to the problem, because it is restricted to describing crystals, since it still relies on the validity of the PGM. Thus, there has still been significant interest in using MD to study phonons more generally, which then requires parameterization of analytical functional forms to reach the length and time scales needed. In this sense, the process associated with parameterizing analytical potentials has been considered a daunting task within the phonon transport community [34,56]. Although a few authors made attempts at parameterizing potentials purely for the study of phonons and accurate thermal transport properties, these attempts still resulted in inaccurate thermal property predictions [81,82]. Some of the earliest work on parameterizing potentials with phonon properties in mind included a series of studies starting in 2006 by Powell, in where he optimized the Tersoff

potential to reproduce experimental mechanical properties and phonon frequencies in group III-IV semiconductors [83].

Powell noted that the Tersoff functional form was unable to simultaneously reproduce elastic constants and phonon properties [83]. The following few years saw an increase in the number of attempted parameterizations using Tersoff by Powell, but experimental phonon fitting targets only included frequencies at a few points of the Brillouin zone [80]. Work in this area continued to progress until 2012 when Powell attempted the creation of an entirely new functional form in order to properly describe phonon frequencies, but his new potential was still not guaranteed to accurately predict phonon transport properties since he was more concerned with elastic properties [84,85]. Parameterization against experimental quantities, as performed by Powell and many others, still had not seemed to produce potentials guaranteed to accurately predict thermal transport [84].

In 1994, Ercolessi introduced the concept of parameterizing potentials to reproduce quantum mechanical quantities such as forces [86]. This sparked a surge in re-parameterizing potentials to match quantum mechanical data instead of experiments, in attempts to computationally scale up the expensive quantum mechanical, or *ab initio*, results to computationally cheaper analytical potentials [82,87,88]. This was a powerful realization, because it suggested that empirically parameterized potentials that were fit to *ab initio* inputs, could one day offer predictive capability. Success in fitting to quantum mechanical quantities such as energies were seen with metals using the embedded-atom method, which is based on a physical rationalization of the overlapping electron density in metals [88,89]. Attempts to fit analytical potentials such as Tersoff to *ab initio* quantities in covalent solids,

where phonon transport is a dominant mode of heat transfer, however, remained unsuccessful; the potentials that were fit to *ab initio* data still possessed inaccurate phonon and thermal properties [82,90]. While work in this area for covalent solids is slim, Umeno *et. al.* for example attempted to re-parameterize the original Stillinger-Weber potential for silicon-silica systems by only modifying a few of the original parameters to reproduce quantum mechanical forces; the resulting phonon and thermal properties, however, still exhibited poor agreement with experiments [82].

Much of the inability to reproduce quantum mechanical forces in previous studies could have presumably lay in the fact that the search space for the parameters of the potentials was largely constrained to reside near the original parameter sets, which were parameterized against experiments [91]. Many authors would impose these constraints due to lack of a robust fitting algorithm to easily perform such multi-objective and highly multi-dimensional optimizations, along with attempts to maintain the stability of existing potentials, while still helping them reproduce quantum mechanical data [82,91]. These difficulties in parameterizing potentials, along with the lack of work to optimize potentials specifically for the study of phonons and thermal transport, have led to a lack of potentials that accurately predict phonon properties [56]. This lack of potentials is one of the biggest roadblocks hindering progress in the field of thermal property prediction, as there are now methods such as GK [52], GKMA [35] and ICMA [54] that allow for general prediction of bulk properties from atomistic dynamical quantities, and there are methods to perform fast MD by efficiently integrating the equations of motion [92], but there are no methods that aid in the creation of potentials for the study of phonon properties [56]. Since potentials are at the heart of a MD simulation and are the most important input, the lack of potentials for

studying phonons translates to an inability to study many different systems [56,57]. This results in a gap between theoretical understanding and experimental confirmation, since the lack of potentials prevents the usage of MD to study many of the systems that are of interest experimentally [93,94].

1.4.2 Bridging the Theoretical-Experimental Gap

Many experimental methods provide ways to measure thermal transport properties without restrictions or constraints associated with the underlying chemistry i.e., measuring pure crystals [94], interfaces [95], amorphous materials [96], alloys and polymers [97,98] are all possible with the same techniques. MD simulations, applicable to any material or phase of matter, also provide a general method to study and predict thermal transport in such systems [99]. Furthermore, MD simulations and modal analysis provide more insight into the underlying dynamics and vibrational modes giving rise to thermal properties [35]. Theoretical pursuits, namely MD simulations and modal analysis, can therefore aid in experimental research by providing a deeper and more detailed level of understanding, since most experimental techniques only yield the overall transport property and provide no insight into the comprising contributions associated with different phonons. Contrarily, experiments can aid in theoretical research by providing a plethora of observed phenomena to further develop and confirm the predictions of theoretical models [100-102]. This collaboration between theory and experiment aids progress in our overall understanding of the underlying physics [103]. Currently, however, the number of systems studied and published experimentally greatly outweighs the number of appropriately corresponding systems studied theoretically via classical MD simulations [103]. For the past few decades, experimentalists have developed methods to measure thermal transport in systems ranging

from pure simple crystals to disordered materials and interfaces [95,96,104]. Yet, there has not been a corresponding increase in the study of these systems using MD simulations, and the use of MD simulations to study whatever systems potentials do exist for, including pure simple crystals, are often inaccurate [56,57,76,105,106]. This is due to the lack of interatomic potentials that allow for accurate MD simulations and thermal property prediction [107]. As a result, it has been generally recognized that the creation of a method to help in the seemingly daunting process of potential creation and parameterization would enable the community to close the gap between theory and experiment.

The creation of potentials, specifically for the study of phonons, has not been an explicit subject of research and has eluded researchers in theoretical phonon transport for many years [76,81]. While a few attempts have been made by Lindsay [81], Umeno [82], and mainly Powell [80,83,85] to create or optimize potentials that accurately predict phonon properties, they have still resulted in inaccurate descriptions. Furthermore, these existing studies did not thoroughly investigate how to create or parameterize potentials that accurately predict phonon properties, or what is involved in such a process. Optimizing potentials for phonon properties therefore invites many unanswered questions, several of which are the subject of the remainder of this thesis.

1.5 Questions and Hypotheses

Since lattice thermal conductivity and thermal transport depends on the motions and vibrations of atoms, the goal is to obtain potentials that accurately capture the thermal motion of atoms so that accurate phonon properties can be calculated using these motions. The lack of existing work towards this goal leads to a fundamental question (Question 1);

namely, how does one create (i.e., optimize or parameterize) a potential that will accurately predict phonon properties and thermal transport? More specifically, what quantities should the potential be optimized to reproduce by varying the fitting parameters? It is not desirable to only fit to phonon dispersion curves, since this is not general; phonon dispersions are only well-defined for pure crystals [26]. We also cannot directly fit to thermal conductivity values, since thermal conductivity is not unique. Thermal conductivity represents a summation of many individual phonon level properties/interactions that can be represented in many different ways, yet can still yield the same overall thermal conductivity [56]. Additionally, full calculations of thermal conductivity are computationally expensive and might be impractical to use in an objective function for optimization. Thus, more general and easily calculable quantities are desired for the optimization process.

Atomic vibrational motion, in part, depends on the stiffness of the interactions [108]. The stiffness between interacting bodies is described by how the forces change with respect to displacements of the bodies [108]. It is therefore hypothesized (Hypothesis 1) that a potential which accurately reproduces interatomic forces, calculated via quantum mechanics, will accurately capture phonon and thermal transport properties by possessing accurate vibrational motions that give rise to such properties. Specifically, fitting only to forces should be sufficient in obtaining a potential that accurately predicts phonon and thermal properties. This hypothesis is supported by MD trajectories being dictated by forces, which also dictate the GK thermal conductivity [52]. More quantitatively, it is hypothesized for this reason that the error in forces for a potential is likely to directly translate to an associated level of error in thermal conductivity. For example, a 10% error in forces might lead to roughly a 10% error in thermal conductivity. Accurate forces are

attainable as fitting targets via quantum mechanical methods, which solve for the electronic structure of a group of atoms, from which forces are calculated. A powerful quantum mechanical method for solids is DFT, which offers excellent predictive power when calculating the energetics, forces and dynamics from first-principles (i.e., the Schrödinger equation) [109]. To prove or disprove Hypothesis 1 of fitting to forces, DFT will therefore be used in this thesis to obtain the forces to optimize potentials against.

This raises another question (Question 2); how closely can quantum mechanical forces and vibrational properties such as phonon frequencies be matched when using traditional potentials for solids (e.g., Tersoff, Stillinger-Weber, Morse, etc.)? It is not known how well quantum mechanical forces can be captured using relatively simple analytical functional forms. Previous work in this area, especially for covalent solids, involved only slight changes to the traditional parameter sets of these potentials without fully exploring the parameter search space [91]. It is hypothesized (Hypothesis 2), that for small displacements around equilibrium positions, the percent error in quantum mechanical forces using traditional functional forms for semiconductors (Tersoff and Stillinger-Weber) can reach below 10% if the parameter search space is searched thoroughly enough. Hypothesis 2 is supported by existing force-fitting work with simple metals, in which embedded atom potentials reached a 20% force error after thorough fitting to phase transition configurations [110]. Furthermore, traditional potentials for semiconductors should be able to resolve small forces about equilibrium atomic positions since these traditional potentials were used to study seemingly more complex tasks such as bulk elasticity and fracture [111], defect formation [112], liquid flow [113,114], and chemical reactions [114]. Atoms in these situations move much further from their equilibrium positions than the mean squared

displacements associated with thermal motions giving rise to thermal transport properties [26]. Due to this excess flexibility of traditional functional forms, one could say that traditional forms are "overdesigned" for the study of phonons. For this reason, it is hypothesized that the functional forms carry more than enough complexity than what is needed to simply describe vibrations around equilibrium. Thus, it is suspected that parameters exist that should be able to reduce the force error to within 10%, if the search space is probed in a sufficiently diverse way. Some traditional potentials result in accurate thermal property prediction, but these potentials were not designed for this purpose; it is a matter of luck that a potential will accurately predict a property when it has been optimized for another purpose [51]. Such traditional potentials can still possess large errors with respect to quantum mechanical forces [57]. Hypotheses 1 and 2, if correct, together state that traditional functional forms for solids (e.g., Tersoff, Stillinger-Weber, Morse, Coulomb, etc.) will accurately predict phonon properties if optimized for such a purpose (i.e., parameterized against forces).

Traditionally, potential parameters were thought to possess some physical meaning and authors always publish a single best parameter set that describes their phenomena of interest [58,66,71,72,112]. Since these traditional functional forms were not designed for the study of phonons, however, many of their parameters may not possess any relevant physical meaning for phonons. This raises a question (Question 3); will parameters that accurately predict phonon and thermal properties be obtained if we do not infer any physical meaning to the parameters of a potential, and just perform brute force multi-objective fitting in a large region of the parameter search space? Due to the overdesign of traditional potentials for the atomic phase space of thermal vibrations it is hypothesized (Hypothesis 3) that

many parameter sets exist to describe thermal phenomena; these parameter sets may not be physically meaningful and may be obtained via brute-force fitting, without spending unnecessary time to deduce individual parameter values based on physical or chemical insight. This is a major shift in thinking with how researchers traditionally obtain parameters; it has been customary to analytically or experimentally deduce the values of each parameter, or based on physical or chemical intuition [51,58,66]. While the concept of overdesign should result in enough flexibility for the study of phonons using traditional potentials, one known limitation of traditional potentials for studying phonons in semiconductors is the exclusion of long-range interactions [58,66].

Phonon frequencies have been shown to depend on long-range interatomic interactions, so excluding them results in inaccurate frequency prediction [115,116]. Brillouin zones, or primitive cells in reciprocal space, serve as spaces to calculate phonon frequencies and plot them as a function of directions in reciprocal space via phonon dispersion curves [117]. The phonon frequencies near the edges of Brillouin zone boundaries are associated with long-range interatomic interactions, so phonon frequencies in these regions cannot be accurately predicted using traditional short-range potentials that only include nearest neighbors [115,116]. Many semiconductor and insulating materials possess face-centered cubic or diamond structured Brillouin zones, shown in Figure 1.

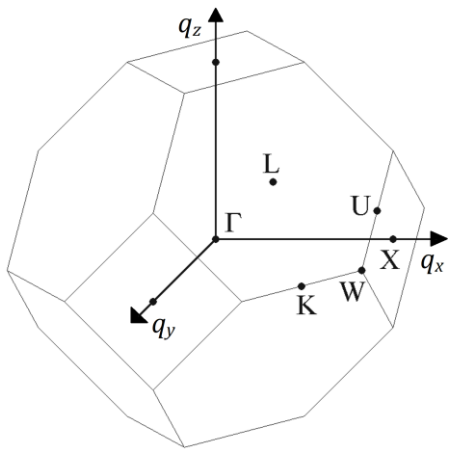

Figure 1 – Brillouin zone for a diamond lattice, residing in reciprocal space with reciprocal coordinates (q_x, q_y, q_z). The capital letters are symmetry points of the Brillouin zone, with the Γ point residing at the center of the Brillouin zone. The points at the edge of the boundaries are X and L, which are also symmetric (identical) for all edges.

The X and L points in Figure 1, for example, show regions of the Brillouin zone with inaccurate phonon frequency calculations according to traditional short-range potentials for covalent solids (e.g., Tersoff[58] and Stillinger-Weber[66]) [118]. This raises another important question (Question 4); will the addition of traditional long-range potentials (e.g., Coulomb, Buckingham, van der Waals interactions) allow accurate phonon frequency prediction for the entire Brillouin zone if these potentials are parameterized to match long-range interatomic forces? Traditional long-range potentials, like their short-range counterparts, have also been successfully used in the past to study larger and more complex regions of phase space, including phase transitions[119] such as melting[120]. The overdesign principle should therefore also apply to traditional long-range potentials, thus allowing for the resolution of phonon frequencies at Brillouin zone boundaries. It is therefore hypothesized (Hypothesis 4) that the addition of traditional long-range interactions (e.g., Coulomb, Buckingham, van der Waals interactions) will alleviate the known issue of capturing

phonon frequencies at the Brillouin zone boundaries. Answering these questions and testing the hypotheses involves a variety of tasks that pose major challenges in potential optimization. It therefore important to highlight the main challenges which hinder investigation of the proposed questions and hypotheses, to better understand the tools that must be developed to begin addressing such problems.

1.6 Challenges

Aside from the fact that the proposed questions are unanswered, therefore rendering the production of potentials for phonon properties as uncharted scientific territory, optimizing potentials is also a time-consuming and daunting procedure in general [86,121-123]. No convenient tools exist to simplify this task. Although some authors began attempts at tools to easily create potentials [124], such tools lack desirable features as: (1) generality across any potential or fitting target that would aid in answering Question 1, (2) speed which would allow for more efficient investigation, and (3) a user-interface to conveniently change optimization settings, thus further aiding in potential fitting experiments. Aside from plaguing the general scientific community that uses MD [86,119,120], these challenges limit the tractable investigation of the proposed questions and hypotheses since answering the proposed questions involves experimenting with different functional forms and fitting quantities, along with thoroughly searching the parameter space for solutions that describe quantum mechanical forces and phonon properties well. Question 1, for example, involves identification of which fitting quantities are necessary to produce a potential that accurately describes phonons. The general applicability of a fitting method to a variety of reference quantities is therefore of utmost importance. The generality must extend to the use of different potentials as well, to answer Question 2 regarding how well analytical potentials

can reproduce quantum mechanical quantities and phonon properties. Further flexibility in the ability to parameterize a variety of potentials is needed, since Question 3 involves the need to thoroughly search the parameter search space, and answering Question 4 involves the addition of long-range potentials. Aside from optimization generality, lack of speed and a convenient user-interface to change optimization settings limit the ability to answer these questions by hindering the amount of potential fitting experiments that can be done in a reasonable amount of time. Answering Question 3 requires effective scanning of many parameters in the parameter search space to confirm the possible existence of many parameter sets that describe phonon properties, which again is limited by these known challenges. A prerequisite task for answering the proposed questions is therefore to develop a tool, a computer program, which alleviates these existing challenges in potential optimization. Such a tool will allow for the tractable investigation of the proposed questions and hypotheses, as well as aid the general scientific community that uses MD, in their efforts to develop interatomic potentials.

Chapter 1 has introduced the problem of developing potentials for phonon properties, along with the necessary prerequisites to address the problem. The remainder of this thesis will cover my approach to solving the problem of a lack of potentials, along with answering the proposed questions and hypotheses. Chapter 2 covers interatomic potential modelling and optimization, as well as introducing the fitting problem and methods used to accomplish the fitting. Chapter 3 covers the methods used in this thesis to predict phonon properties, and will also serve as a basis for the theory which is used to develop phonon optimized potentials (POPs). Chapter 4 combines the material of Chapters 2 and 3 to introduce the procedure of developing POPs. The powerful open-source program POPs is

also introduced in Chapter 4, which alleviates the challenges in potential optimization highlighted in Chapter 1. Chapter 5 covers applications to some simple systems, and Chapter 6 discusses limitations of the current method as well as attempted solutions. Chapter 7 concludes the thesis and discusses future work needed to overcome the remaining challenges. Challenges arise in investigating and answering the proposed questions and hypotheses due to the lack of tools that aid in the convenient optimization of potentials; it is therefore a secondary goal of this thesis to create a tool, or computer program, that alleviates these known issues. Such a tool will aid in the investigation of the proposed questions and hypotheses by providing a tractable method to quickly parameterize a variety of potentials to a variety of fitting targets. To begin at accomplishing such a task, and investigating the questions and hypotheses raised, a more thorough discussion on interatomic potential modelling and optimization is first needed.

CHAPTER 2. INTERATOMIC POTENTIALS

The mathematical and analytical approximation of interatomic interactions i.e., the interatomic potential, forms the foundation of classical MD simulations. This chapter further covers the basics of potentials and how they are optimized, to offer a better understanding of the proposed questions and hypotheses.

2.1 Introduction to Interatomic Potentials

Analytical potentials seek a relation between an atom's environment and its potential energy [51]. Specifically, this should be a closed-form analytical relation so that the exact spatial gradient may be performed when calculating the force in MD simulations via Equation 3. An example of an atomic environment is shown in Figure 2, where the circles represent atoms. The red atom in Figure 2, for example, possesses a potential energy that depends on the positions of all the atoms in its environment. All atoms within some cutoff radius r_c of the atom under consideration make up the atomic environment, which is termed a neighbor list inside a typical MD program. Positions of atoms in the atomic environment, or the environmental geometry, dictate the potential energy of an atom. Traditional analytical potentials assume that the total potential energy can be expanded into contributions from single atoms, 2-body interactions, 3-body interactions, and so forth, represented by Equation 6 [51]

$$U = \sum_i U_i(\mathbf{R}_i) + \sum_{i,j} U_{ij}(\mathbf{R}_i, \mathbf{R}_j) + \sum_{i,j,k} U_{ijk}(\mathbf{R}_i, \mathbf{R}_j, \mathbf{R}_k) + \ldots \tag{6}$$

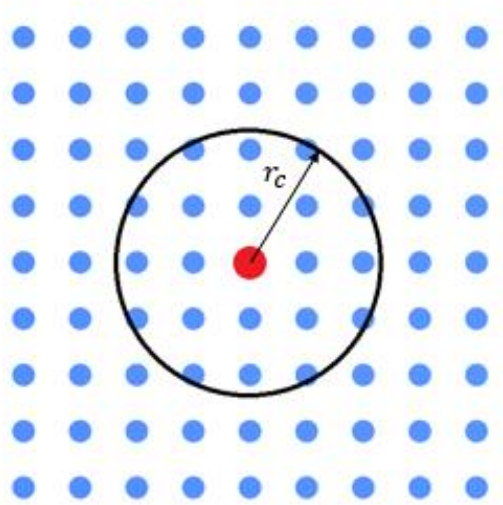

Figure 2 – Representation of an atomic environment. The environment, or neighbor list, of the red atom includes all atoms within some cutoff distance.

where $U_i(\mathbf{R}_i)$ is the self-interaction potential energy of atom i, as a function of its position vector $\mathbf{R}_i$, $U_{ij}(\mathbf{R}_i, \mathbf{R}_j)$ is the 2-body interaction potential between atoms i and j, as a function of the positions $\mathbf{R}_i$ and $\mathbf{R}_j$ of atoms i and j, and similarly for higher order interactions. For a single atom i, the interactions between other atoms for the higher-order terms in Equation 6 must be truncated to some cutoff r_c to restrict enormous amounts of atoms from entering the neighbor list, thus rendering the potential calculation more expensive. The higher-order terms in Equation 6 sum over all atoms in the neighbor list of each atom i. For a given atom i, the self-energy of the first term in Equation 6 would only include contributions from itself. The 2-body energy of atom i would include contributions from all pairs of atom i and atoms j in its neighbor list. The 3-body energy of atom i would include all the triplets of atoms i, j, and k atoms in the neighbor list of atom i, and so forth. Interatomic potentials are simply functional forms that give potential energy

in terms of these N-body interactions. Analytical potentials, according to the expansion in Equation 6, cast the environmental geometry of any atom i into a specific function of the positions of all atoms in the environment (the neighbor list), along with fitting parameters to tailor it to a specific set of atomic species. A general form of such potentials, for a single atom i, is given by Equation 7

$$U_i = U_i\left(\overline{\mathbf{R}}, \boldsymbol{\lambda}\right) \tag{7}$$

where U_i is the potential energy of atom i, $\overline{\mathbf{R}}$ are all the positions of all atoms in the environment of atom i, and $\boldsymbol{\lambda}$ are a set of fitting parameters. This form of potential energy, in which the energy can be written for each atom, is also required in Hardy's heat flux operator of Equation 4 where per-atom energies are assumed to be definable [50]. The total potential energy for the system now results as a sum of per-atom contributions, which is the potential energy we take the spatial derivative of to calculate forces on atoms in Equation 3. While the potential energy represented by analytical interatomic potentials are functions of atomic positions, plain Cartesian coordinates of atoms are poor candidates for the description of environmental geometry [51]. Aside from the fact the plain Cartesian coordinates by themselves do not offer unique information into the geometry of a group of atoms, their values change under mathematical operations such as translation and rotation. In other words, Cartesian coordinates by themselves are not translationally or rotationally invariant [125]. Invariance, or symmetry, describes a property of a system that is unchanged under a mathematical transformation [126]. Such transformations apply to all positions of all atoms in a system. An important theorem in classical mechanics called Noether's theorem states that for every invariance in a system, there is a corresponding conservation law [126].

Translational and rotational invariance are intuitive necessities, since simple translation or rotation of an atomic system (e.g., a crystal) will not change the interatomic interactions, or bulk properties of the material, in the absence of external fields [125]. It is therefore necessary to cast the positions of atoms into invariant mathematical descriptions, or geometric descriptors, of the atomic environment.

2.2 Geometric Descriptors

Geometric descriptors are transformations of atomic coordinates into quantities that can be more easily used in a mathematical potential model [125]. More importantly, these transformations cast the environmental geometries from plain Cartesian coordinates into invariant descriptions of geometry. For example, a potential possessing simple translational invariance defined by Equation 8

$$U\left(\overline{\mathbf{R}}\right) = U\left(\overline{\mathbf{R}} + C\right) \tag{8}$$

involves the addition of a constant number C to the positions of all atoms $\overline{\mathbf{R}}$. Such a potential, possessing translational invariance, would result in dynamics that conserve translational or linear momentum [126]. Another important invariance for interatomic potentials, rotational invariance, denotes an unchanging potential energy when rotating the system; rotational invariance ensures conservation of angular momentum [125]. These invariances, translational and rotational, are especially important in classical MD simulations since all modes of vibrations, including translational modes, can be excited; the translational modes should therefore conserve energy for stable dynamics (i.e., no unphysical increases in total energy) to be realized. Invariant descriptions of the geometry

of a group of atoms therefore results in potentials that conserve linear and angular momentum, thus resulting in stable MD simulations. The most traditionally used geometric descriptor for interatomic potentials, dating to early works of Lennard-Jones[62] and Morse[61], is the simple pairwise distance between two atoms r_{ij}. This distance does not change when a system of two atoms is translated, and therefore the potential energy of the system is also unchanged; likewise, for rotation. The advent of potentials for covalently bonded solids resulted in potentials with 3-body descriptors including angles between triplets of atoms; these angles are also unchanged under total system transformations such as translation and rotation. Illustrations of these commonly used and traditional descriptors are shown in Figure 3.

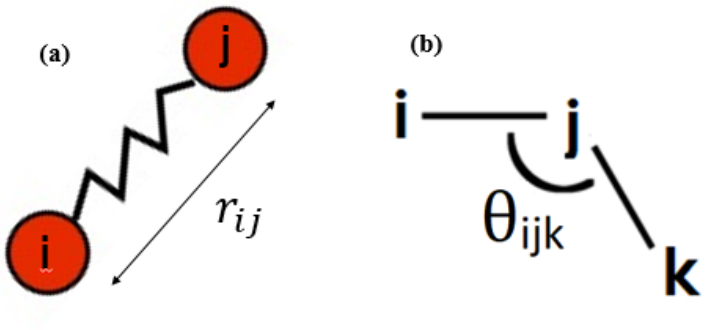

Figure 3 – Traditionally used geometric descriptors. Simple examples are (a) the pairwise distance between pairs of atoms and (b) angles between triplets of atoms.

Central potentials utilizing the pairwise distance between atoms i and j, r_{ij}, have traditionally been and still are the most common. Traditionally used descriptors for semiconductors and insulators, where phonon transport dominates heat conduction, also included the angular descriptor θ_{ijk} between triplets of atoms. These are the only two

geometric descriptors, represented in Figure 3, that are employed in the traditionally used semiconductor potentials (e.g., Tersoff and Stillinger-Weber) involved in Question 3 of whether traditional potentials for such materials will accurately predict phonon properties if parameterized for such properties. These geometric descriptors were used by traditional potentials to describe seemingly more complex phenomena per the concept of overdesign, and should therefore possess the necessary flexibility to describe thermal transport. The traditional long-range potentials (e.g., Coulomb and Buckingham) involved in Question 4 of whether the addition of long-range potentials will more accurately predict phonon frequencies, only incorporate the 2-body radial geometric descriptor r_{ij}. Hypothesis 4, stating that traditional long-range potentials can accurately reproduce phonon frequencies at the Brillouin zone boundaries, therefore assumes that the radial geometric descriptor is sufficient for describing such phenomena in diamond structured semiconductors. More modern geometric descriptors exist to bring more flexibility in describing interatomic interactions, namely with the recent machine learned interatomic potentials [125]. These more modern potentials utilize geometric descriptors with more flexibility in describing the atomic environment compared to simple distances and angles, but are orders of magnitude more expensive in computation [127]; the original questions and hypotheses, however, deal with traditionally used potentials containing desirable computational speed. While different geometric descriptors provide different flexibilities in describing atomic environments, the parameters of the potential ensure that proper energetics in those environments are accurately calculated. Consideration of some common traditional potentials will show how these parameters arise, and where they reside in an analytical functional form in relation to the geometric descriptors.

2.3 Example Potentials

One of the most commonly used potentials in physics and MD simulations is the Coulomb potential, representing the interaction between charged bodies or atoms i and j [128]. The traditional Coulomb potential, serving as a model example potential, is given by Equation 9

$$U\left(r_{ij}\right)=\frac{\lambda_1\lambda_i\lambda_j}{\lambda_2 r_{ij}} \tag{9}$$

where we see the traditional radial descriptor r_{ij}, along with some other parameters that represent the charges λ_i and λ_j of atoms i and j, along with physical constants λ_1 and λ_2. This potential includes the radial descriptor in the denominator, thus stating that the interaction decays with increasing interatomic distance. The sign of the charges can influence the Coulomb potential to be either positive or negative, thus denoting either a repulsive or attractive interaction. Another traditional example is the Morse potential made for anharmonic bonding, given by Equation 10

$$U(r_{ij}) = \lambda_1\left[1-\exp\left(-\lambda_2(r_{ij}-\lambda_3)\right)\right]^2 \tag{10}$$

where we again see a radial geometric descriptor r_{ij}, along with three fitting parameters in the set $\boldsymbol{\lambda}$. Another common example, incorporating traditional van der Waals interactions that decay as the inverse 6th power of the interatomic distance [129], is the Born potential [130] given by Equation

$$U(r_{ij}) = \lambda_1 \exp\left(\frac{\lambda_2 - r_{ij}}{\lambda_3}\right) - \frac{\lambda_4}{r_{ij}^6} + \frac{\lambda_5}{r_{ij}^8} \tag{11}$$

which again utilizes the same radial geometric descriptor r_{ij} along with some fitting parameters. These example traditional radial potentials, often used for long-range interactions, all possess a similar shape when plotted as a function of interatomic distance r_{ij} for a pair interaction. This shape is shown in Figure 4, noting the combination and repulsive and attractive interactions which combine to form a minimum energy equilibrium region in which the atoms vibrate about.

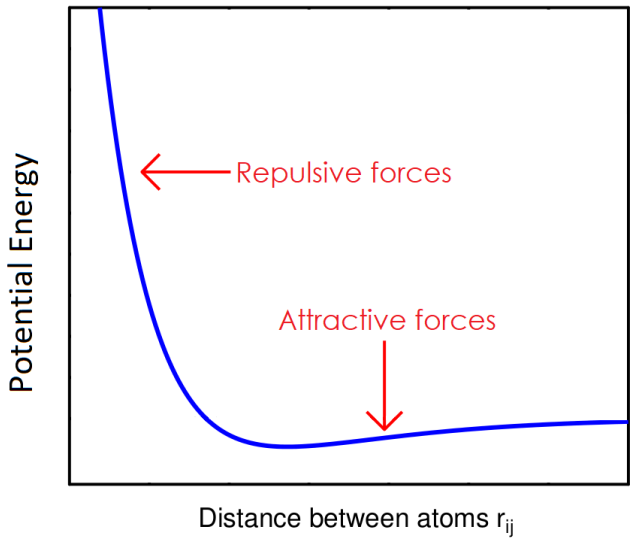

Figure 4 – Potential energy surface (PES) of traditional 2-body potentials as a function of the radial geometric descriptor. Attractive forces bring atoms together at larger separations, and repulsive forces keep atoms from touching each other.

Representations of a potential in terms of geometric descriptors such as in Figure 4 is referred to as a potential energy surface (PES), which becomes a hyper dimensional surface when more than two atoms are involved [131]. The PES, while difficult to visualize for a system of many atoms, is an important concept when referring to the behavior of an analytical potential in terms of its geometric descriptors [131]. For many potentials and

interactions, however, the PES is better understood in terms of more complex descriptors than simple pairwise distances. An example of a simple potential utilizing the angular geometric descriptor θ_{ijk} is given by Equation 12

$$U(\theta_{ijk}) = \lambda_1\left(\theta_{ijk} - \lambda_2\right)^2 \tag{12}$$

where the fitting parameters λ_1 and λ_2 determine the shape of the PES in terms of the 3-body angular descriptor. This harmonic 3-body potential forms a PES that is parabolic about some equilibrium angle λ_2, and the parameter λ_1 influences the shape of the parabola (i.e., strength of the 3-body interaction). Variations of the 3-body potential in Equation 12 appear in more complex potentials used to describe covalent bonding in semiconductors and insulators, such as Tersoff[72] and Stillinger-Weber[66]. The functional forms of Tersoff and Stillinger-Weber contain up to 18 fitting parameters [112], but they are simply analytical functions of atomic positions, particularly geometric descriptors of positions, and some fitting parameters.

Hundreds of functional forms exist today [132], with varying analytical forms, and different representations of atomic geometry, offer varying degrees of flexibility to describe various regions of the PES. The fitting parameters, however, ensure that the PES can be properly described in terms of whatever quantity the potential is fit to. It is therefore worthwhile, especially to better understand what is involved in investigating the proposed questions and hypotheses in Chapter 1, to more deeply consider the parameterization problem associated with fitting potentials to target quantities.

2.4 Optimization

The process of parameterizing interatomic potentials greatly eludes many researchers in computational materials science, especially those studying phonons. This is evident by the plethora of studies which state the difficulties and uncertainties associated with parameterizing potentials for phonon properties [74,76,78,80,84,91,133,134]. For the few researchers who do attempt their own optimizations, they usually start with pre-existing parameter sets that were designed for purposes other than the application they are studying [85,91,135]. This results in parameter sets that are presumably nowhere near as optimized as they could be for a certain task, since the parameter search space is not often well-searched. The reason for the lack of successful parameterizations of a variety of functional forms lies in the lack of tools necessary to perform such daunting optimizations. To better explain this problem, it is important to consider the optimization problem more in depth.

Interatomic potential optimization refers to the process of minimization the errors between quantities calculated with the potential and reference quantities. This optimization problem is represented mathematically via Equation 13

$$\arg\min_{\boldsymbol{\lambda}} \left(Z(\boldsymbol{\lambda})\right) \tag{13}$$

for some error $Z(\boldsymbol{\lambda})$, or objective function, between potential quantities and target quantities, and this error is a function of the parameter set $\boldsymbol{\lambda}$ of the potential (e.g., the three parameters of the Morse potential in Equation 10). The $\arg\min$ operator means that the arguments $\boldsymbol{\lambda}$ are sought that minimize the objective function $Z(\boldsymbol{\lambda})$, thus representing a general parameterization problem. The objective function $Z(\boldsymbol{\lambda})$ between reference quantities and target quantities can take the form of any error metric (e.g., standard

deviation, etc.). A commonly used and simple objective function, to illustrate an example, is the sum of squared errors between potential quantities $q_i(\boldsymbol{\lambda})$ and reference target quantities q_i^0 [121]

$$Z(\boldsymbol{\lambda}) = \sum_i^N \left(q_i(\boldsymbol{\lambda}) - q_i^0\right)^2 \tag{14}$$

where the index i runs over all N quantities being fit to, or fitting targets. It is important to note that the potential calculated quantities, $q_i(\boldsymbol{\lambda})$, are also functions of the potential parameters since these quantities are calculated by the potential. The quantities included in the error $Z(\boldsymbol{\lambda})$ can therefore be anything that is calculable by the potential, and that a reference exists for (e.g., experiments or *ab initio* data). Optimizing the parameters $\boldsymbol{\lambda}$ can be a large multi-dimensional optimization problem, with many functional forms possessing dozens of parameters [51]. This optimization problem was traditionally simplified by attempting to experimentally or analytically deduce the values of most parameters [58,132], and many authors would publish a single best set of parameters that describes their phenomena of interest [72,83,132]. Authors such as Powell would also incorporate local minimization methods starting from regions in the parameter search space near the originally published Tersoff values [85]. This thesis, however, adopts a new philosophy per Hypothesis 3.

Investigation of Hypothesis 3 requires an optimization method capable of searching a large multi-dimensional search space, to obtain many different sets of parameters. Such optimization tools lie within the realm of global optimization, and differ from traditionally

used potential fitting methods of gradient-based local minimization [81,83-85,91]. This will aid in the investigation of other questions and hypotheses by allowing the same algorithm, or program, to be applied when experimenting with different potentials and fitting quantities. Such algorithms fall under the umbrella of optimization methods known as metaheuristics; these algorithms do not require any information about the gradient of the objective function since they depend on stochastic optimization processes [136]. Guided random sampling of the parameter search space also renders metaheuristics as excellent candidates for exhaustive searches, especially compared to gradient-based or numerical optimization techniques [137]. Metaheuristics are therefore excellent candidates of an algorithm choice to investigate the proposed questions and hypotheses by being applicable to any potential or fitting quantity, and will aid in the exhaustive searching required to obtain multiple parameter sets. Their strength as exhaustive multidimensional search algorithms [137] also render metaheuristics as excellent tools to explore the parameter search spaces in testing how well traditional analytical functional forms can reproduce quantum mechanical fitting targets (Question 2), the viability of traditional potentials for phonons (Question 3) and the viability of long-range interactions of phonons (Question 4). While many optimization methods fall under the category of metaheuristics, a powerful class of metaheuristic methods in artificial intelligence belong to evolutionary optimization [138].

Evolutionary optimization refers to a class of bio-inspired algorithms that mimic Darwin's theory of natural selection [138,139]. These algorithms are best understood by considering the evolutionary phenomena from which they are derived. Populations of organisms may undergo biological or physical changes over many generations of reproduction, these changes result in characteristics that aid the organism in its

environment [139]. These changes arise in natural selection since only biologically fit individuals will survive to pass on their genes, thus modifying the gene pool an physical characteristics of organisms over many generations [139]. The evolutionary process can be thought of as a powerful optimization tool, and vocabulary used in biology aids in its understanding as an optimization method [138]; the *population* of *individuals* refers to a collection of all parameter sets, the parameter sets themselves are the *genes* of each individual, and the biological *fitness* is the objective function value. Populations of organisms (individuals), over generations of reproduction, can be thought of as optimizing their genes (i.e., a long parameter set of four base pairs for biological DNA [140]) to minimize or maximize some fitness metric, or objective function. By analogy, Giraffes for example, have minimized the distance between their heads and the trees from which they eat, thus resulting in relatively long necks compared to other animals [141]. In this case, giraffes with long necks possess genes (parameters) that minimize some objective function (the distance between their head and a tree). A more complex example, discovered by Darwin himself, involved the optimization of finch beak shapes in the Galapagos islands to better access their unique food sources on each island [139]. Evolutionary optimization algorithms are often incorporated to apply this process to non-biological problems in science and engineering [142]. Instead of minimizing the distance between a giraffe head and a tree, for example, this thesis aims to minimize the distance between endpoints of quantum mechanical force vectors and a potential calculated force vectors. This sort of generality is a main strength of evolutionary optimization and metaheuristics, since all they require is a metric to minimize without any regard to the mathematical form of the metric, unlike gradient-based optimization methods [142]. Accomplishing this task first involves representing sets of

parameters as artificial genes, so that operations can be performed on these genes that mimic the evolutionary process. The genetic algorithm is a commonly used tool to perform optimization operations on artificial genes, or genetic representations of parameters [143].

2.4.1 Genetic Algorithm

One powerful algorithm that mimics the evolutionary process is the genetic algorithm (GA), which performs operations on artificial genes to simulate the natural selection process [138]; these operations mimic the genetic process of mating and reproduction. Central to the GA, therefore, is the genetic representation of fitting parameters. Biological genes, or DNA, store information in four-valued base pairs, which offers the astounding variability seen in all life on Earth [140]. A simpler representation, commonly employed in GAs, involves using genes with two base pairs, namely zeros and ones (i.e., binary) [143]. Simple artificial genes can therefore be thought of as binary strings of data, from which genetic operations can be performed on. Understanding how fitting parameters are represented as binary strings, especially in the case of potentials, is paramount in showing how the GA can be applied to the potential optimization process. All the parameters in a potential need to be cast into some binary representation to perform bitwise genetic operations, and then the concatenation of these binary sequences represents a single individual of the population. Each parameter λ_i requires a minimum and maximum interval, $\lambda_{\min}$ and $\lambda_{\max}$ respectively, for which the GA will search in. The representation of a parameter value can be converted back and forth between binary and its decimal representation via Equation 15 [144]

$$\lambda = \frac{\lambda_{\max} - \lambda_{\min}}{2^L - 1} d + \lambda_{\min} \tag{15}$$

where L is the length of the binary string and d is the integer decimal value of the binary number. As a simple example, consider a parameter with a encoded by the binary string "1010" in which the intervals $\lambda_{\min} = 1.0$ and $\lambda_{\max} = 2.0$. To solve for the actual decimal value of the parameter, which would be input to the potential, note that the length $L = 4$ and the binary string has an integer value $d = 10$. Here, d is equivalent to 10 by taking the zeros and ones in the binary strings to be the coefficients of increasing powers of two, namely $10 = 0\times 2^0 + 1\times 2^1 + 0\times 2^2 + 1\times 2^3 = (0\times 1) + (1\times 2) + (0\times 4) + (1\times 8)$. Substituting these values into Equation 15 yields $\lambda = \frac{1}{15}10 + 1 = 5/3$, which is indeed a value between the minimum and maximum intervals $\lambda_{\min} = 1.0$ and $\lambda_{\max} = 2.0$. This process of encoding parameters as binary strings occurs for every fitting parameter in the potential. Considering the Morse potential of Equation 10, for example, the GA begins by randomizing a population of individuals with random parameter values and utilizing Equation 15 to convert the values to binary string representations.

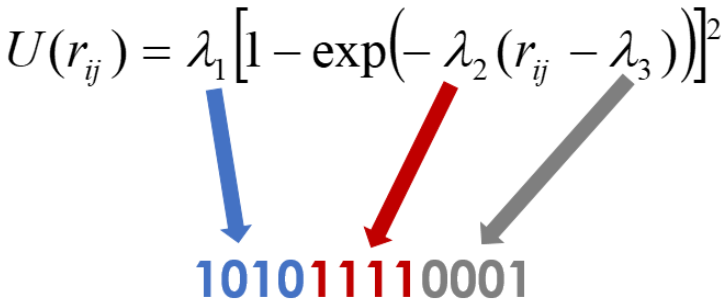

Figure 5 – Example representation of parameters into binary strings of length $L = 4$ for a Morse potential. The different colors represent different parameter representations, and the concatenated binary string represents a single individual in the population.

Figure 5 shows how each parameter in a potential is concatenated into a binary string, and the string represents the "genes" of the "individual", which is a specific set of values for the parameters. A single individual in the population therefore simply refers to a binary string, which encodes a full set of parameters. The GA initializes the optimization procedure by creating a random population of these binary strings, from which random fitting parameters are obtained. This artificial gene now makes it easier to perform GA operations on, to mimic the reproduction of this individual with other individuals.

In each iteration, or "generation", of the GA, a selection process ensues which eliminates individuals containing undesirable objective function values, which depends on their genes and the parameters encoded by genes. In the case of potential fitting, smaller objective function values are favored for minimizing the error between potential quantities and reference quantities. The bottom half of the population, containing the larger objective function values, are discarded. The top half, with smaller objective function values, will survive and form pairs for mating; their genetic material are combined to produce a parameter set that is some mixture of the two parents. This process is known as crossover [143], and involves randomly splicing the genes of two parents to mix their genes. The crossover process is illustrated in Figure 6, continuing from the Morse potential example with three parameters of length $L = 4$ strings.

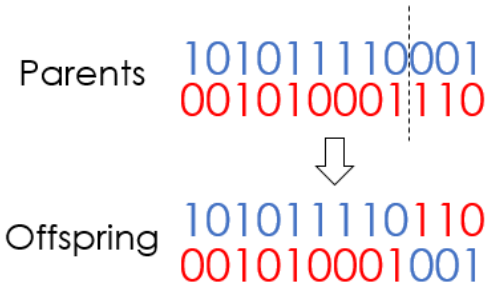

Figure 6 – Example crossover process. Two parents (blue and red strings) are randomly spliced at the dashed line. The genetic material on the right side of the splice are mixed and matched to form two new individuals, or offspring.

In Figure 6, the crossover point for the two parents (red and blue binary strings) occurs at the dashed line, and this point is chosen randomly. The first (blue) parent in Figure 6 is the same individual shown in the Morse potential example of Figure 5, with three fitting parameters represented as length $L = 4$ binary strings, for a total of 12 bits. The parent represented by the blue binary string in Figure 6 randomly pairs with the individual represented by the red binary string, whom will also contain the same genetic structure (i.e., binary string length and parameter interval values) for consistency. Cleaving the binary strings and mixing the ends results in the two children shown in Figure 6 which are now genetic combinations of the two parents. In this example, only the last parameter (last 4 binary digits) of the Morse potential are modified. In practice, however, this splicing occurs at random points for every individual, thus resulting in offspring that are random combinations of one of the two parents. The resulting children now contain mixture of genetic material, or parameter values, of their two parents. Crossover occurs for every parent pair in the population, thus replacing the unfit individuals discarded in the selection process with new children that are mixtures of fit parents. To add further diversity, the children randomly experience genetic mutations at random points in their genes. This is

represented in the GA by randomly flipping a binary digit in the children's binary strings from a "1" to a "0" and vice versa. After mutation the generation comes to an end and the process is repeated starting with selection again for another generation. This process repeats until some sort of convergence is reached; the average objective function value of the population can be used as a convergence criterion, or the objective function of the top individual may be used.

The crossover and mutation processes in the GA are paramount to the success of the GA in both exploiting minima and exploring the search space, respectively [145]. Since crossover involves mixing solutions of fit individuals, and these individuals may reside in similar regions of the search space after many generations, crossover aids in exploiting local minima [145]. Mutation, on the other hand, offers an opportunity for the offspring of two parents to jump out of local minima into a better (lower) minima. Exploration of the search space is therefore thoroughly achieved via the mutation process, thus heavily aiding in global optimization [145]. Mutation probability is defined by some user-defined probability, or mutation rate. A lower mutation rate results primarily in crossover operations, thus resulting in better local optimization or exploitation. A higher mutation rate, on the other hand, results in more population diversity, thus resulting in better global optimization (or exploration). Too high of a mutation rate (e.g., near 100%) renders the GA no better than a random search, and small mutation rates (< 50%) are used in practice [145].

Algorithmically, the GA is summarized as follows:

1) **Initialization – form a population of N individuals.** Individuals represent a complete set of parameters that can be used to evaluate the potential. However, in a GA they are not represented as real numbers, but instead in binary format, which facilitates subsequent manipulation according to the evolutionary process. Individuals (e.g., parameter sets) are represented as binary strings, which are termed the genotypes and are initialized as random binary strings (random zeros and ones). Each genotype is a concatenation of P "substrings" of length L, and each substring represents one of the P parameters being optimized.
2) **Gene expression – decode the genotypes into phenotypes.** Phenotypes are the actual observable representation of genotypes in genetics. In this case, the phenotypes are a set of real numbers which are the actual parameters being fit. Each substring in the binary string (genotype) can be converted to a real number using Equation 15.
3) **Assess fitness – calculate the objective function for each individual.** Using the set of parameters (phenotype) from Step 2, we calculate the objective function $Z = Z(\lambda_1,...,\lambda_P)$ for each individual. This is where the potential is evaluated to calculate quantities that enter the objective function. This step can also be easily parallelized since the order of which individuals are evaluated does not matter if a list of objective function values is gathered at the end.
4) **Selection – choose the fittest individuals to be parents.** In the case of minimization, a low Z value represents a high fitness or a low error with respect to the *ab initio* results being fit to. The individuals are first sorted from lowest to highest in terms of their objective function value Z and then a process known at

elitism is performed in which a user-defined percentage of the best individuals are chosen to be parents, with 100% chance of surviving until the next generation. The rest of the population is chosen at random until the parent population is composed of N/2 individuals, where N is the total population size.

5) **Crossover – allows parents to mate.** Crossover involves the combination of solutions. This is accomplished by randomly selecting two parents and splicing their binary strings (genotypes) at a random point, and then mixing the end pieces. The resulting combinations are termed children and join the parents in the new population of the next generation. Crossover ensures exploitation of the search space, meaning that crossover aids more in local minimization than global minimization. This is because after many generations, all individuals possess similar genotypes since the population converges to a set of genes. Mixing these similar solutions results in better exploitation of whatever local minima the GA is converging to.
6) **Mutation – randomly change the genotype of the children.** Mutation is accomplished by choosing a random binary digit in the genotype of the children and flipping its value (i.e., a "1" becomes a "0" and vice versa). This process happens for every child solution with a user-defined probability known as the mutation rate, below 50% in practice [146]. Mutation ensures exploration of the search space, thus aiding more so in the task of global minimization as opposed to local minimization. This is because randomly perturbing the solutions helps the algorithm step far away from local minima. If the mutation rate is too high, the GA

becomes no better than a random search and will be more difficult to converge to a single solution.

7) **Evolve.** The algorithm returns to Step 2 and repeats until a user-defined number of generations have elapsed.

The algorithm listed by Steps 1 – 7 is the GA used in this thesis to parameterize potentials. It is important to realize that the GA process generally applies to any objective function regardless of the unique potentials being parameterized or fitting quantities being fit to. This will aid in the answering of Question 1, since it allows for a variety of fitting quantities to be tested (i.e., changing the objective function), without spending time changing the underlying optimization algorithm. The GA process described in this section applies the same operations and rules to any parameter of any fitting problem, and therefore requires no extra coding when changing the objective function. This is especially useful when attempting to answer Question 1 regarding which quantities to fit the potential to, since no modifications to the fitting algorithm arise when testing new fitting quantities as the GA requires no knowledge of the form of the objective function, only its value. This provides a powerful tool needed to answer the proposed questions and test the hypotheses, since different fitting quantities can easily be added and experimented with. Specifically, this means that the objective function $Z(\boldsymbol{\lambda})$ of Equation 14 could contain any fitting quantity without changing the underlying GA used to accomplish the minimization.

Traditional fitting quantities include experimental values that are calculable with analytical potentials, such as lattice parameters, bulk moduli and elastic constants [58,66,112,121]. For phonons, some notable authors, such as Powell, fit directly to experimental phonon frequencies at a few points in a Brillouin zone [80]. Fitting to experimental quantities

is not general, however, since calculation of phonon dispersions and elastic constants must be modified for different crystal structures. The availability of such experimental quantities is also another limitation, along with the time to obtain them. Pseudopotentials that can be used in DFT calculations, however, exist for the majority of elements in the periodic table [147] and DFT has been shown to calculate interatomic interactions and forces so accurately that the vibrational and phonon frequencies resulting from these forces agree almost exactly with experimental values. This agreement is quite consistent across many different classes of materials and thus the approach of using DFT as a reference for potential optimization is ideal and it also enables predictive power [34 109]. [109,148 149].

2.5 Density Functional Theory (DFT)

DFT is a computational quantum mechanical method that solves for the electronic structure of a group of atoms. The system potential energy and forces are dictated by the electronic structure, and the electronic structure is dictated by the positions of ions [150]. The electronic structure, namely the electron density as a function of ionic positions, determines the ground-state energy of electrons associated with a group of atoms, along with the forces on ions [150-152]. DFT codes such as Vienna Ab-initio Simulation Package (VASP)[153] and Quantum Espresso[154] solve for this electronic structure, or density, from which system potential energy and forces are obtained. Revolutionary work by Hohenberg and Kohn in the 1960s, which lead to their winning the Nobel Prize in Chemistry in 1998 showed that the ground-state energy is a unique functional of the electron density, and that the density which minimizes the ground-state energy is the true electron density [152]. This ground-state electron density uniquely determines all properties, such as energies and forces [109]. The

electron density is therefore the key variable in DFT calculations, and is calculated from the individual pseudo electron wavefunctions ψ_i via [155]

$$n(\mathbf{r}) = \sum_i \psi_i^*(\mathbf{r}) \cdot \psi_i(\mathbf{r}) \tag{16}$$

where the summation runs over all electrons and both spins of each electron [156]. A DFT calculation begins by initializing a random electron density $n(\mathbf{r})$ in terms of randomly initialized wave-functions ψ_i. To calculate the electron ground-state energy for minimization, which according to Hohenberg and Kohn is a functional $E[n(\mathbf{r})]$ of the electron density, we must incorporate the Schrödinger equation.

The Schrödinger equation can describe time-dependent electron dynamics in the absence of any time-independent assumptions [157]. However, their ground-state energy is practically time-independent since their mass is three to four orders of magnitude lower than the ions, and therefore the ions move much slower than the electrons [158]. For this reason, the time dependent nature of the pseudo wave functions is usually neglected and time-independent Schrödinger equation is given by

$$\left[-\frac{\hbar^2}{2m} \sum_{i=1}^{N_e} \nabla_i^2 + \sum_{i=1}^{N_e} U(\mathbf{r}_i) + \sum_{i=1}^{N_e} \sum_{j<i} U(\mathbf{r}_i, \mathbf{r}_j) \right] \psi = E\psi \tag{17}$$

where the bracketed term on the left includes all contributions to the Hamiltonian, ψ is a set of solutions or eigenstates of the Hamiltonian and E is the ground-state energy of the system that we wish to solve for. The electron mass is given by m, $\hbar$ is the reduced

Planck's constant, and N_e is the number of electrons in the system. The three terms in the bracketed Hamiltonian of Equation 17 define the summed kinetic energy of all electrons i, the summed interaction energy between each electron and the field of nuclei, and the pairwise sum of interaction energies between all pairs of electrons i and j. Equation 17 is an example of a many-body Schrodinger equation, for which analytical solutions are sparse [159]. Kohn and Sham, however, in the 1960s, showed that the many-electron Schrodinger equation can be simplified by solving a set of single-electron Schrodinger equations [160]. The Kohn-Sham equations have the form

$$\left[-\frac{\hbar^2}{2m}\nabla^2 + U_C(\mathbf{r}) + U_H(\mathbf{r}) + U_{XC}(\mathbf{r})\right]\psi_i(\mathbf{r}) = \varepsilon_i\psi_i(\mathbf{r}) \tag{18}$$

which are like the full Schrodinger equation in Equation 17, except lack the summation over all electrons. The bracketed terms on the left-hand side are the electron kinetic energy, the Coulomb interaction $U_C(\mathbf{r})$ between the electron and collection of atomic nuclei, the Hartree potential $U_H(\mathbf{r})$ describing electron repulsion with the single electron and the total electron density, and the exchange-correlation potential $U_{XC}(\mathbf{r})$ which includes all effects that are not described by the other potentials. The Coulomb interaction $U_C(\mathbf{r})$ between the single electron and all nuclei is a known term that does not depend on the electron density [161]. The Hartree potential is readily calculated from a volume integral of the electron density via [155]

$$U_H(\mathbf{r}) = e^2 \int \frac{n(\mathbf{r}')}{|\mathbf{r}-\mathbf{r}'|} d^3\mathbf{r}' \tag{19}$$

where e is the electron charge. The exchange-correlation potential is formally defined as a functional derivative of the exchange-correlation energy with respect to the electron density as [155]

$$U_{XC}(\mathbf{r}) = \frac{\partial E_{XC}(\mathbf{r})}{\partial n(\mathbf{r})} \tag{20}$$

where $E_{XC}(\mathbf{r})$ is the exchange-correlation energy, often called the exchange-correlation functional. Electronic exchange and correlation are quantum mechanical phenomena referring to the effect that is associated with the Pauli exclusion principle, and the lack of self-interaction between an electron and its own charge density, respectively [162]. While the true form of the exchange-correlation functional is not known, it can be determined for the idealized case of a homogenous electron gas possesses constant electron density at all points in space [163,164]. The exchange-correlation potential $U_{XC}(\mathbf{r})$ in this case is therefore the known exchange-correlation potential for a uniform electron gas at the electron position. This approximation uses only the local electron density to define $U_{XC}(\mathbf{r})$, and is therefore referred to as the local density approximation (LDA) [163]. Although seemingly simple due to the homogenous electron gas assumption, the LDA functional is useful for systems with slowly varying electron densities such as metals [165]. Covalently bonded solids, where phonon transport is dominant and are therefore of primary interest in this thesis, however, contain more complex variations in charge density [166]. To describe more

complex charge densities, an approach utilizing both the local electron density and the local gradient of the electron density was formulated, known as the generalized gradient approximation (GGA) [167]. The GGA class of exchange-correlation functionals has seen more success than the LDA in describing properties with covalently bonded solids [168-170]. More modern functionals based on the GGA approach include the Perdew-Wang (PW91) [171] and Perdew-Burke-Ernzerhof (PBE) [172] functionals. Many researchers have applied these functionals successfully to describe vibrational properties of covalent solids with excellent experimental agreement [33,34,76,116,173].

Since there are many exchange-correlation functionals, it is up to the user to determine which one is best for a system under consideration. Regardless, once it is chosen, the exchange-correlation potential for a single electron can be solved via Equation 20, which is required to solve the Kohn-Sham equations of Equation 18. The single-electron wave functions of the Kohn-Sham equations are also known from the charge density, along with the Hartree potential in Equation 19. Solving the Kohn-Sham equations for every electron yields a new set of single-electron pseudo wave functions, from which a new electron density $n_{KS}(\mathbf{r})$ defined by the Kohn-Sham equations can be calculated. If the original electron density $n(\mathbf{r})$ is the same as the Kohn-Sham electron density, then this is the true electron density since $E[n(\mathbf{r})] = E[n_{KS}(\mathbf{r})]$; the ground-state energy functional is the ground-state energy corresponding to the Schrodinger equation in this case. If the two original and Kohn-Sham electron densities are not the same, or nearly the same, the trial electron density $n(\mathbf{r})$ is updated and the entire process repeats. A variety of density update techniques exist in many software packages [174]. This self-consistent loop, rooted in the

Schrödinger equation, is a powerful method for finding the ground-state electron density. A summary of the DFT process to find the ground-state electron density is as follows:

1) Define an initial electron density $n(\mathbf{r})$.
2) Calculate the Hartree potential and exchange-correlation potential using $n(\mathbf{r})$, via Equations 19 and 20.
3) Solve the Kohn-Sham equations for every electron in the system, Equation 18, using the calculated Hartree and exchange-correlation potentials to solve for the new single-electron wave functions.
4) Calculate the new electron density resulting from the Kohn-Sham equations, $n_{KS}(\mathbf{r}) = \sum_i \psi_i^*(\mathbf{r})\psi_i(\mathbf{r})$.
5) Compare $n_{KS}(\mathbf{r})$ and $n(\mathbf{r})$. If they are the same, then the ground-state electron density is reached, and this electron density can be used to calculate the total energy via the Hartree potential and single electron-wave functions. Otherwise, update the electron density and repeat from Step 2.

Once the electron density is found, various quantities relevant for potential fitting such as energies and forces are obtained [175].

The Hellman-Feynman theorem allows the calculation of forces on ions due to the electron density [151]. These forces are often used to calculate bulk phonon frequencies in crystals [116]. This process revolves around using DFT to numerically approximate the derivative of the total energy with respect to displacement. The 2nd order force constants, or 1st derivatives of force with respect to atomic positions, are also useful quantities, as

they form the elements of the Hessian matrix for all atoms. The Hessian is used by the dynamical matrix to calculate phonon frequencies in the Brillouin zone, since it represents the stiffness of interaction between every pair of atoms. Since the phonon dispersions calculated for a wide variety of crystals using this method agree almost exactly with experimental phonon dispersions, and the forces are the only inputs, it is well accepted that DFT forces are close to the true forces on atoms [33,116]. For this reason, fitting to DFT forces is sufficient to obtain POPs, according to Hypothesis 1. At this point, however, it may seem futile to parameterize analytical potentials to match DFT quantities since DFT yields accurate forces.

The entire DFT process possesses cubic computational scaling with the number of electrons in the system N_e, represented in Big O notation as $O(N_e^3)$. This cubic scaling arises since solving the Kohn-Sham equations for every electron in the system involves diagonalizing the total Hamiltonian to obtain every electron eigenstate, and matrix diagonalization scales cubically with the number of matrix elements [176]. Classical MD based on analytical potentials, however, possesses linear scaling $O(N)$ with the number of atoms N in the system [92]. This can be realized from the decomposition of total potential energy into per-atom contributions in analytical potentials, seen in Equation 6. As more atoms are added to the system, the total potential energy required for force calculation simply requires an extra per-atom energy contribution to calculate, hence linear scaling. Fitting computationally cheap models (i.e., analytical potentials) to DFT therefore allows us to scale up computationally; DFT accuracy could then be used to study larger systems for longer times using classical MD simulations based on analytical potentials. Creating analytical potentials that reproduce DFT data therefore bridges an important gap in

multiscale modelling, between quantum and classical methods. This is further illustrated in Figure 7.

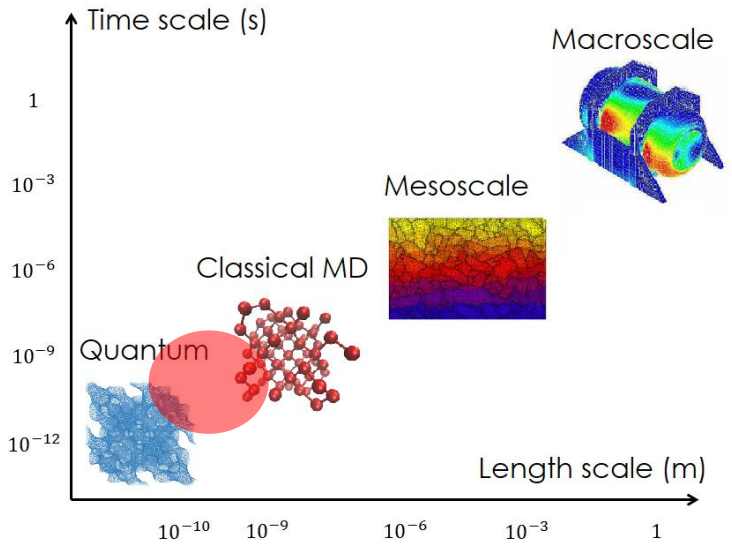

Figure 7 – Material modelling methods as a function of length and time scales which they are applicable to. The red circle shows the connection established by obtaining analytical potentials that reproduce DFT data, thus bridging the gap between quantum and classical methods.

As shown in Figure 7, quantum mechanical modeling methods such as DFT are applicable in the regime of femtoseconds and angstroms. Classical MD based on analytical potentials are computationally tractable in the nano regime, with modern computers handling up to 320 billion atoms [177]. Mesoscopic and macroscopic finite element methods cover the micro regime and above. The red circle in Figure 7 shows the gap that is bridged by fitting analytical potentials to DFT data; this connects quantum and classical methods in multiscale modeling. Bridging this gap allows us to study systems in the nano regime by taking advantage of the linear scaling of classical MD simulations, with the accuracy of DFT; this would otherwise not be possible or tractable on modern computing hardware. To specifically perform this task for phonons, and create POPs, it is necessary to consider the

lattice dynamics (LD) theory which describe phonons. This will show how phonon properties are calculated using modern computational techniques, and provide insight into which quantities give rise to phonon properties.

CHAPTER 3. PREDICTING PHONON PROPERTIES

BTE based calculations rely on LD calculations of phonon frequencies and dispersion as well as 3rd order and higher force constants to evaluate anharmonic phonon quantities. This chapter formally introduces these approaches so that their integration into the POPs tool can be justified and clarified.

3.1 Lattice Dynamics

Deeper insights into the true nature of the shape of the PES can be obtained via derivatives of the PES with respect to Cartesian atomic positions. These derivatives are called the interatomic force constants (IFCs). A mathematical definition of the IFCs can be obtained by assuming the PES of a crystal can be written as a Taylor expansion about the equilibrium Cartesian positions of atoms, which we term herein a Taylor expansion potential (TEP), given by [173]

$$U = U_0 + \sum_{i,\alpha} \Pi_i^{\alpha} u_i^{\alpha} + \frac{1}{2!} \sum_{ij,\alpha\beta} \Phi_{ij}^{\alpha\beta} u_i^{\alpha} u_j^{\beta} + \frac{1}{3!} \sum_{ijk,\alpha\beta\gamma} \Psi_{ijk}^{\alpha\beta\gamma} u_i^{\alpha} u_j^{\beta} u_k^{\gamma} + \ldots \quad (21)$$

where Π_i^{α}, $\Phi_{ij}^{\alpha\beta}$, and $\Psi_{ijk}^{\alpha\beta}$ are the IFCs of 1st, 2nd and 3rd order, and u_i^{α} is the displacement of atom i in the α direction. The constant U_0 energy does not provide any information on the shape of the PES so it can be ignored, since it has no effect on the dynamics. The first derivative term becomes zero, by definition, when all atoms are exactly located at their equilibrium sites, thus the TEP can be written as[173]

$$U = \frac{1}{2!}\sum_{ij,\alpha\beta}\Phi_{ij}^{\alpha\beta}u_i^{\alpha}u_j^{\beta} + \frac{1}{3!}\sum_{ijk,\alpha\beta\gamma}\Psi_{ijk}^{\alpha\beta\gamma}u_i^{\alpha}u_j^{\beta}u_k^{\gamma} + \ldots \tag{22}$$

The mathematical definition of the displacement is given by

$$u_i^{\alpha} = \alpha_i - \alpha_i^0 \tag{23}$$

where α_i^0 is the equilibrium Cartesian coordinate α of atom i and α_i is the current coordinate. The indices i, j, and k in the TEP of Equation 22 run over all atoms in the system under consideration, and the superscripts α, β, and γ denote general Cartesian directions. The 2-body term, for example, includes a sum over all pairs of atoms i and j, and all 2nd order IFCs $\Phi_{ij}^{\alpha\beta}$ between each ij pair. Since there are three possible Cartesian coordinates in the two terms denoted by the superscript $\alpha\beta$, there are nine possible IFC values for each ij pair. These nine IFC values can be represented as a 3×3 matrix for each 2-body interaction:

$$\Phi_{ij}^{\alpha\beta} = \begin{bmatrix} \Phi_{ij}^{xx} & \Phi_{ij}^{xy} & \Phi_{ij}^{xz} \\ \Phi_{ij}^{yx} & \Phi_{ij}^{yy} & \Phi_{ij}^{yz} \\ \Phi_{ij}^{zx} & \Phi_{ij}^{zy} & \Phi_{ij}^{zz} \end{bmatrix} \tag{24}$$

There are therefore nine 2nd order IFCs, or 2nd derivatives of the potential energy with respect to displacement, for each 2-body interaction. By a similar logic there are 27 definable 3rd order IFCs $\Psi_{ijk}^{\alpha\beta\gamma}$, or 3rd derivatives of the potential with respect to displacement, for every triplet ijk. For a given N-body interaction, there are 3^N IFCs,

representing the spatial derivatives of the potential energy in all combinations of Cartesian directions.

To model phonon properties using the IFCs, the IFCs must first be calculated and there are two main methods used, namely: (1) the direct displacement method (DDM) and (2) density functional perturbation theory (DFPT). The DDM simply fits the TEP of Equation 22 to force-displacement data obtained from DFT calculations [116]. The number of IFCs in a unit cell is equal to $3N \times 3N$, but the fitting problem and number of parameters can be simplified by assuming certain symmetry operations for the IFCs in a crystal. One of these symmetries, for example, assumes the diagonal terms of the IFC matrix are identical, and ij pairs are commutable [116], which must be true by Newton's third law. This is represented by

$$\Phi_{ij}^{\alpha\beta} = \Phi_{ji}^{\beta\alpha} \tag{25}$$

thus simplifying the 9-element 2nd order IFC matrix to six unique elements. A similar relation holds for 3rd order IFCs [33,116]. Density functional perturbation theory (DFPT) perturbs the wave functions in DFT to varying orders to calculate IFCs of varying orders [149]. Due to the relative ease of fitting a TEP to force-displacement data compared to perturbing the wave functions, the DDM is used in this thesis to obtain force constants instead of DFPT.

The fitting procedure to obtain the IFCs in Equation 22 involves using the TEP to perform the minimization problem of Equation 13 in Chapter 2. The target quantities in the objective function are forces. With known displacements u_i^{α} and the corresponding forces

on all atoms, the IFCs can be readily obtained by fitting the TEP to reproduce these quantities [116]. The TEP forces are given by the negative gradient of the potential in Equation 22 with respect to position, thus yielding

$$F_i^{\alpha} = -\sum_{j,\beta} \Phi_{ij}^{\alpha\beta} u_j^{\beta} - \sum_{jk,\beta\gamma} \Psi_{ijk}^{\alpha\beta\gamma} u_j^{\beta} u_k^{\gamma} \qquad \ldots \tag{26}$$

A least squares local minimization algorithm can then be used since this is a convex problem if the crystal displacements are small enough, whereby one approaches the harmonic limit in which the PES possesses a shape that can be well resolved with the TEP [116]. Once the IFCs are obtained, various LD theories allow for the calculation of phonon properties.

The simplest quantities calculable with LD take the limiting case, termed the harmonic limit, whereby we truncate the Taylor expansion in Equation 22 to include only harmonic terms. Useful representations of harmonic phonon behaviour include phonon dispersion and phonon density of states. The group velocity and frequency of each mode are required to calculate these quantities, so their calculation will be discussed first. Phonon frequencies are eigenvalues of the dynamical matrix, whose components depend on the 2nd order IFCs via [26]

$$D_{ij}^{\alpha\beta} = \frac{1}{\sqrt{m_i m_j}} \sum_{l} \Phi_{ij}^{\alpha\beta} e^{i\mathbf{q}_l \cdot \mathbf{R}_l} \tag{27}$$

Where m_i is the mass of atom i, $\mathbf{R}_l$ is the position of primitive cell l, and $\mathbf{q}_l$ is the primitive cell position in reciprocal space. Diagonalizing the dynamical matrix yields the

3N eigenvalues and corresponding eigenvectors $\mathbf{e}_{\mathbf{q}s}$ for each $\mathbf{q}$ point in reciprocal space and atomic polarization s. The eigenvalues $\omega_{\mathbf{q}s}$ of the dynamical matrix $\mathbf{D}$ are given by [26]

$$\omega_{qs}^2 = \left(\mathbf{e}_{qs}^*\right)^T \mathbf{D}\mathbf{e}_{qs} \tag{28}$$

which are the frequencies of phonon mode $\mathbf{q}s$. Diagonalizing the dynamical matrix for each $\mathbf{q}$ point in reciprocal space allows for the construction of a $\omega(\mathbf{q})$ plot, representing frequency as a function of directions in the Brillouin zone, which is termed the phonon dispersion. The group velocity, another harmonic quantity, is given by the slope of the phonon dispersion curves by:

$$\mathbf{v}_{\mathbf{q}s} = \frac{\partial \omega_{\mathbf{q}s}}{\partial \mathbf{q}} \tag{29}$$

This derivative is calculated numerically in this thesis using the Alamode program [116]. Harmonic properties (i.e., frequencies and group velocities) describe individual vibrational modes and how they behave [35]. Phonon transport properties such as thermal conductivity, however, arise due to anharmonic effects associated with larger displacements and higher order interactions in the TEP.

Anharmonic LD relieves the truncation of the TEP associated with the harmonic approximation. The 3rd order IFCs $\Psi_{ijk}^{\alpha\beta\gamma}$ are obtained using the DDM in the same way as the 2nd order IFCs, by simply fitting the TEP to DFT force-displacement data. One of the

key quantities required to calculate anharmonic phonon transport properties is the phonon lifetime, or relaxation time $\tau_{\mathbf{q}s}$ of mode $\mathbf{q}s$. The relaxation time can be estimated as [116]

$$\tau_{\mathbf{q}s}^{-1}(T) \approx 2\Gamma_{\mathbf{q}s}^{anh}(T, \Psi_{ijk}^{\alpha\beta\gamma}) \tag{30}$$

where $\Gamma_{\mathbf{q}s}^{anh}(T, \Psi_{ijk}^{\alpha\beta\gamma})$ is the imaginary part of the phonon anharmonic self-energy as a function of temperature and third order IFCs in Equation 22. The Alamode program [116] is used in this thesis to calculate $\Gamma_{\mathbf{q}s}^{anh}(T, \Psi_{ijk}^{\alpha\beta\gamma})$ via Fermi's golden rule, and the tetrahedron method in reciprocal space aids in its calculation [179]. Calculation of the relaxation time in Equation 30 is crucial in PGM based thermal conductivity expressions, which require the mean free path $\Lambda_{\mathbf{q}s}^{\alpha} = v_{\mathbf{q}s}^{\alpha}\tau_{\mathbf{q}s}$.

Although DFT can be used to calculate harmonic and anharmonic phonon properties by obtaining the IFCs from quantum mechanical force-displacement data, the same force-displacement data can come from an analytical interatomic potential as well. Understanding how harmonic and anharmonic phonon properties arise from underlying quantities such as forces, namely the IFCs or derivatives of the forces, further supports Hypothesis 1 that optimizing an analytical potential against DFT forces should produce a potential that yields accurate phonon quantities such as frequencies, eigenvectors (modes) and relaxation times.

3.2 Phonon Thermal Conductivity

3.2.1 Boltzmann Transport Equation

The BTE can be applied to study the properties of a system of interacting particles, and if one invokes the PGM for phonons, the BTE can subsequently be used to calculate thermal conductivity. As mentioned in Chapter 1, this approach of treating phonons as boson particles yields accurate results for crystals, and thus it is used in this thesis for prediction of crystal thermal conductivity. The general BTE is derived from the Louville equation, and can be written for each phonon mode $\mathbf{q}s$ as [28]

$$\frac{\partial f_{\mathbf{q}s}}{\partial t} + \mathbf{v}_{\mathbf{q}s} \cdot \frac{\partial f_{\mathbf{q}s}}{\partial \mathbf{r}} + \mathbf{a}_{\mathbf{q}s} \cdot \frac{\partial f_{\mathbf{q}s}}{\partial \mathbf{v}_{\mathbf{q}s}} = \left[\frac{\partial f_{\mathbf{q}s}}{\partial t}\right]_{coll} \tag{31}$$

where $f_{\mathbf{q}s}$ is the Bose-Einstein distribution of phonon mode $\mathbf{q}s$, $\mathbf{v}_{\mathbf{q}s}$ is the phonon group velocity, $\mathbf{a}_{\mathbf{q}s}$ is the particle acceleration and $\left[\frac{\partial f_{\mathbf{q}s}}{\partial t}\right]_{coll}$ is the collision term, that describes how the phonons interact and scatter with each other. Solving the BTE is greatly simplified by introducing the relaxation time approximation (RTA), where the collision term is replaced by[28]

$$\left[\frac{\partial f_{\mathbf{q}s}}{\partial t}\right]_{coll} = \frac{f_{\mathbf{q}s}^{0} - f_{\mathbf{q}s}}{\tau_{\mathbf{q}s}} \tag{32}$$

where f_0 is the equilibrium distribution and the relaxation time $\tau_{\mathbf{q}s}$ can be assumed to be independent of group velocity in the RTA [28]. It is important to note that this is the same relaxation time that can be calculated from the 3rd order IFCs via Equation 30. Rewriting the BTE under the RTA and neglecting acceleration gives

$$\frac{\partial f_{\mathbf{q}s}}{\partial t} + \mathbf{v}_{\mathbf{q}s} \cdot \frac{\partial f_{\mathbf{q}s}}{\partial \mathbf{r}} = -\frac{f_{\mathbf{q}s} - f_{\mathbf{q}s}^{0}}{\tau_{\mathbf{q}s}} \tag{33}$$

where $f_{\mathbf{q}s} - f_{\mathbf{q}s}^{0}$ represents the perturbed phonon distribution from the equilibrium distribution. Assuming a steady-state distribution, we have $\frac{\partial f_{\mathbf{q}s}}{\partial t} = 0$. The distribution function is assumed to vary spatially only, and can be written as $\frac{\partial f_{\mathbf{q}s}}{\partial \mathbf{r}} = \frac{\partial f_{\mathbf{q}s}}{\partial T}\nabla T$ utilizing the chain rule and spatial gradient of temperature. Designating the perturbed phonon distribution as $\hat{f}_{\mathbf{q}s} = f_{\mathbf{q}s} - f_{\mathbf{q}s}^{0}$, applying the steady-state assumption, and substituting the new spatial gradient of the distribution, the BTE can be written as

$$\mathbf{v}_{\mathbf{q}s} \cdot \frac{\partial f_{\mathbf{q}s}}{\partial T}\nabla T = -\frac{\hat{f}_{\mathbf{q}s}}{\tau_{\mathbf{q}s}} \tag{34}$$

The specific heat of a phonon mode $\mathbf{q}s$ is given by the Bose-Einstein specific heat $c_{\mathbf{q}s} = \hbar\omega_{\mathbf{q}s}\partial f_{\mathbf{q}s} / \partial T$, so we can incorporate this into Equation 34 and rearrange to give

$$-c_{\mathbf{q}s}\tau_{\mathbf{q}s}\left(\mathbf{v}_{\mathbf{q}s} \cdot \nabla T\right) = \hbar\omega_{\mathbf{q}s}\hat{f}_{\mathbf{q}s} \tag{35}$$

for each phonon. This relation holds true for all Cartesian directions specified by the group velocity vector and spatial gradient of temperature; for any general Cartesian direction β we therefore have

$$-c_{\mathbf{qs}}\tau_{\mathbf{qs}}v_{\mathbf{qs}}^{\beta}\frac{\partial T}{\partial \beta}=\hbar\omega_{\mathbf{qs}}\hat{f}_{\mathbf{qs}} \tag{36}$$

Since this relation is valid for every phonon mode $\mathbf{qs}$, it is also valid for the sum of all phonon modes in the system given by

$$-\frac{\partial T}{\partial \beta}\sum_{\mathbf{qs}}c_{\mathbf{qs}}\tau_{\mathbf{qs}}v_{\mathbf{qs}}^{\beta}=\sum_{\mathbf{qs}}\hbar\omega_{\mathbf{qs}}\hat{f}_{\mathbf{qs}} \tag{37}$$

Adding another group velocity in any Cartesian direction α on both sides of this relation, for every phonon mode, yields

$$-\frac{\partial T}{\partial \beta}\sum_{\mathbf{qs}}c_{\mathbf{qs}}\tau_{\mathbf{qs}}v_{\mathbf{qs}}^{\beta}v_{\mathbf{qs}}^{\alpha}=\sum_{\mathbf{qs}}\hbar\omega_{\mathbf{qs}}v_{\mathbf{qs}}^{\alpha}\hat{f}_{\mathbf{qs}} \tag{38}$$

The term on the right hand side is the heat flux Q^{α} in the α Cartesian direction, defined as [31,32,50]

$$Q^{\alpha}=\frac{1}{V}\sum_{\mathbf{qs}}\hbar\omega_{\mathbf{qs}}v_{\mathbf{qs}}^{\alpha}\hat{f}_{\mathbf{qs}} \tag{39}$$

and V is the crystal volume. Substituting Equation 38 into the heat flux, and solving for Q^{α} yields:

$$Q^{\alpha}=-\left(\frac{1}{V}\sum_{\mathbf{qs}}c_{\mathbf{qs}}\tau_{\mathbf{qs}}v_{\mathbf{qs}}^{\alpha}v_{\mathbf{qs}}^{\beta}\right)\frac{\partial T}{\partial \beta} \tag{40}$$

According to Fourier's law $Q^{\alpha} = -\kappa^{\alpha\beta} \frac{\partial T}{\partial \beta}$ for an anisotropic medium, this now defines the thermal conductivity tensor $\kappa^{\alpha\beta}$ as

$$\kappa^{\alpha\beta} = \frac{1}{V} \sum_{\mathbf{qs}} c_{\mathbf{qs}} v_{\mathbf{qs}}^{\alpha} v_{\mathbf{qs}}^{\beta} \tau_{\mathbf{qs}} \tag{41}$$

which is the same as the thermal conductivity obtained from the kinetic theory of gases in Chapter 1, Equation 2, noting that the mean free path $\Lambda_{\mathbf{qs}}^{\alpha} = v_{\mathbf{qs}}^{\alpha} \tau_{\mathbf{qs}}$ [30-32]. This expression will be used in this thesis to calculate crystal thermal conductivity. This BTE-RTA thermal conductivity result yields excellent agreement with experimental thermal conductivities for many semiconductors and insulator crystals [34]. More importantly, the BTE derivation in Equation 41 shows how fundamental phonon quantities (group velocities and relaxation times), which depend on changes in force with respect to atomic positions, dictate the thermal conductivity. According to GK theory, thermal conductivity also depends on forces via Hardy's flux operator [50]. Thermal conductivity via the GK approach utilizes the autocorrelation of the heat flux, calculated from equilibrium MD simulations.

3.2.2 Equilibrium Molecular Dynamics

Thermal conductivity calculations using MD simulations include equilibrium MD (EMD) and non-equilibrium (NEMD) simulation methods. EMD simulations involve sampling the phase space around the equilibrium structure of group of atoms under a NVE ensemble, and using the resulting dynamical quantities as a function of time to calculate the atomistic heat flux via Equation 4 and the GK thermal conductivity via Equation 5 [180]. This method has been shown to be equivalent to and yield the same results as the BTE

thermal conductivity, at least when applied to systems where the PGM is applicable (i.e., crystals) [56,181]. Some studies even found that the GK method is more accurate than the BTE approach [99]; this is especially true for high temperatures where anharmonic interactions are stronger, and MD naturally includes anharmonicity to full order, unlike the truncated TEP. This benefit of MD is fully realized when one considers the phase space of atoms that can be sampled in an MD simulation; when starting from random velocities on all atoms in a crystal, the phase space of all atom is explored in dynamics consistent with the ensemble. In the case of thermal conductivity calculation, the phase space dynamical properties of positions, velocities and forces are used to calculate the heat flux in Equation 4 which is then used with GK theory to get thermal conductivity. Phase space can be sampled in a MD simulation via time averaging or ensemble averaging [182]. Time averaging involves probing the phase space sequentially for a single trajectory until a representative average has been obtained. Ensemble averaging samples the phase space with independent trajectories, which can be interpreted as separate MD simulations starting from different initial velocities. Independent trajectories can be more quickly simulated in parallel, compared to a single long run used in time averaging. In other words, ensemble averaging can be up to 200 times faster than time averaging when utilizing parallel processing for different ensembles [182]. As a result, ensemble averaging with EMD simulations are used herein. Ensembles of EMD simulations provide the atomic trajectories and dynamical quantities required to calculate the heat flux, and then the thermal conductivity at the autocorrelation of the heat flux.

Like the BTE thermal conductivity based on the PGM, which depends on group velocities and relaxation times calculated from force derivatives, the GK thermal

conductivity also depends on forces. Atomic trajectories, namely the positions, velocities and forces, are direct inputs to Hardy's heat flux operator [50]. Since the forces determine the dynamics and trajectories of atoms in MD simulations, this further supports Hypothesis 1 that optimizing potentials against accurate quantum mechanical forces will yield a potential that accurately predicts phonon and thermal properties. Furthermore, fitting to many DFT forces for many configurations of atoms (i.e., many displacements) should allow the potential to capture the spatial derivatives of forces (IFCs), required by the LD formulations of phonon group velocity and relaxation time; these quantities are also direct inputs to the PGM thermal conductivity derived from the BTE. This hypothesis is therefore supported by all the theories covered in this chapter. While the two main methods of calculating phonon thermal conductivity, the BTE and GK method using EMD simulations, provide theoretical support for Hypothesis 1, this still needs to be investigated by fitting analytical potentials to DFT forces.

CHAPTER 4. CREATING PHONON OPTIMIZED POTENTIALS

Phonon properties and thermal conductivity depend mainly on the interatomic forces, and how those forces change with respect to displacement, as seen Chapter 3; this further supports Hypothesis 1. Although supported in theory, this hypothesis still needs to be tested. In the process, Question 2 of how well can quantum mechanical quantities such as forces be reproduced by an analytical potential will be investigated as well. Hypothesis 3, that idea many different parameter sets can describe phonons well via traditional potentials, will be investigated by using the GA to perform more complete assessments of the parameter search space. Prior to these investigations, the underlying methodology and goals associated with the POPs tool are worthwhile to highlight – i.e., the basic tenets that underpin it. Many of these tenets are based on the proposed questions and hypotheses, and they also describe the philosophy behind the POPs approach [57].

4.1 The POPs Tenets

Based on the original hypotheses, these Tenets pose a hypothesized recipe for the creation of POPs, along with the underlying methods to create them.

Tenet 1: It is believed that many traditional analytical potentials, especially for semiconductors, are overdesigned for the study of phonons by possessing features and flexibility that aid in studying regions of phase space beyond thermal vibrations around equilibrium. This is the main idea behind Hypotheses 2, 3 and 4. Given this assumed overdesign, a core part of the POPs philosophy is to treat the fitting parameters are purely mathematical objects that are devoid of any physical meaning whatsoever. From this first

Tenet, we can justify usage of the GA to randomly sample the large parameter search space and find many unique parameter sets.

Tenet 2: For an analytical potential to be optimized for describing phonons, the key quantities that must be well described are the forces and their spatial derivatives. Hypothesis 1 stated that fitting the potential only to forces should accomplish this task, and therefore result in accurate thermal properties, since fitting to the forces in many configurations (atomic displacements) should provide information about the derivatives of these forces with respect to displacement. The formalism presented in Chapter 2 shows that the velocities and relaxation times for the crystalline thermal conductivity based on the BTE requires accurate 2nd and 3rd order IFCs, or spatial derivatives of force. Therefore, an analytical potential that reproduces these derivatives will accurately predict phonon and thermal properties based on this formalism. Although, in concept one would need an infinite number of derivatives to be exact, we note that in practice only the first three or four derivatives of energy ($\frac{dE}{d\mathbf{R}_i}$, $\frac{d^2E}{d\mathbf{R}_i d\mathbf{R}_j}$, $\frac{d^3E}{d\mathbf{R}_i d\mathbf{R}_j d\mathbf{R}_k}$) are actually needed for most systems/temperatures, but higher order terms can be included as deemed necessary [183]. Here, it is also important to clarify that the goal of POPs is to make potentials that replicate the results of quantum DFT calculations and not necessarily experiments. In this sense the goal is to make POPs based purely on first principles data, thereby enabling them with predictive power.

Tenet 3: Assuming the basis of Tenet 2 is correct, one can use a form of error between target quantities and potential quantities to assess the viability of a POP. This then can provide a universal scale upon which any potential can be assessed. It may happen, for

example, that a certain potential exceeds 20% error in forces and therefore may not be suitable for the study of phonons in a system of interest. A goal of the POPs methodology is to provide a way to assess the suitability of a given parameter set for any functional form without having to perform any expensive thermal conductivity calculations. By performing an exhaustive search via the GA, this should elucidate the viability of a specific functional form to reproduce thermal properties. It is therefore a goal of this methodology to enable assessment of the suitability of the functional form itself, without spending unnecessary amounts of time with expensive thermal conductivity calculations for every potential under consideration. It should be noted that this is a powerful attribute of the approach as it seeks for example to be able to state that a given function form, such as Tersoff's potential, is incapable of reproducing the DFT forces in a certain system to with, say 40%. By conducting a sufficiently exhaustive search, such a statement allows one to rule out an entire functional form altogether, rather than always leaving room for future modification of parameters to improve its description. In this way, this approach seeks to identify the fundamental limitations of a functional form.

Tenet 4: A major goal of the POPs approach is to easily create potentials for any system in an easy and quick fashion. The term "easy" here implies minimal user input, and that the procedure is capable of handling most of the effort. It is highly desirable to have the approach be built in such a way that it does not require excessive coding by the user. This therefore allows less time to be spent debugging the optimization process, and more time to be spent on the creation of POPs to study the physics of phonons. It is therefore highly desirable to have the approach be built in such a way that there are no difficult deterrents (long optimization times or excessive coding).

These tenets highlight the goals in this work to create POPs, along with the hypotheses involved in performing such a task. Furthermore, according to Tenet 4, a goal of the POPs method is convenience. This tool, the POPS optimization program, was therefore developed to bring ease and simplicity to the potential optimization process. Along with aiding in the investigation of the questions and satisfying the POPs Tenets, the value of such a program is well-known in the MD community where no current tools exist [123].

4.2 POPS Optimization Program

The issue of generality (Issue 1) is important since it allows for the convenient testing of a wide variety of potentials, across a wide variety of fitting quantities. It is therefore of interest to link the POPS optimization program with some sort of existing library of potentials, along with a calculator that computes quantities associated with these potentials for fitting. An excellent and renowned choice is the Large-scale Atomistic/Molecular Massively Parallel Simulator (LAMMPS), developed at Sandia National Labs [92]. LAMMPS contains a library of interatomic potentials that are easily invoked by simple user commands, along with parameter settings for such potentials. Furthermore, various quantities associated with the potential (e.g., forces and energies) can readily be computed via the LAMMPS compute class. The object-oriented C++ structure of the LAMMPS code allows for the intuitive extension of LAMMPS to add user-defined potentials and quantities to compute. The great number of potentials and calculable quantities, combined with the convenient extendibility, renders LAMMPS as an excellent choice to interface with the POPS program so that these quantities can be invoked to satisfy Issue 1.

In the spirit of the object-oriented nature of LAMMPS, offering convenient extendibility in the form of C++ classes, the POPS program will also contain an object-oriented framework with modules that aid in the addition of new settings. A user-interface module, for example, will aid in Issue 3 by providing a convenient way to change settings and experiment with different fitting procedures without wasting as much time coding such features. Code organization resulting from these modules will aid in the development of fast code, aiding in Issue 2 of speed as well. The modular design of the POPS program is therefore of utmost importance in understanding how this program will aid in the investigation of the proposed questions and hypotheses.

4.2.1 Program Organization and Modules

It is important to note that to be fast and efficient, the POPS program does not simply use the operating system to perform file input/output on LAMMPS input files and execute LAMMPS. POPS is a C++ library extension to LAMMPS, and therefore communicates with LAMMPS through its own library. During runtime, therefore, it is required that the entire POPS program and its connection to LAMMPS be compiled as a single package. This low-level connection of code allows for much quicker and efficient runtime as opposed to simply executing LAMMPS via a system command, thus further aiding in Issue 2 of speed. For the same reason that the modular structure of LAMMPS provides convenience, in the sense that users can easily add their own features and modules, the POPS program is also object-oriented and modular. The modules of the POPS program are designed so that users can add features such as their own fitting targets, objective functions, and fitting algorithms without having to recompile the entire program, thus further aiding in Issue 1 of generality.

The only two external libraries required by the POPS program are LAMMPS and Open MPI, a Message Passing Interface (MPI) C++ library. The MPI library is not used to take advantage of the parallel features of LAMMPS, but instead to parallelize the GA. This highlights another advantage of the GA, it can be evaluated using "embarrassingly parallel" operations; this means that separate parts of the optimization procedure can be executed in isolation of each other and do not require communication. Thus they can be evenly distributed across computing processes for a near linear increase in speed with respect to increasing the amount of assigned processors. High performance computing allows the connection of many separate computers, or "nodes", to incorporate their combined power for accomplishing a task, and the MPI library handles the passing of information between nodes. This process is easily applied to the GA, noting that there is a population of individuals as explained in Chapter 2. All individuals must undergo evaluation of the objective function, which adds to the overall compute time of the GA. If we parallelize the fitting process over individuals in the population, it is possible to separate the computing so that each processor handles $N_P = \frac{N_{tot}}{N_{procs}}$ individuals, where N_{tot} is the total number of individuals and N_{procs} is the number of processes being incorporated. These N_P individuals are sent to their own computing process to evaluate their objective functions, instead of a single process evaluating all objective functions. [184]. While the speed-up as a function of incorporated computing processes does not result in exactly 100% parallel efficiency due to the need for some level of inter-process communication via MPI, the efficiency remains well above 90% for many processes with the POPS program. Figure 8 shows the parallel efficiency of the POPS program as a function of computing processes, calculated by

performing five GA generations with 256 individuals in the population. This benchmark was performed on a cluster of 24-core Intel® Xeon® CPUs E5-2680 at 2.50 GHz with 64 GB of memory.

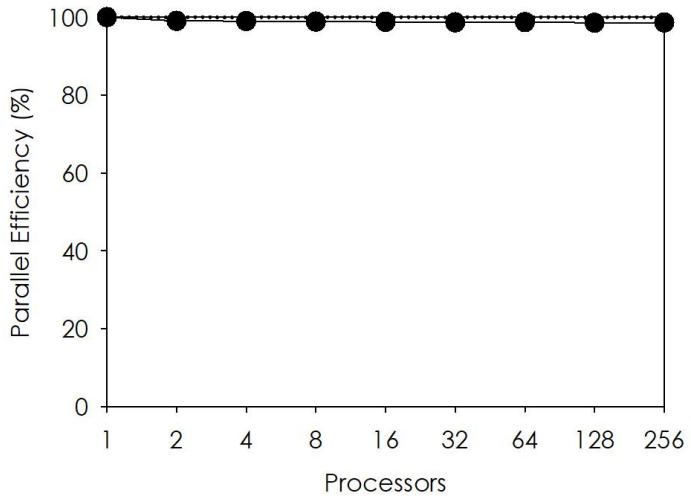

Figure 8 – Parallel efficiency of the POPS program. The large black dots are the actual speedup efficiency values and the dotted line is the theoretically ideal value.

If one has access to a certain number of computing cores, they should be able to decrease the training time to achieve a potential by a significant amount. This significant increase in speed from traditionally serial fitting algorithms [85,124], or algorithms incorporating only a single computing process, further alleviates Issue 2.

The parallelization module, utilizing the MPI libraries, ensures fast potential optimization, other modules in the POPs program work together to complete the optimization process. The LAMMPS potential module allows for potential quantities to be calculated for every parameter set, or every individual in the GA population. The user-

interface module allows the convenient modification of optimization settings, thus alleviating Issue 3. An optimization module must be incorporated, which will house the GA, so that operations can be performed on parameters to minimize the objective function. In this regard, another module which has not been mentioned is the objective function, or error module. The error module contains the definition of the error, $Z(\boldsymbol{\lambda})$, between reference quantities and DFT quantities to be minimized. Existence of such a module allows one to easily extend the POPS program to include a variety of fitting targets without modifying the rest of the code, thus alleviating Issue 1 of generality. A high-level organization of these five modules is shown in Figure 9, along with how potential parameters flow through the program during optimization.

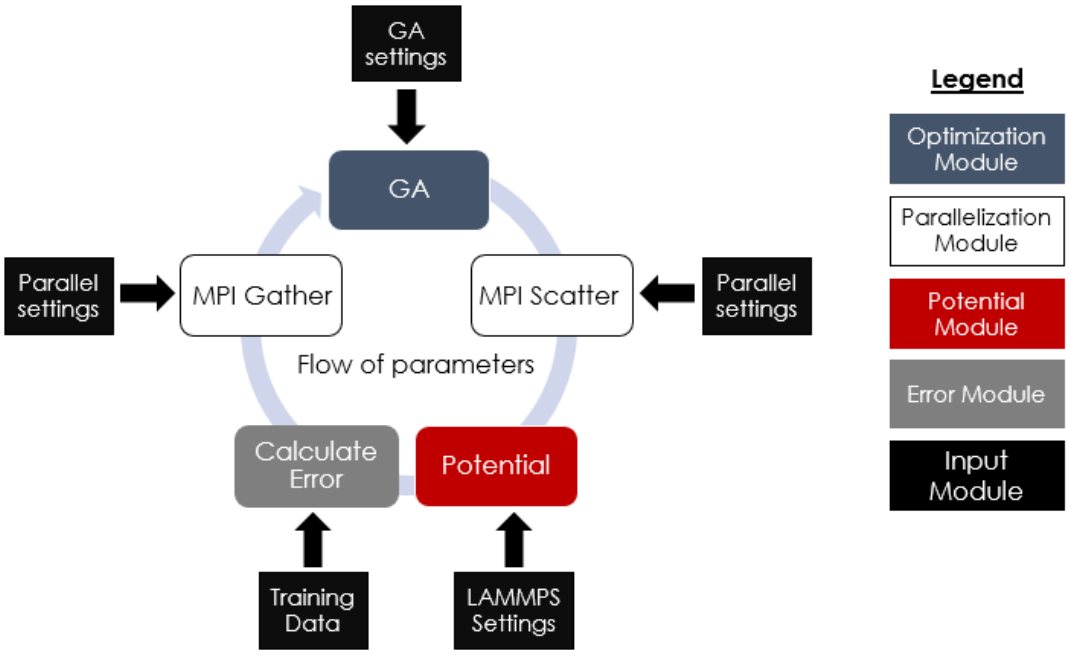

Figure 9 – High-level organization of the POPS program. The circular arrow represents the flow of parameters through the modules during the potential optimization process. The blue box is the fitting module, for which we use the GA. White boxes represent the parallelization modules, in which MPI is used to scatter and gather the parameters across processes. The red box is the potential module which calls the LAMMPS potential library. Objective function calculation is handled by the error module, the grey box. The black boxes are tasks performed by the user-input module, in which settings influence all modules, and training data is input to the error calculation.

This high-level organization shows the main modules which drive the POPs program, and the circular arrow shows the flow of parameters through the program as they are optimized with the GA in the optimization module (blue box).

Fitting begins by initialization in the optimization module, and then parameter sets (population individuals in the GA) are distributed across processors. White boxes represent the parallelization module, utilizing the MPI libraries, which first scatter the parameters across processors for potential and error calculation, and then gather the resulting errors back before performing the GA operations mentioned in Chapter 2. The red box, the

potential calculator module driven by LAMMPS, contains the library of potentials and the code to calculate fitting quantities with the potentials. Error is calculated after potential quantities are obtained via the error module given by the grey box. Resulting errors for every individual in the population are then gathered from all processors onto a single master node which performs GA operations on individual parameter sets. As seen in Figure 9, the user-input module represented by black boxes affects all the other modules via settings declared by the user. This results in an easy-to-use program that allows the convenient changing of a wide variety of settings for potential fitting experimentation. The POPS program modules all combine to form a coherent package that optimizes potential parameters, as shown in Figure 9. These modules culminate together to alleviate the three main existing issues in potential optimization, and these issues posed major barriers to answering the key scientific questions of interest and testing of the noted hypotheses in this thesis.

4.3 Discovering the POPs Recipe

Model systems to investigate the proposed questions and hypotheses will include semiconductor crystals, mainly crystalline silicon (c-Si) and crystalline germanium (c-Ge). Traditional analytical potentials for these systems, namely Tersoff and Stillinger-Weber, will serve as functional forms to reproduce quantum mechanical forces. Since c-Si is a simple and technologically relevant material, this was the first material used for testing. The Tersoff potential was the original potential used for c-Si, so this original fitting tests involved this functional form. The key question is what is the "recipe" or set of quantities (i.e., ingredients) that must be included in an objective function for it to consistently and accurately optimize for reproduction of phonon properties determined from DFT? The

objective function can be any form of error, such as mean percent error (MPE), root mean squared error (MSE), etc. The MPE is a convenient way to assess a fit, and it therefore made sense to choose the force MPE as the original objective function. This led to an objective function of the form

$$Z = \frac{1}{M}\sum_{m=1}^{M}\sum_{n=1}^{N_m}\frac{1}{N_m}\frac{\left\|\mathbf{F}_{mn}^{0}-\mathbf{F}_{mn}\right\|}{\left\|\mathbf{F}_{mn}^{0}\right\|} \tag{42}$$

where M is the total number configurations, N_m is the number of atoms in configuration m, $\mathbf{F}_{mn}^{0}$ is the reference DFT force on atom n in configuration m and $\mathbf{F}_{mn}$ is the potential force on atom n in configuration m. The double brackets indicate magnitudes of the vectors. While Equation 42 allowed for convenience in thinking about quality of fit to forces, it was not a suitable candidate for optimization. This was clear when the error of this optimization hardly decreased as a function of generations in the GA. Further investigation of this issue led to the realization that small forces on the order of 10^{-6} eV/Å caused Equation 42 to diverge, and when using 100 configurations of 64 atoms, these occurrences were not uncommon. This led to the abandonment of fitting to MPE, but the quantity is still useful to assess the validity of training errors. A more appropriate and simple force objective function was developed, resulting in

$$Z = \sum_{m}^{M}\sum_{n}^{N}\left\|\mathbf{F}_{mn}^{0}-\mathbf{F}_{mn}\right\|^{2} \tag{43}$$

which is not unitless. This objective function led to better force fitting success, and it was still possible to track the evolution of the more meaningful MPE quantity in Equation 42

as Equation 43 was optimized. Before any fitting needs can be performed, a training set needs to be clarified. The training set for this first test includes 50 ($M = 50$) c-Si configurations of 64 atoms, where each configuration contains atoms randomly displaced from equilibrium by up to 0.3Å. The forces were calculated using DFT with the PBE exchange-correlation functional, which has been shown to predict accurate forces and IFCs in c-Si [34]. Using Equation 43 as the objective function, the Tersoff potential was optimized against these forces and Figure 10 shows the evolution of the MPE as a function of GA iterations.

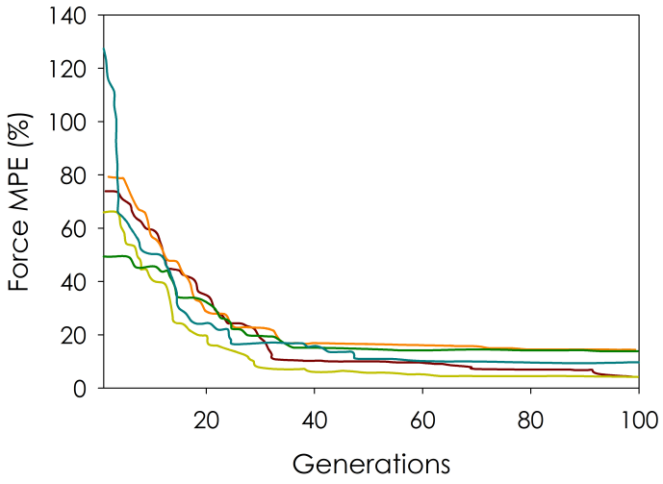

Figure 10 – Force MPE evolution vs. GA generations for 5 trials of Tersoff c-Si fitting to forces in 50 configurations of 64 atoms. Each line in this figure is a separate trial GA fit, starting from a different random population. All trials converged around 40 generations with an average of 9.4% error in forces.

Figure 10 was the first successful fitting experiment in the sense that some fits were below the original target of 10% error in forces. All 5 trials in Figure 10 all started from random positions in the parameter search space according to the GA, and all trials achieved below a 20% error in forces. It is important to note here that this successful fitting experiment was only possible by allowing the parameter ranges in the GA optimization to span a large

enough range. This was realized since original fitting experiments, containing small ranges for parameter searches, resulted in many parameters approaching the boundary of the allowed interval. This showed that the best minimum according to the GA existed outside of the allowed parameter interval. Performing this analysis for many trials of GA optimization, and finding that some trials result in parameters that lie on the boundary of allowed intervals, is a convenient way of showing that the parameter intervals must be expanded. This procedure was repeated through trial and error until it was found that a parameter range spanning 2 orders of magnitude was chosen for each Tersoff parameter. Of the 5 GA trials in Figure 10, all starting from random positions in search space, only one resulted in a potential that exhibited stable MD simulations. While this was concerning and will soon be addressed, it was still of interest to test the hypothesis of 10% error in forces yielding a 10% error in thermal conductivity via the GK formula. At 300 K the thermal conductivity error of this optimized Tersoff potential with experimental values[185] was over 100%, thus disproving our hypothesis that a 10% error in forces, will automatically lead to a ~ 10% error in thermal conductivity. This further confirms that Hypothesis 1 is incorrect; fitting only to forces is not sufficient to obtain a potential that will accurately predict phonon properties. This result was surprising. Even more problematic was the fact that 6 out of 7 of the potentials in this test yielded unstable dynamics in MD simulations. Instability in MD, herein, is defined as unrealistic and sudden changes in quantities such as the potential energy and temperature, which therefore lead to unrealistic dynamics (e.g., c-Si explodes and behaves like a gas at room temperature). This is a domino effect, since unrealistic interactions can result in large displacements that increase the potential energy and force, which tend to cause the system to fall apart as the

simulation proceeds. This problem was more drastic than the inaccurate thermal conductivity, since stable potentials are needed just to perform MD simulations in the first place.

Although most previous works involve fitting to experimental values of elastic constants [80,85], they still never explicitly discuss the issue of stability. This is because by fitting to experimental elastic constants, satisfaction of the Born elastic, elastic stability criteria is automatically ensured [65,186-188]. Fitting to elastic constants is undesirable, however, since elastic constant calculation and corresponding stability criteria are not general for any crystal structure or material [65]. Relying on the availability of experimental data would also be restrictive and disable predictive capability. Previous works also fit to structural quantities like the lattice parameter [80,85], under the proper assumption that by reproducing the structural parameters of the lattice that stability should be increased. The average error in DFT lattice parameter for the results in Figure 10 was 5%, which is actually quite poor, as the widely used parameterizations developed by Tersoff himself possessed a ~1% error in experimental lattice parameters [71]. This suggests that fitting only to forces does not ensure structural property agreement, which may be the reason for a corresponding instability of the potentials. Analytical derivation of the lattice parameter from the potential is a challenging mathematical task, as it would have to be coded for every specific potential that is fit to. Instead, fitting to the DFT energy of many configurations with different volumes was identified as an alternative to capture the volume associated with the minimum energy (i.e., the lattice parameter).

4.3.1 Energy Shape and Lattice Parameter

In theory, by fitting to the energies of DFT configurations containing various volumes, the lattice parameter be accurately captured. The objective function of Equation 43 was therefore modified to include energies of each configuration, resulting in

$$Z = w_e z_e + w_f z_f \tag{44}$$

where z_e is some normalized error for energy and z_f is some normalized error for force, and the w values are their corresponding weights. A successful normalization was found by dividing the square error of each quantity by the sum of all the references quantities, thus resulting in

$$z_f = \frac{\sum_{m=1}^{M}\sum_{n=1}^{N}\left\|\mathbf{F}_{mn}^{0} - \mathbf{F}_{mn}\right\|^2}{MN\sum_{m=1}^{M}\sum_{n=1}^{N}\left\|\mathbf{F}_{mn}^{0}\right\|^2} \tag{45}$$

for forces, where N is the total number of atoms in the entire training set and

$$z_e = \frac{\sum_{m=1}^{M}\left(E_m^0 - E_m\right)^2}{M\sum_{m=1}^{M}\left(E_m^0\right)^2} \tag{46}$$

for energies, where E_m^0 is the reference DFT energy and E_m is the potential energy of configuration m calculated via the potential. It is important to note here that the absolute value of energy is not of interest in the development of POPs. This is most apparent when considering the TEP of Equation 22, since the IFCs determine phonon properties, and the

scaling of the PES by an arbitrary constant would not influence its derivatives, and therefore has no impact on the dynamics. To better capture the relative contributions of different configurations to the potential energy, the energies in Equation 46 are all subtracted by the energy of the equilibrium structure with the lowest (i.e., most negative) energy. With the definitions of z_e and z_f, Equation 44 will serve as the objective function when testing the ability of a potential to reproduce the DFT energy-volume curve and lattice parameter, and will enable assessing whether this will improve MD stability.

Performing the same c-Si Tersoff fitting discussed previously, with 50 randomly displaced configurations and 50 GA trials, more "volume configurations" were added to the training set. These included 20 configurations with the equilibrium lattice parameter and other volumes with lattice parameters +/- 5% from the equilibrium value, along with 10 configurations extending beyond +/- 2.0 A. The results confirmed that fitting to different volumes of DFT training data reduced the error in lattice parameter between the potential and DFT. This also resulted in more stable c-Si Tersoff potentials. Out of the 50 trials, about 60% were stable in MD. To test the generality of the POPs program, the Tersoff potential was parameterized for a material with 2 atom types – zinc-blende GaAs. The results for fitting to the energy-volume curve are shown in Figure 11. This GaAs Tersoff potential resulted in stable MD simulations, and the force error averaged 15% for all 50 trials.

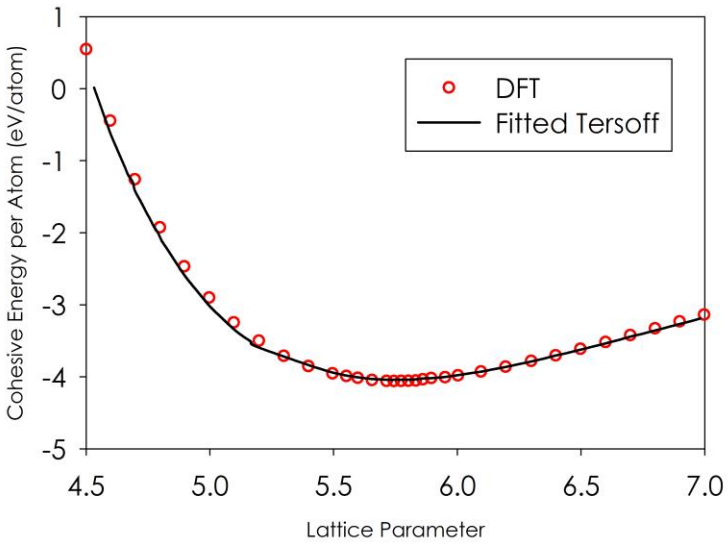

Figure 11 – Energy-volume curve fitting for GaAs. The error in lattice parameter for this fit was on the order of 0.1%, which is more than an order of magnitude increase from fitting experiments where the volume configurations were not included.

The potentials at this point were optimized with Equation 44 as the objective function, resulting in excellent lattice parameter agreement ~ 0.1%. While the number of stable potentials obtained via 50 GA trials increased compared to just fitting to forces, yet there were still occurrences of unstable potentials. In these unstable potentials, the expansion associated with elevated temperatures in NPT simulations caused volumetric and pressure instabilities in the lattice. A graphical picture of the observations leading to this analysis is shown in Figure 12 below

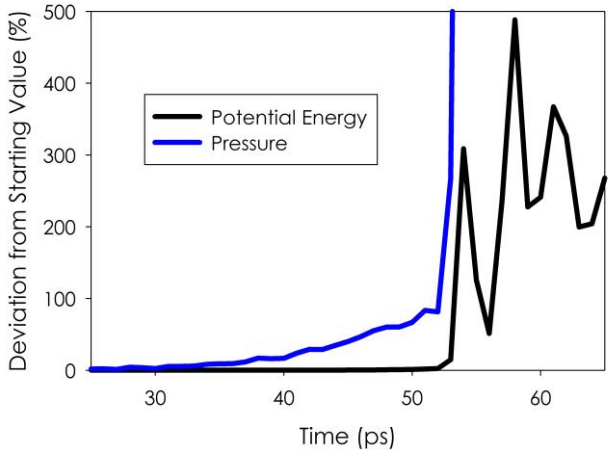

Figure 12 – Pressure instabilities occurring before potential energy instability in a MD simulation. Notice how the pressure deviation from the starting value begins to go unstable (rise) before the potential energy deviation begins to rise.

Further analysis of the MD quantities as a function of time showed that pressure instabilities occur in sync with volume instabilities during a NPT simulation. It could be the case that although the forces possess low errors, errors in the pressure virial contribute to massive errors in the stress tensor. This was indeed the case, judged by taking configurations at the point before total instability of the system occurs (i.e., potential energy and pressure oscillations deviate over 100% from initial values) and comparing the stress tensor components of these configurations with the stress tensor components from DFT calculations. The errors were on the order of 1,000%, thus showing that the current potentials optimized for energy and force are not accurately reproducing the stress tensor. Although the analysis in Figure 12 does not prove that pressure instabilities lead to unstable MD simulations, it does show that the stresses calculated by the potential can exhibit large errors that coincide with destabilization of the supercell. This is further supported by the fact that the potential energy, which only depends on the position of atoms, oscillates near

zero error until the pressure reaches an unreasonably large value, thus causing the system to collapse. This sort of analysis led to the idea of including stress in the objective function.

4.3.2 The Need for Stress

The potentials in Section 4.1.1, fit only to forces and energy as a function of volume, experienced instabilities seemingly due to pressure oscillations as shown in Figure 10. Other authors included elastic constants to overcome this problem and guarantee Born's elastic stability criteria [65] as discussed in Chapter 2, but they cannot be easily generalized to any potential or structure. Alternatively, since the elastic constants depend on the stress tensor for a variety of strains, it was hypothesized that fitting to the stress tensor on a variety of system volumes would result in increased stability. The stress tensor components for a static configuration can be calculated in a system of atoms from the virial theorem via [189]

$$\sigma_{\alpha\beta} = \frac{1}{V}\sum_{n=1}^{N} \alpha_i F_i^{\beta} \tag{47}$$

where α and β represent Cartesian coordinates, α_i is the α coordinate of atom i, and F_i^{β} is the force on atom i in the β direction. The objective function of Equation 44 was then extended to incorporate a stress error term, resulting in

$$Z = w_f z_f + w_e z_e + w_s z_s \tag{48}$$

where the stress error z_s is given by

$$z_s = \frac{\sum_{m=1}^{M}\sum_{p=1}^{6}\left(\sigma_{mp}^{0} - \sigma_{mp}\right)^2}{6M\sum_{m=1}^{M}\sum_{p=1}^{6}\left(\sigma_{mp}^{0}\right)^2} \tag{49}$$

where σ_{mp}^{0} and σ_{mp} are the p^{th} symmetric stress tensor components of configuration m for the reference and potential, respectively. The normalization by 6 and sums over 6 components come from the fact that the 9-element stress tensor is symmetric since $S_{\alpha\beta} = S_{\beta\alpha}$. Using the objective function in Equation 48 to parameterize the Tersoff potential for c-Si resulted in, again for 50 GA trials, resulted in nearly all stable potentials, especially at higher temperatures. Even with the increase in stability, however, the thermal conductivity error calculated via the GK method was still large at 62% for the best fit. In order to achieve better thermal conductivity predictions, the objective function requires a property related to phonons that can easily be calculated on the fly for the potentials. The formalism in Chapter 3 stems from the IFCs, or 2nd and 3rd derivatives of the energy, these were the next quantities to be added.

4.3.3 Higher Order Derivatives of Energy

There are two main reasons for fitting to the IFCs: (1) fitting to the derivatives of forces can help further resolve the force accuracy for the GK calculation and (2) according to the PGM, the IFCs directly influence the thermal conductivity. Here it is important to note a rather surprising finding from these preliminary optimizations, namely that it is possible that a potential can reproduce total forces well, with incorrect force contributions coming from different atoms. Initially, it was assumed that calculating nearly correct forces

for many different atoms averaged over many different configurations would filter down to a unique set of force contributions coming different neighboring atoms. However, it was deduced from the preliminary fitting tests that this is actually not true, and it is therefore necessary to force the potentials to try and reproduce the actual force contributions arising from different neighbors. This is a much more stringent requirement, but fitting to the derivatives of a function also allows for a better representation of the function itself, especially in the case of an interatomic PES [190]. Fitting to higher derivatives should therefore allow for better fits, since more information about the surface is provided. The 2nd order 3rd order IFCs were therefore added to the objective function due assuming that this would also improve the poor thermal conductivity predictions of previous fits which were only fit to force, energy and stress. Inclusion of the IFCs into the objective function requires separate error terms for the 2nd and 3rd order IFCs. Following the normalized format of previous errors, the error for 2nd order IFCs z_{ifc-2} is given by

$$z_{ifc-2} = \frac{\sum_{i}^{N_{IFC2}} \left(\Phi_i^0 - \Phi_i\right)^2}{\sum_{i}^{N_{IFC2}} \left(\Phi_i^0\right)^2} \tag{50}$$

where Φ_i^0 are the reference 2nd order IFC and Φ_i are the 2nd order IFCs for the potential, and the sum runs over N_{IFC2} number of 2nd order IFCs. The error for 3rd order IFCs z_{ifc-3} is given by

$$z_{ifc-3} = \frac{\sum_{i}^{N_{IFC3}} \left(\Psi_i^0 - \Psi_i\right)^2}{\sum_{i}^{N_{IFC3}} \left(\Psi_i^0\right)^2} \tag{51}$$

where Ψ_i^0 are the reference 3rd order IFCs and Ψ_i are the 3rd order IFCs for the potential and the sum runs over N_{IFC3} number of 3rd order IFCs. The number of IFCs included in the error of Equation 50 and Equation 51 depend on the cutoff of the interactions used in the potential. Inclusion of these errors into the total objective function of Equation 48 yields

$$Z = w_f z_f + w_e z_e + w_s z_s + w_e z_e + w_{ifc-2} z_{ifc-2} + w_{ifc-2} z_{ifc-3} \tag{52}$$

Crystalline germanium (c-Ge) served as a test system for the new objective function in Equation 52. Following the same experiments in the previous sections, the fitting composed of 100 GA trials, 100 randomly displaced configurations and 20 volume configurations, using 1000 individuals and a mutation rate of 0.5. The chosen potential as a combination of a short range Tersoff potential plus a long-range van der Waals and Coulomb potential (TVC). The long-range terms were added to give more flexibility to the potential. The best result from all trials yielded a TVC potential with 4.9% force error, which was about twice as good compared to previous attempts. MD simulations with the potential were also stable since the stress and volume were also included. The thermal conductivity was calculated via the ensemble method [182] using the GK formula over a variety of temperatures, and the results are shown below compared to experiments

[185,191,192] for isotopic and natural compositions of c-Ge.

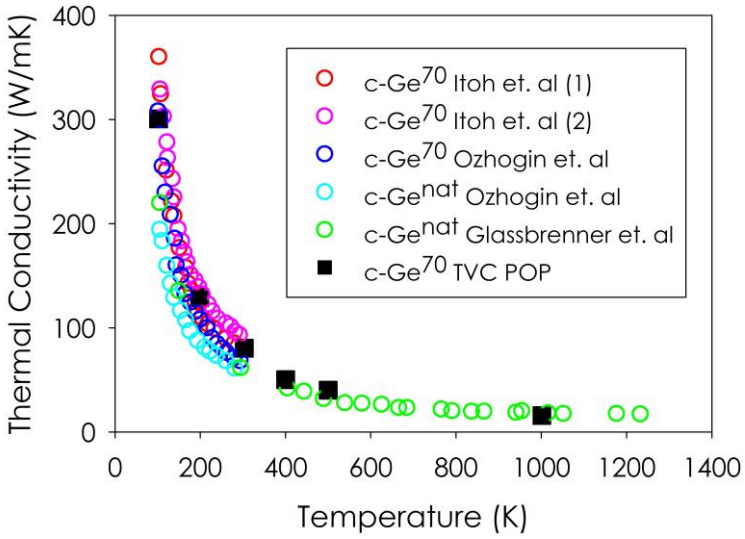

Figure 13 – Thermal conductivity as a function of temperature for c-Ge using the optimized TVC potential, calculated via the GK method. Excellent agreement with experiments as a function of temperature are shown.

The thermal conductivity values were calculated using the ensemble averaging method with 100 ensembles for each temperature, and a simulation time of 2 ns. The thermal conductivity was extracted from the thermal conductivity accumulations using the first avalanche method [193]. An example of the application of this method is shown in Figure 14 to extract the thermal conductivity value at 200 K in Figure 14.

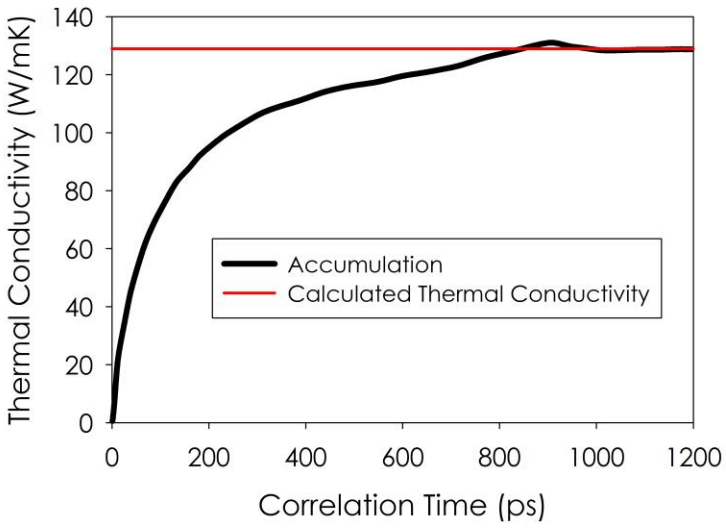

Figure 14 – Thermal conductivity accumulation for c-Ge at 200 K. The black line is the accumulation and the red line is the value of 129 W/mK extracted from the first avalanche method.

The final components needed to create a potential that can reproduce the thermal conductivity, were the 2nd and 3rd order IFCs. The results using the full objective function in Equation 52 yield potentials with both stable MD and accurate phonon transport properties. These preliminary fitting tests therefore concluded the investigation of a recipe to create POPs, confirms the utility of the POPs Tenets, and answers many of the proposed questions and hypotheses.

4.4 Answered Questions

First and foremost, Question 1 of what quantities to use in the potential fitting process was answered. Hypothesis 1, that fitting only to forces are sufficient, turned out to be false. Originally, fitting only to forces yielded potentials with unstable dynamics (i.e., large fluctuations in potential energy leading to unphysical dynamics). Even when stability was

improved by fitting to energy-volume curves and stresses, force errors of < 10% still resulted in inaccurate thermal conductivity calculations. Inclusion of the force derivatives or IFCs, inspired by LD theory in Chapter 3, resulted in accurate thermal conductivity predictions for c-Ge. These results answer question, at least for this system, and provide the recipe of five main quantities (force, energy-volume, stress, 2nd order IFC, 3rd order IFC) to produce a stable POP. Question 2, involving how closely can analytical potentials match quantum mechanical quantities such as forces in covalent solids, was also answered to show that it is at least possible that analytical functional forms can achieve a < 10% error in forces. This is surprising since previous work for metals, which contain a more homogenous and less complicated electronic structure [166], resulted in force-fitting errors of 20% [194]. It also seems that traditional analytical potentials, such as Tersoff, will reproduce thermal conductivity if parameterized for such a purpose (i.e., to the forces and IFCs), thus confirming Hypothesis 2. Hypothesis 3 regarding the existence of different parameter sets to reproduce small forces about equilibrium was shown to be true with the force fitting experiment of Figure 10. The main remaining question to be answered is Question 4, of whether fitting to long-range forces will result in accurate phonon frequency calculations at the Brillouin zone boundaries. To further investigate this question and confirm the viability of the POPs Tenets and approach, a formal application of the recipe discovered herein will be applied to a few different potentials for c-Si and c-Ge.

CHAPTER 5. EXAMPLES: CRYSTALLINE SILICON AND GERMANIUM

This chapter applies the knowledge from Chapters 2, 3 and 4 to worked examples for two simple systems – diamond structured crystalline silicon and germanium (c-Si and c-Ge, respectively). Attaining the training set/fitting targets, will first be discussed with special considerations regarding the number of certain configurations and types of configurations. Choosing the potentials to test the POPs Tenets, method, and the POPs program will also be discussed, along with their respective functional forms. Results will be presented in terms of errors in training quantities, along with how these errors relate to the target goal of reproducing phonon properties.

5.1 Obtaining the Training Set

Before parameterization of potentials ensues, a set of fitting quantities and their associated atomic positions must be obtained. This training set will contain everything that the potential is parameterized against, and the first step in obtaining it is choosing DFT settings that will produce accurate fitting quantities. Accurate in this sense means accurate forces for varying displacements around the equilibrium positions, and therefore accurate force constants and phonon properties. The phonon properties can be tested by taking force-displacement data obtained from DFT, fitting the TEP of Equation 21 to obtain force constants, and then using these force constants with Equations 28 and 41 to calculate phonon dispersion and thermal conductivity. These quick checks at least show that the force constants obtained from the DFT data are accurate, and therefore the forces and DFT

settings are accurate. For non-crystalline systems, where phonon dispersion and thus PGM based expressions for thermal conductivity cannot be defined, other parameters such as the bulk modulus can be verified from DFT energy-volume and pressure-volume data.

5.1.1 DFT Settings

The DFT calculations for c-Si were performed on 64 atom supercells using VASP [153], employing the GGA, with plane augmented wave pseudopotentials [195] and the PBE functional [172] was used for the exchange-correlation energy. For both c-Si and c-Ge, pseudopotentials with s^2p^2 valence electron hybridizations were used, resulting in 4 valence electrons that enter the electronic structure calculation. Energy cutoffs of 245.3 eV and 174.0 eV were employed for the wave functions in c-Si and c-Ge, respectively. For both c-Si and c-Ge, a $6\times6\times6$ Monkhorst-Pack [196] $\mathbf{q}$-point grid was used as the domain for charge density calculations, and electronic structure was converged to within 10^{-5} eV. The forces were converged to 10^{-4} eV/Å. These settings were applied to obtain the energy and forces associated with configurations where atoms are randomly displaced from their equilibrium site, as well as the configurations where atoms are positioned on their geometric lattice site, but the lattice parameter is varied. All atoms in the randomly displaced configurations were displaced up to 0.1 Å, resulting in forces on the order of 0.1-1 eV/Å for each atom.

GGA and PAW pseudopotentials were chosen since these yielded accurate lattice parameters under DFT relaxation of the primitive cell for both c-Si and c-Ge. Energy cutoffs and $\mathbf{q}$-point grids must be chosen such that a measure of energy is converged in the DFT calculations. A convenient and meaningful measure of energy is the cohesive energy; the difference between the total calculated ground-state energy of the atomic

system and the sum of all single-atom ground-state energies [117]. For example, the cohesive energy of a 64-atom c-Si system is the total ground-state energy of the 64-atom system minus 64 ground-state energies of single silicon atoms. By this definition, the cohesive energy is the energy required to separate the atoms of the system (i.e., break the bonds) [117]. The energy cutoffs and $\mathbf{q}$-point grids were both chosen such that the total cohesive energy of the system converged to within 10^{-2} eV. This was accomplished by sampling increasing numbers of $\mathbf{q}$-points in the grid using a literature recommended values for the energy cut-off, until the total cohesive energy converged. Using these converged $\mathbf{q}$-point values, the energy cut-off was then sampled with increasing values until the cohesive energy again converged within 10^{-2} eV, and these converged energy cut-offs were only slightly higher than values recommended in literature for phonons [34].

5.1.2 Equilibrium Structures

The goal here is to capture configurations of atoms that are perturbed about from their equilibrium sites, so that the fitting captures these perturbations and associated forces and force constants that underlie the LD formalism introduced in Chapter 2. The assumptions for eliminating the first two terms of the TEP in Equation 22 also hinge on the requirement that the structure is at an energetic minimum with zero forces on the atoms. Thus, an equilibrium structure must be obtained. It is also important to obtain an equilibrium structure with an equilibrium lattice parameter since the lattice parameter influences the phonon calculations based on reciprocal lattice vectors, as seen in Chapter 2. To calculate the DFT lattice parameter, configurations with equilibrium diamond structure positions were sampled over a variety of volumes. The resulting energy-volume

dataset was then fit to the Birch-Murnaghan isothermal equation of state [197], which gives the cohesive energy E as a function of volume V as,

$$E(V) = E_0 + \frac{9V_0B_0}{16}\left\{\left[\left(\frac{V_0}{V}\right)^{2/3} - 1\right]^3 B_0' + \left[\left(\frac{V_0}{V}\right)^{2/3} - 1\right]^2\left[6 - 4\left(\frac{V_0}{V}\right)^{2/3}\right]\right\} \quad (53)$$

Where E_0 is the minimum energy of the energy-volume curve, V_0 is the volume associated with the minimum energy, B_0 is the bulk modulus, and B_0' is the derivative of bulk modulus with respect to pressure. These quantities can all be treated as fitting parameters to the energy-volume dataset. The GA can be used to calculate these parameters for a given energy-volume dataset. To test the accuracy of the equilibrium lattice parameter, which is the cubed root of the V_0 parameter in Equation 53, energy-volume data from DFT can be taken over a range of volumes and then fit to the Birch-Murnaghan equation of state. The result for c-Si is shown in Figure 15.

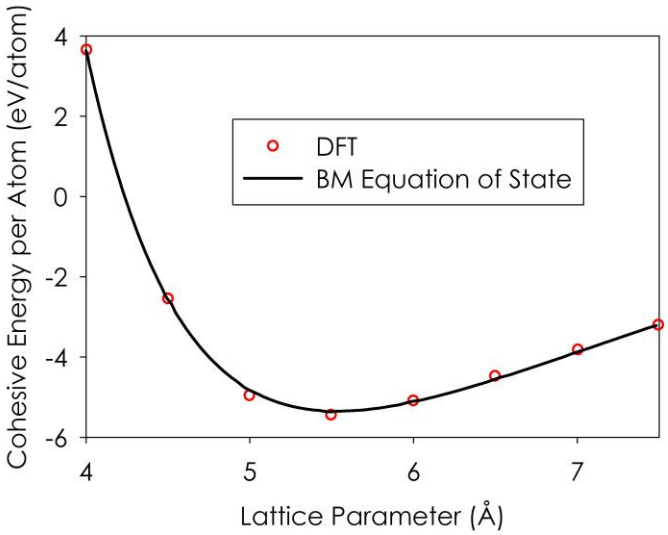

Figure 15 – Energy-volume data for c-Si fit to the BM equation of state.

The energy-volume data in Figure 15 was chosen over a few angstroms, and the fit to the BM equation of state yielded a better idea of where the equilibrium zero pressure lattice parameter for the DFT calculations lies, around 5.5 A as shown. A more accurate resolution can be obtained by fitting a parabola to the small region around this value, plus or minus a few hundredths of an angstrom. The results showing the c-Si lattice parameter are shown in Figure 16.

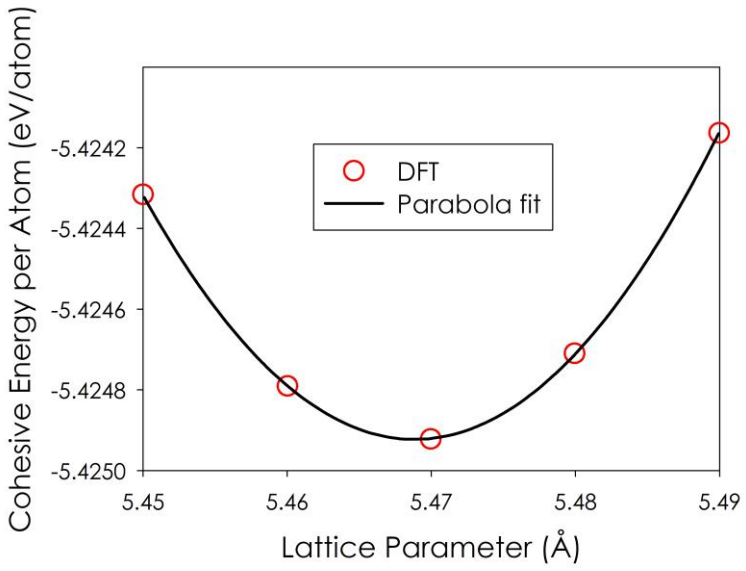

Figure 16 – Narrow energy-volume from c-Si DFT with a parabola fit.

After the range of DFT lattice parameter is found via a BM fit, the exact lattice parameter can be calculated from a fit to smaller spaced volume data as shown in Figure 16. This procedure was performed for both c-Si and c-Ge, yielding lattice parameters that were 0.70% and 0.49% off from experimental values [198,199]. Obtaining these equilibrium structures with accurate agreement to experimental structural parameters is important for the generation of more training data, as well as ensuring the Brillouin zone is accurately sampled during phonon dispersion calculations via Equation 28. With equilibrium

structural quantities like the lattice parameter obtained in agreement with experiment, it is now safe to construct fitting data such as forces and stresses arising from perturbing the atoms about their equilibrium positions.

5.1.3 Perturbed Structures

It was shown in Chapters 3 and 4 that structures perturbed from equilibrium are necessary to include in fitting to capture forces, energies and stresses associated with these perturbations, thus ensuring various types of stability in MD simulations. The training set here for both c-Si and c-Ge included 300 displaced configurations and 50 volume configurations, consisting of the lattice parameter spanning +/- 5% around the equilibrium value. The amount of displacements chosen for the displaced configurations was motivated by the desire to reproduce forces near the regime where the harmonic approximation is most valid. Small displacements only 0.01 Å have been shown to reproduce harmonic forces leading to accurate phonon frequencies in both crystals [33]. To determine the magnitude required to capture anharmonic forces and ensure dynamical stability in a MD simulation, DFT-MD simulations of small unit cells showed the root mean squared displacement of atoms to have an average of 0.3 Å at 600 K. The randomly displaced configurations therefore included displacements up to 0.5 Å to better resolve the high temperature phase space.

Random displacements were generated by taking the equilibrium relaxed structure corresponding to the minimum of the energy-volume curve in Figure 16, and then adding random displacements from [-0.3 Å, 0.3 Å] to the Cartesian position components. The choice of 0.3 Å for each coordinate is chosen such that the maximum norm of the

displacement vector corresponds to the previously mentioned 0.5 Å. Half of the 300 displaced configurations consisted of these "large" displacements, while the other half consisted of small displacements up to 0.01 Å. Inclusion of the smaller displaced configurations ensured that the harmonic phase space associated and phonon frequencies could accurately be captured. Although the forces are a first step in obtaining a full training set to create POPs, fitting to force derivatives is also necessary for stability and accurate phonon properties. Perturbed configurations and their resulting forces were used to calculate these derivatives.

5.1.4 IFC Calculation

IFCs were calculated using the DDM discussed in Chapter 2, in which force-displacement data from perturbed configurations were fit to a TEP. Fitting parameters in the TEP represent the IFCs, so these values can be obtained by fitting directly to DFT forces. In theory, only a displacement of one atom in a single Cartesian direction is needed to calculate accurate 2nd order IFCs in diamond structured materials [33]. In practice, however, when developing a potential optimized for phonon properties while remaining stable in MD simulations, it is of interest to ensure that the IFCs are still accurate when calculated using more diverse configurations. For this reason, the IFCs were calculated during the optimization process by using 50 of the randomly displaced configurations. This ensures that the IFCs calculated by the potential are still accurate in this more complex part of phase space, instead of just at a single point given by one displacement. The cutoff of the TEP calculating during the optimization process was chosen so that the phonon dispersion converged in both c-Si and c-Ge, which includes 9th nearest neighbors. The discussion in the next section on choosing functional forms for this system was influenced

by these findings, as the cutoff for the potential for each atom must include interactions that extend to the 9th nearest neighbor of that atom.

5.2 Choosing Interatomic Potentials

Semiconductor and insulator materials already have many functional forms made for their study in MD simulations, created by previous researchers decades ago [66,71]. While these potentials have been shown to perform stable MD with semiconductor materials, they are still short-range potentials that lack the necessary long-range interactions required to reproduce correct phonon dispersions [80]. The potentials chosen for this study were therefore be a combination of traditional short-range and long-range potentials. Traditional short-range potentials have been shown to stabilize diamond lattices [58,66], so this is a necessity. Traditional long-range potentials utilize the 2-body radial descriptor discussed in Chapter 2, and Hypothesis 4 assumes these potentials can capture long-range interactions associated with phonon frequencies at Brillouin zone boundaries. Long-range 3-body potentials have not been developed or used extensively in the literature, therefore this work only includes long range 2-body terms. The difficulty in applying long-range 3-body potentials lies in the fact that the existing functional forms for 3-body potentials possess a single parameter for the angle in a triplet of atoms, and this only makes sense for 1st nearest neighbors, since all 1st nearest neighbors possess identical angles with respect to a central atom. If one were to extend a 3-body interaction beyond first nearest neighbors, then defining the equilibrium angle would require different definitions for different triplets, which would be cumbersome to implement and would only make sense for the single crystal structure being studied, i.e., the potential would not be transferable. Another difficulty lies in the computational expense of using long-range 3-body interactions, as the number of triplet evaluations would scale

with radius to the fourth power. For short-range interactions, however, a classical functional form for semiconductors is the Tersoff potential [71], so this was chosen. Another traditional choice is the Stillinger-Weber potential [66]. To deviate from traditional choices for these functional forms, a Morse + 3-body harmonic potential was also be chosen as a combination of Equations 10 and 12. These short-range potentials possess the necessary physics (3-body interactions) to stabilize a diamond-structured lattice [65]. For the long-range potentials, there are a few traditional options to address Question 4, regarding whether these traditional forms can accurately capture phonon frequencies.

Based on traditional physical knowledge of long-range interactions in atomic systems, especially crystals, prior work has shown that these interactions exist in the form of van der Waals forces and Coulomb forces [117]. The van der Waals interactions have been shown to decay as $\frac{1}{r^6}$ and Coulomb forces decay as the inverse of interatomic distance[117]. Recent advances in computing the Coulomb potential allow for quicker and more accurate calculations in terms of force cutoffs, particularly with the damped-shifted-force (DSF) model [128]. This form of the Coulomb potential was therefore used in this study. More flexibility for long-range interactions can be added with the addition of other potentials, such as the van der Waals type Buckingham and Born potentials. A combination of short-range 3-body interactions and long-range 2-body interactions was hypothesized to possess the necessary physics to both stabilize the diamond lattice, along with providing the long-range interactions necessary to reproduce proper phonon dispersion. The three potentials to illustrate the POPS method with c-Si and c-Ge were therefore the (1) Tersoff + Buckingham + Coulomb (TBC) potential, (2) Stillinger-Weber + Buckingham + Coulomb

(SWBC) potential and (3) the Morse + 3-body + Born + Coulomb (M3BC) potential. With these functional forms declared, and the training set obtained from Section 5.1, the fitting procedure utilizing the POPS program and recipe were ready for testing.

5.3 GA Fitting

The GA in the POPS program was used to minimize the objective function in Equation 52. The weights for fitting quantities were chosen such that $w_f = 0.15$, $w_e = 0.25$, $w_s = 0.2$, $w_{ifc-2} = 0.2$, $w_{ifc-3} = 0.2$. Before the fitting is accomplished, however, settings for the GA must be chosen so that the fitting has guidelines to abide by. Previous fitting experiments in Chapter 4 found that most fits converged within 150 generations of the GA, and a population size of 1,000 was sufficient, so these settings were chosen. It was also helpful to employ a high mutation rate and therefore avoid local minima in the first round of fitting. For the first fitting trial, a mutation rate of 0.5 was chosen to seek out more diverse regions of the parameter search space. The elite percentage was chosen to be 5%, thus ensuring that the top 5% of the population for each generation survived the selection process. A mutation rate of 10% was used in the second round of fitting so that the converged local minimum found by the first round could be optimized further. The above procedure was repeated in parallel for 50 different trials, resulting in many local minima, although some trials found the same local minimum. The training set included a total of 350 configurations as mentioned in Section 5.1, namely 150 randomly displaced configurations up to 0.5 Å, 150 randomly displaced configurations up to 0.01 Å, and 50 volume configurations. The 1,000 individuals in the population were parallelized over 25 processes for each trial, thus resulting in a total fitting time of 2 hours for 150 generations.

It should be noted that fitting potentials within 2 hours is a major step forward in terms of speed, as many previous works have required months of computational time to find a single solution [51,56,121,122,132,200]

5.4 Results

The average objective function convergence for both c-Si and c-Ge for all three potentials as a function of iterations is shown in Figure 17.

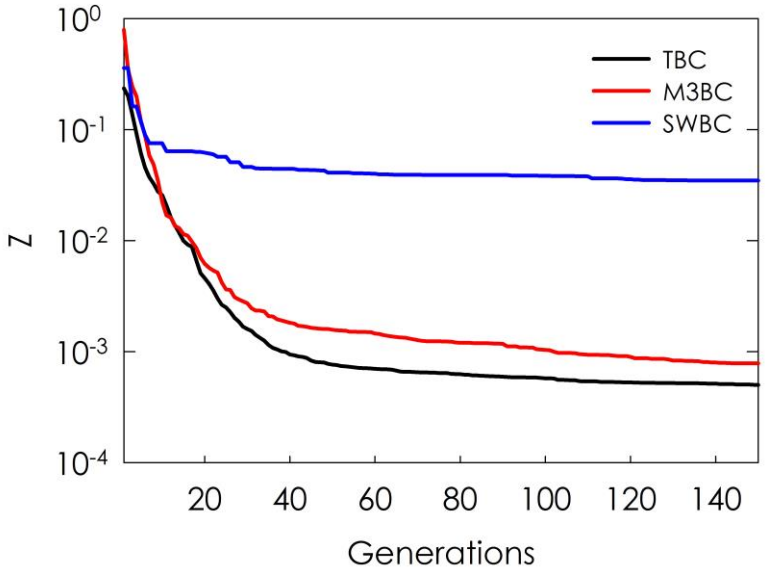

Figure 17 – Objective function convergence as a function of iterations. The black line represents the TBC potential, the red line is the M3BC potential, and the black line is the SWBC potential. Each line in this figure is an average over all 50 trials performed in the fit, for both c-Si and c-Ge.

As seen in Figure 17, the TBC and M3BC potentials decreased the objective function error of Equation 52 by about 3 orders of magnitude. The SWBC potential, however, did not decrease over a single order of magnitude. This shows that at least in the parameter space that was being searched, the SWBC potential cannot simultaneously reproduce the forces, energies, stresses and IFCs of the training data. It is important to note here that the

parameter space being searched in SWBC was the same as the other potentials; all parameters spanned 2 orders of magnitude. This range was found, also in agreement with the first Tersoff fitting experiment in Chapter 4, to result in fitted parameters that did not approach the intervals of allowed parameter values. The failure of the SWBC potential was attributed to the fact that stresses and IFCs were could never decrease in error simultaneously – all fits either possessed low stress errors and high IFCs errors or vice versa. Regardless, this type of analysis is beneficial in the sense that it shows that it is possible for this approach to determine that a given potential is incapable of reproducing the training data in the parameter search space under consideration. Thus, it can be largely concluded that the SWBC functional form cannot be used to model c-Si accurately for phonons. Even more beneficial is the fact that the training can take a couple hours as opposed to a couple days or weeks presented by other methods and programs [124], so ruling out an entire functional form no longer takes large amounts of time. Furthermore, this brings more confirmation to Hypothesis 3 that many different parameter sets exist for traditional potentials to describe thermal properties, since each line in Figure 17 is the average objective function error of 50 random GA trials converging to vastly different regions of the parameter search space. Due to the failure of SWBC in the parameter search space under consideration, the top three TBC and M3BC potentials with the lowest objective function errors were selected for deeper evaluation of their errors and phonon properties.

5.4.1 Errors in Training and Validation Data

While the evolution of the objective function is shown in Figure 17, the value of the Z itself is not particularly useful, judging by its form in Equation 52. A much more intuitive

measure of error, which is not suitable for fitting, as mentioned in Chapter 4, is the mean percent error (MPE) given by

$$MPE = 100\% \times \frac{1}{M} \sum_{m}^{M} \frac{t_m - p_m}{t_m} \tag{54}$$

Where t_m is the target value (DFT) and p_m is the predicted value (potential calculated value) of configuration m. The target and predicted values in Equation 54 can be any quantity included in the training, such as forces or energies. The errors on the training data are not as useful as errors for validation data, namely data that was not included in the fitting procedure. Validation errors are of more interest since the potentials will be used in MD simulations that sample phase space outside of which they were trained for. The validation data therefore included 50 randomly displaced configurations for which the potentials were not trained on. The errors presented in this section apply Equation 54 to each of the quantities included in the objective function to calculate the MPE of these quantities. Taking the top three candidates of the fitting process for each of the three potentials, Table 1 summarizes the errors in terms of percentage for each of the training quantities for c-Si. The values entered in this table are the mean percent error (MPE) for each training quantity, given by Equation 54. The IFC2 and IFC3 quantities are the 2nd and 3rd order IFCs, respectively.

Table 1 – MPE (%) Validation Set Errors for c-Si

	TBC-1	TBC-2	TBC-3	M3BC-1	M3BC-2	M3BC-3
Force	3.1	3.7	4.4	3.9	5.8	6.2
Energy	0.09	0.06	0.14	0.11	0.07	0.15
Stress	16	13	19	15	26	18
IFC2	17	22	26	29	22	24
IFC3	8.2	10	10	9.5	15	18

The results for c-Si show that all potentials yielded force errors less than 10%. The low errors in energy contribute to almost exact agreements with the lattice parameter. Table 2 summarizes the MPE metrics for c-Ge.

Table 2 – MPE (%) Validation Set Errors for c-Ge

	TBC-1	TBC-2	TBC-3	M3BC-1	M3BC-2	M3BC-3
Force	2.8	4.7	5.1	6.3	4.9	7.5
Energy	0.05	0.03	0.06	0.09	0.14	0.07
Stress	14	18	15	22	19	13
IFC2	20	22	26	41	31	19
IFC3	14	9.7	12	15	11	24

Table 2 shows that the validation errors for the TBC and M3BC potentials for c-Ge are like c-Si in Table 1, in the sense that energy agreement is the best, followed by force as the next best. Stresses and IFCs exhibit worse agreements in percent error. The difficulty in exhibiting stress errors below 10% is due to the complicated off-diagonal stress tensor components associated with randomly displaced configurations. The stress errors for only the volume configurations exhibited errors around 1%, since these configurations possessed equilibrium lattice sites and therefore no off-diagonal stress tensor components.

For both c-Si and c-Ge it is apparent that the IFC errors were the highest, especially the IFC2 errors. Further investigation showed that the majority of the IFC2 error was due to long-range 2nd order IFCs, which was surprising due to the fact that long-range 2-body potentials were included, and it was hypothesized that the GA would therefore be able to match these IFCs. In contrast, the first nearest neighbor 2nd order IFCs exhibited nearly

exact agreement. The 3rd order IFCs also exhibited somewhat better agreements to training data compared to 2nd order IFCs, mainly since the 3rd order IFCs in the training data only extended out to first nearest neighbors. A deeper discussion on these IFC errors is given in Chapter 6.

5.4.2 Structural Property Agreement

Table 1 and Table 2 show that energy errors for all the fitted potentials exhibited excellent agreement consistently below 1%. It is important to recall here that 50 configurations of varying volumes were included in the training set. The low energy errors therefore included these configurations, thus accurately capturing the energy as a function of volume. This excellent agreement in energy as a function of volume directly leads to excellent agreements in equilibrium lattice parameters for c-Si and c-Ge. Figure 18 shows a graphical example of this agreement for c-Si.

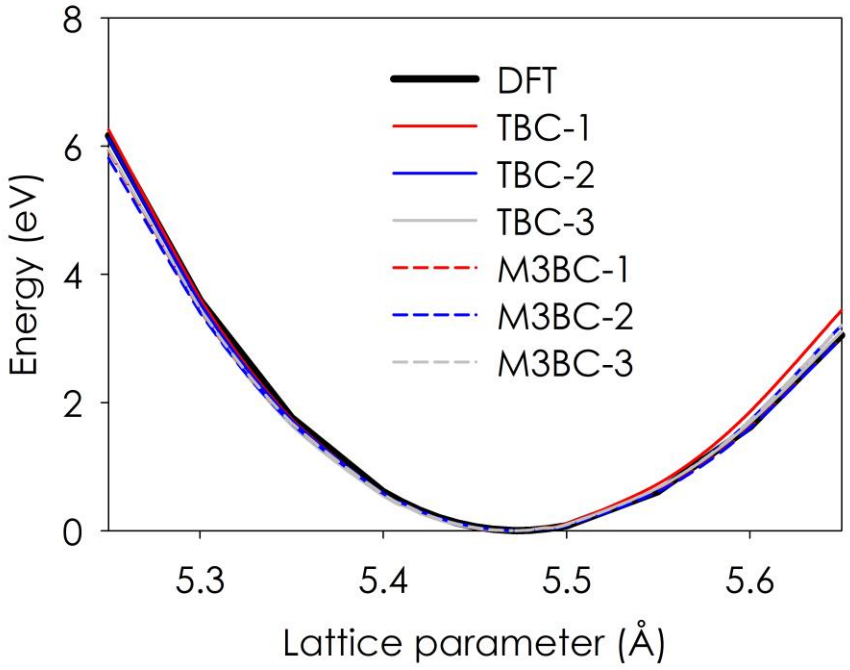

Figure 18 – Energy vs. lattice parameter for DFT and various c-Si POPs.

The energy associated with the lattice parameter in Figure 18 is taken to be 0 eV due to the all configuration potential energies being subtracted by the minimum energy at the equilibrium lattice parameter. This figure shows how the lattice parameter, or cubed root of the system volume, matches the DFT value for all the c-Si POPs. Similar results ensued for c-Ge. Table 3 below shows the percent errors in lattice parameter for c-Si and c-Ge across the top 3 candidates for TBC and M3BC potentials. The lattice parameters are shown to be consistently below 0.1% error from the DFT value.

Table 3 – Lattice parameter percent errors for various POPs in c-Si and c-Ge.

	TBC-1	TBC-2	TBC-3	M3BC-1	M3BC-2	M3BC-3
c-Si	0.010	0.013	0.009	0.010	0.025	0.008
c-Ge	0.012	0.007	0.018	0.014	0.006	0.022

The DFT lattice parameter values of 5.47 Å and 5.74 Å for c-Si and c-Ge, respectively, exhibited small errors from the experimental values of 5.43 and 5.66 [198,199]. Since the target for the POPs is DFT, however, errors with respect to DFT values are of interest. The excellent agreement with DFT lattice parameter for all the POPs ensures that the Brillouin zone itself is scaled correctly via Equation 28 to obtain the frequencies as a function of directions in the Brillouin zone. This is the first and most fundamental step in achieving accurate phonon frequencies, since Brillouin zone space is defined in terms of inverse lattice parameter. With these fitting errors in mind, calculating thermal conductivity with these potentials further answers Question 1, specifically was it sufficient to fit to these quantities to yield accurate thermal property prediction? To answer this question, the top three POPs containing the lowest objective function errors for each functional form and each system were chosen for phonon property calculations.

5.4.3 Phonon Thermal Conductivity

Phonon thermal conductivity is an example of an anharmonic property, depending explicitly on IFCs beyond 2nd order. The thermal conductivity of the POPs generated in this study was calculated via the BTE using the RTA, via Equation 41. In the limit of applicability to crystals, the BTE method has been shown to be equivalent to GK

calculations using EMD [42,201]. However, the BTE method is much faster to evaluate, and can conveniently be done using Alamode. Using the BTE based approach will then allow for the comparison of POPs thermal conductivities to DFT thermal conductivity utilizing DFT IFCs in the BTE approach. The 3rd order IFCs required for this calculation were generated using randomly displaced configurations up to 0.05 Å, and fitting the resulting force-displacement data to the TEP of Equation 22 via least squares. The fitting procedure is the same as obtaining the 2nd order IFCs, except that the force-displacement data contains configurations of larger displacements to sample anharmonic regions of the potential. The thermal conductivity results for the c-Si TBC potentials are shown in Figure 19, compared to low and high temperature experimental results of Inyushkin [202] and Glassbrenner [185].

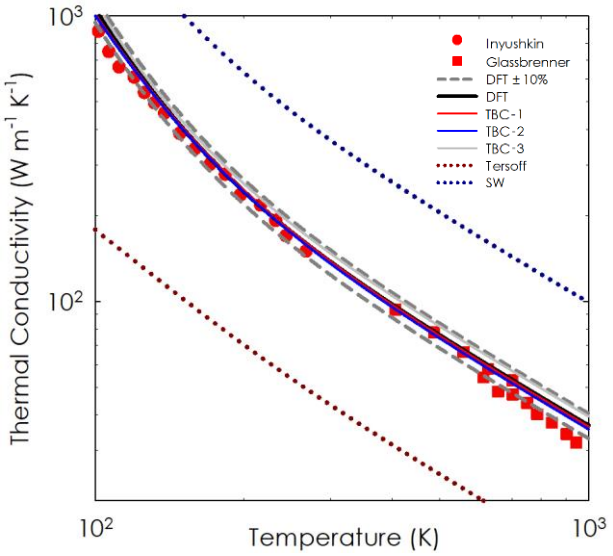

Figure 19 – Thermal conductivity of c-Si for the TBC POPs. The red, blue and grey lines are the TBC-1, TBC-2 and TBC-3 POPs, respectively. The black line is DFT and circles and squares are experiments. Dashed lines are added to show that the c-Si TBC potentials are well within 10% of DFT values across the entire range of temperatures. The blue and red dotted lines show original Tersoff and SW calculated values, respectively. Red circles and squares are experimental results from literature.

The c-Si TBC potentials exhibit excellent agreement to the DFT thermal conductivity with across the entire range of temperatures in Figure 19, with the TBC-1 potential only deviating by a few percent. The c-Si M3BC potential thermal conductivities are shown in Figure 20. The circles and squares in Figure 19 and Figure 20 are experimental values [185,202], and dotted red and blue lines are the original Tersoff [71] and Stillinger-Weber [66] parameter sets.

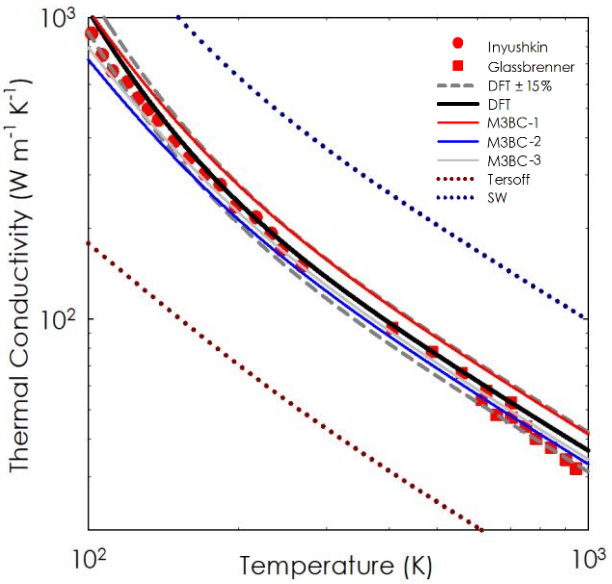

Figure 20 - Thermal conductivity of c-Si for the M3BC POPs. The red, blue and grey lines are the M3BC-1, M3BC-2 and M3BC-3 POPs, respectively. The black line is DFT and circles and squares are experiments. Dashed lines are added to show that the c-Si M3BC potentials are within 15% of DFT values across the entire range of temperatures.

The c-Si M3BC potentials exhibit thermal conductivity errors compared to DFT up to 13%, due to poorer agreement in 3rd order IFCs shown in Table 1. The TBC potentials were able to more accurately reproduce these higher order IFCs due to the inherent flexibility of the Tersoff portion of the potential, which well exceeds the flexibility of the short-range Morse + 3-body harmonic potentials. The thermal conductivity for the c-Ge TBC potentials is shown in Figure 21, compared to experiments of Ozoghin [191] and Glassbrenner [185].

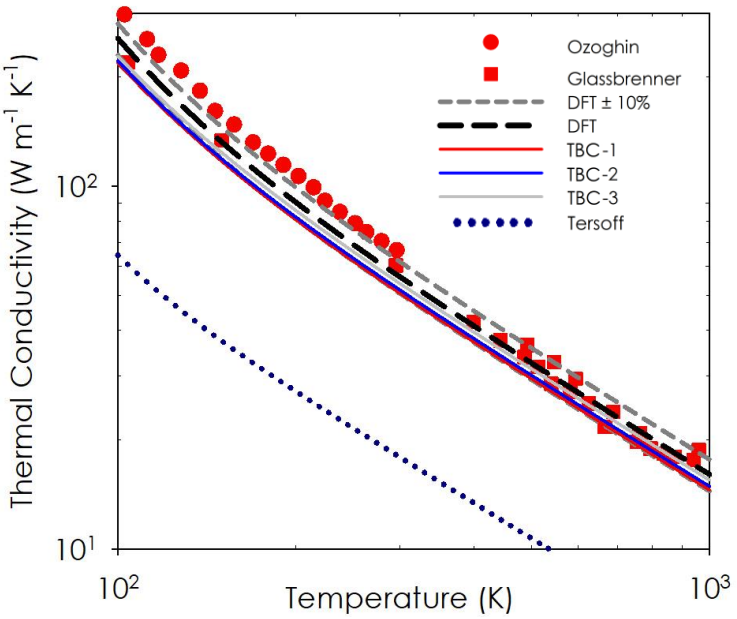

Figure 21 - Thermal conductivity of c-Ge for the TBC POPs. The red, blue and grey lines are the TBC-1, TBC-2 and TBC-3 POPs, respectively. The black line is DFT and circles and squares are experiment. Dashed lines are added to show that the c-Ge TBC potentials are within 10% of DFT values across the entire range of temperatures. The original Tersoff parameter set for c-Ge is shown as a dotted blue line.

The c-Ge TBC POPs fall within 15% error from DFT thermal conductivity. The circles and squares, again, are experimental values [185,191] and the blue dotted line is the thermal conductivity using the original Tersoff parameters [112]. The thermal conductivity results for the top three c-Ge M3BC POPs are shown in Figure 22.

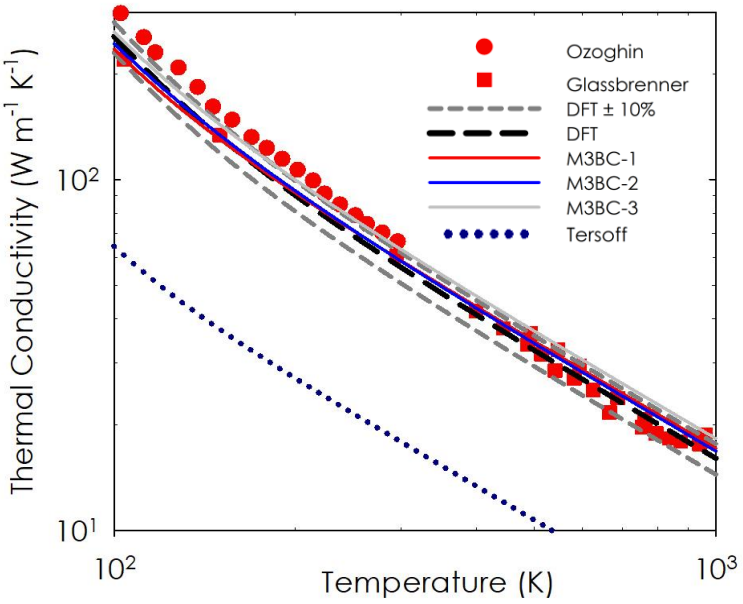

Figure 22 - Thermal conductivity of c-Ge for the M3BC POPs. The red, blue and grey lines are the M3BC-1, M3BC-2 and M3BC-3 POPs, respectively. The black line is DFT and circles and squares are experiments. Dashed lines are added to show that the c-Ge M3BC potentials are within 15% of DFT values, except for deviations in M3BC-3 which deviate up to 17% at higher temperatures.

The thermal conductivities of all POPs for c-Si and c-Ge show excellent agreement with DFT over the range of temperatures from 100 K to 1000 K, especially compared to original potentials for such systems. The best agreements, seen with the c-Si TBC-1 potential, corresponds with excellent agreements in 3rd order IFCs from Table 1. Contrarily, the worst agreement with DFT thermal conductivity with c-Ge M3BC-3 is seen from the poorer agreements in 3rd order IFCs in Table 2. These thermal conductivity results suggest that all

the POPs sufficiently reproduce the necessary quantities to predict thermal conductivity within ~10% error of accurate DFT predictions. This also suggests that the POPs developed herein accurately capture the anharmonic properties of the potential sufficiently to achieve such agreement. The c-Si TBC-1 potential, for example, possessed the best agreement to DFT thermal conductivity (< 2% error across all temperatures) and possessed the lowest IFC3 error (< 10%) as seen in Table 1. While the anharmonic properties of the lattice are well described using these POPs, it is equally important to accurately describe harmonic properties since these determine modes in the material [35]. Phonon frequencies as a function of directions in the Brillouin zone, or phonon dispersions, are an excellent measure the harmonic behaviour [26] and will therefore be used to further investigate the efficacy of these POPs.

5.4.4 Phonon Dispersions

Harmonic properties are observed via the 2nd order IFCs, which enter phonon frequency calculations or phonon dispersions for crystalline materials [116]. Phonon dispersions for DFT and the obtained POPs are calculated via the direct displacement method herein, by obtaining the 2nd order IFCs via fitting force-displacement data to the TEP in Equation 22. The IFCs are then used to calculate the phonon frequencies as a function of directions in the Brillouin zone via Equation 28. This procedure was replicated for c-Si and c-Ge for all the POPs, using randomly displaced configurations up to 0.01 Å for the force-displacement data involved in TEP fitting. The TEP fitting process involved least squares minimization in the Alamode program [116]. Alamode was also used to solve for the phonon frequencies via Equation 28. Despite the relatively large 2nd order IFC (IFC2) errors in Table 1 and Table 2, compared to other fitting quantities, the phonon

dispersions of POPs for c-Si and c-Ge exhibited qualitative agreement to DFT quantities. The phonon dispersion for the c-Si TBC potentials are shown in Figure 23, along with DFT and neutron scattering experimental values [203].

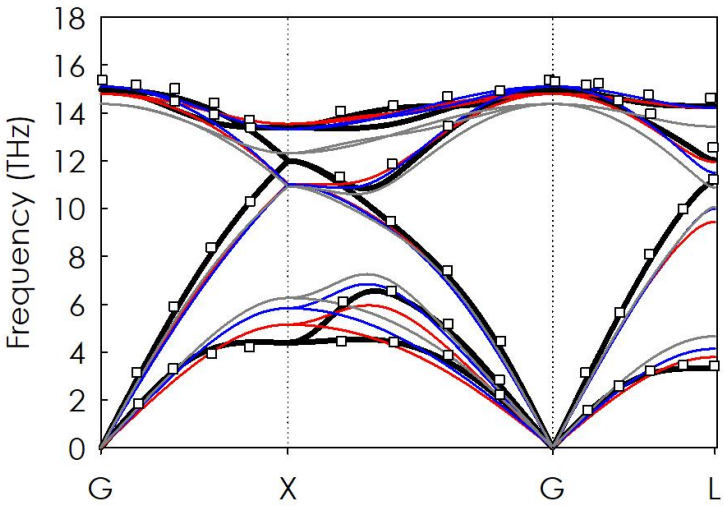

Figure 23 – Phonon dispersion for c-Si TBC POPs. The red, grey and blue lines are the TBC-1, TBC-2 and TBC-3 potentials, respectively. The black lines are the DFT (target), and the white squares are experimental neutron scattering values from literature.

The phonon dispersions for the c-Si M3BC potentials are shown in Figure 24.

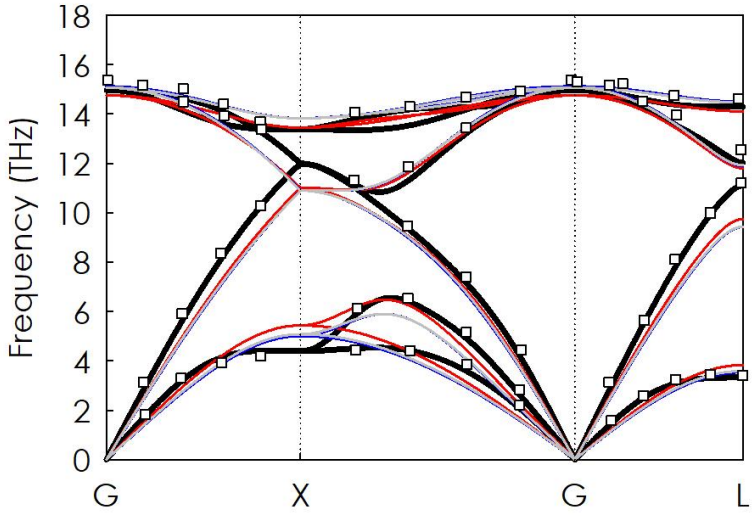

Figure 24 – Phonon dispersion for c-Si M3BC POPs. The red, grey and blue lines are the M3BC-1, M3BC-2 and M3BC-3 potentials, respectively. The black lines are the DFT (target), and the white squares are experimental values.

While Figure 23 and Figure 24 show qualitative agreement to DFT and experimental results, DFT still vastly outperforms the POPs in experimental phonon dispersion agreement. It is important to compare to existing parameter sets, however, to show that the POPs at least outperform traditionally used potentials. Phonon dispersions compared to DFT and experimental results for the original Tersoff [71] and Stillinger-Weber [66] are shown in Figure 25.

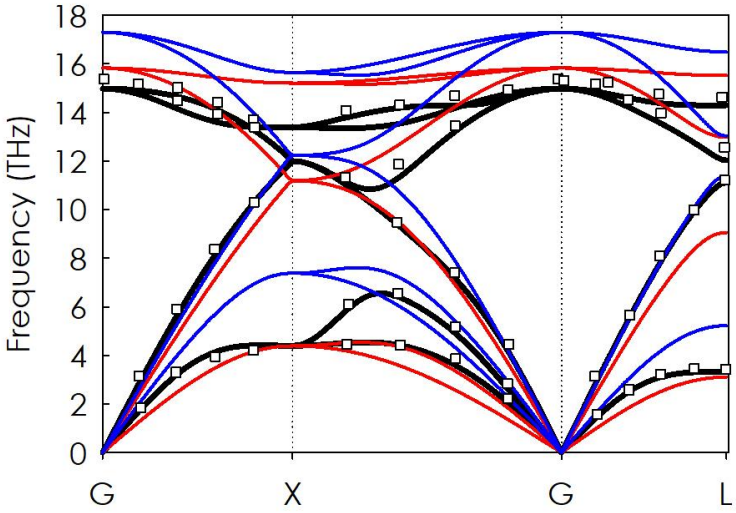

Figure 25 – Phonon dispersion curves for c-Si using the original Tersoff and Stillinger-Weber potentials (blue and red lines, respectively) compared to DFT and experimental values (black lines and white squares, respectively).

Although the c-Si POPs don't exactly match DFT phonon dispersions, they still perform much better than existing potentials still used today as seen in Figure 25. Especially in the optical phonon branches (higher frequencies), the original Tersoff [71] and Stillinger-Weber [66] potentials tend to overestimate the frequencies. The POPs developed herein are therefore a major improvement over these original potentials in terms of harmonic phonon

properties. Similar qualitative agreement was seen with c-Ge, the phonon dispersions for the c-Ge TBC potentials are shown in Figure 26 compared to experimental values [204]

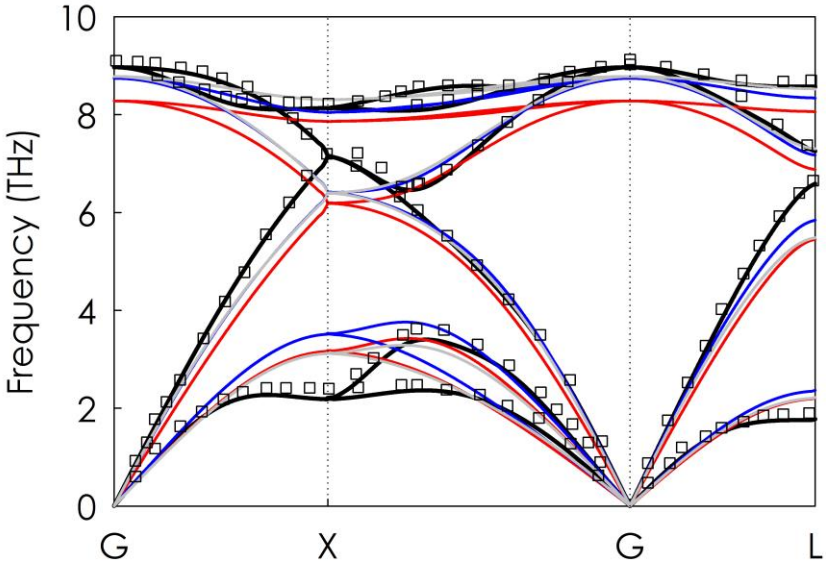

Figure 26 – Phonon dispersions for c-Ge TBC potentials. The red, grey and blue lines are the TBC-1, TBC-2 and TBC-3 potentials, respectively. The black line is the DFT (target) phonon dispersion, and white squares are experimental values.

The phonon dispersions for the c-Ge M3BC potentials are shown in Figure 27, along with DFT and the same experimental values [204].

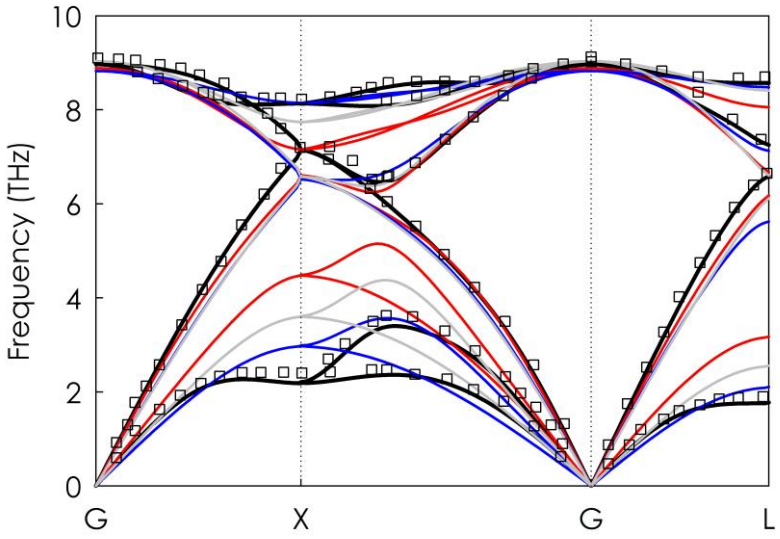

Figure 27 - Phonon dispersions for c-Ge M3BC potentials. The red, grey and blue lines are the M3BC-1, M3BC-2 and M3BC-3 potentials, respectively. The black line is the DFT (target) phonon dispersion, and white squares are experimental values.

As seen in the phonon dispersion figures, all the of the c-Si and c-Ge POPs exhibit decent agreement in dispersion. Figure 27 is notable due to the worsening trend of phonon dispersions between the POPs. Referring to Table 2, the IFC2 errors for c-Ge M3BC potentials follow the same trend as seen in Figure 27. This example shows that, at least for this test case, the agreement in 2nd order IFCs can be proportional to the qualitative agreement and frequency accuracy in the Brillouin zone. Such an observation better supports Tenet 3 of the POPs approach, noting that the viability of a potential to predict phonon frequencies is determined by its agreement in 2nd order IFCs. All the POPs, however, were unable to reproduce the well-known flattening of the acoustic branch at the X point of the Brillouin zone boundary. The Brillouin zone boundary corresponds to long-range interatomic interactions and IFCs [115,116]. According to Hypothesis 4, inclusion of traditional long-range potentials should have accurately captured these long-range

interactions, thereby resulting in the characteristic flattening at the X point. None of the potentials were able to resolve these long-range IFCs nor the corresponding phonon branch flattening and thus we conclude that Hypothesis 4 is incorrect/not true. Furthermore, IFC2 errors for all potentials seemed to be the highest error quantities associated with these POPs (Table 1 and Table 2). Investigating this further, it is apparent that over 90% of the IFC2 errors are the long-range harmonic IFCs. This is rather surprising since 50 trials of the GA, all finding vastly different parameter sets, were not able to achieve accurate long-range harmonic IFCs despite the addition of long-range potentials. Inability of traditional long-range potentials to properly match the phonon dispersion curves shows that Hypothesis 4 was wrong, and that this issue warrants further investigation.

5.5 Summary

This chapter walked through application of the POPs Tenets to c-Si and c-Ge, namely the attempted reproduction of forces, 2nd and 3rd order IFCs by fitting via the GA for three different functional forms. Brute force fitting for 50 trials with the GA showed that some potentials, namely SWBC in this case, are not able to simultaneously reproduce all quantities in the objective function. Average error in DFT fitting targets across all fitting trials for the TBC and M3BC potentials decreased by three orders of magnitude, thus confirming Hypothesis 3 and the validity of Tenet 4 that multiple parameter sets exist to match quantities relevant to phonons (i.e., forces and IFCs). This is further confirmed by showing that the top three POPs for each case resulted in accurate thermal conductivity predictions (<10% error in experiments). Despite accurate thermal conductivity prediction, especially compared to the original Tersoff and Stillinger-Weber potentials, none of the POPs could properly match DFT or experimental phonon dispersions. This was surprising

since traditional long-range 2-body interactions were included, thus showing that Hypothesis 4 is false; it seems that traditional long-range interactions cannot accurately capture long-range harmonic IFCs. This is not an issue of the fitting procedure but rather an issue of the underlying descriptions of atomic geometry in these potentials; the 2-body radial geometric descriptor discussed in Chapter 2. It is desirable to accurately predict both thermal conductivity and harmonic modal properties so that we may calculate accurate thermal conductivity for the proper underlying reasons (i.e., the vibrational modes that contribute to it) [35,54]. This therefore warrants an investigation on the failure of traditional long-range potentials to properly predict harmonic phonon properties, so that such issues may be alleviated.

CHAPTER 6. MODELING LONG-RANGE INTERACTIONS

While the POPs obtained in Chapter 5 performed well at predicting thermal conductivity, they failed to properly predict phonon dispersion curves. This main discrepancy was mainly seen at the Brillouin zone boundaries, associated with long-range interatomic interactions [43,115,116]. Since parameters of long-range central potentials, utilizing the pairwise distance geometric descriptor, were exhaustively searched using the GA, this shows that something may be wrong with the functional forms of such potentials that limits their ability to describe long-range interactions.

6.1 Limitations of Central Potentials

Central potentials assume that the energy of interaction between two bodies depends only on the radial distance between those bodies. The radial symmetry associated with a potential depending on this geometry assumes that changes in the perpendicular directions about a given radial axis are all equivalent, and therefore the potential cannot resolve differences in these directions if they exist. In fact, radial potentials can mathematically only experience two unique IFCs in the radial and tangential direction. Therefore, it is clear that a radial based functional form is intrinsically incapable of describing the 9 different (6 unique) 2nd order IFCs needed for every pair. This is mathematically realized since a central potential only possesses 2 unique 2nd derivatives in the radial and tangential directions, $\frac{\partial^2 U(r)}{\partial r^2}$ and $\frac{1}{r}\frac{\partial U(r)}{\partial r}$, respectively. Since central potentials can only possess two unique IFCs, they cannot capture the true nature of IFCs given by their definition in the TEP of Equation 22. The true 2nd order IFCs form a matrix of 9 IFCs for each 2-body interaction.

This is often a symmetric matrix, resulting in 6 unique IFCs for each 2-body interaction [173]. In many crystalline materials, especially those with more than a single basis such as diamond c-Si and c-Ge, these 6 IFCs can all be unique [34,173]. Central potentials are unable to resolve these unique IFCs for a single 2-body interaction, due to the fact they only have two unique IFCs. This limitation is more readily visualized in three dimensions in Figure 28, which further elucidates the issue of radial symmetry with central potentials.

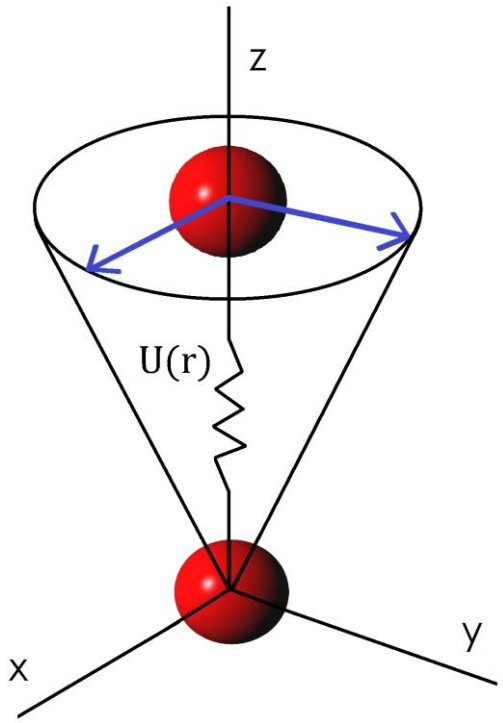

Figure 28 – Visualization of a radial 2-body interaction described by a central potential. All motions of the top atom in any direction in the plane of the cone (e.g., the blue vectors) are considered equal due to radial symmetry.

The top atom in Figure 28 may move in the plane of the cone, which is parallel to the xy axis. Two blue vectors represent possible motions in the x or y direction, and every other motion in this plane is defined as a linear combination of these vectors. According to central

potentials, these two motions result in identical forces and therefore yield identical IFCs, due to radial symmetry. Originally unknown prior to the investigation of Question 4, this assumption was shown in early works to be incorrect for covalent solids due to their highly inhomogeneous electronic structure [205]. Earlier researchers in LD also noted that central forces are not sufficient to achieve phonon frequency flattening at Brillouin zone boundaries [206], but such work has eluded the modern use of long-range central potentials for phonon properties [79]. This further confirms that Hypothesis 4 is incorrect; traditional long-range potentials do not possess the necessary flexibility to properly describe phonon frequencies at the Brillouin zone boundaries in semiconductors, no matter how they are parameterized. Therefore, central potentials will never in general result in accurate phonon dispersions at the edges of the Brillouin zone, although some special cases may work (e.g., a noble element crystal).

This limitation of central potentials has greatly eluded the modern phonon transport community, with many reports stating that they were simply unable to reproduce elastic properties properly [85]. More recent studies simply state the inability of typical pairwise central potentials to exactly reproduce phonon dispersions, without further investigation or discussion [81,207-209]. Since a major goal of atomistic phonon transport is to accurately study phonon transport properties in terms of the correct modes and frequencies, and accurate frequencies may only be obtained via long-range interactions [116], it is important to highlight and alleviate this issue associated with traditionally used long-range central potentials. This is a limitation of the models used and not of the parameterization process. To progress further, traditionally used potentials must be abandoned in favor of potentials that can more accurately reproduce modal characteristics and phonon frequencies. Specifically,

potentials possessing flexibility for long-range radially asymmetric interactions are required to describe all of the unique IFCs.

6.1.1 Long-Range Radially Asymmetric Interactions

Uniqueness of the IFCs for different directions in long-range interactions cannot be explained in terms of simple 2-body radial geometry descriptors, and these interactions extend well beyond 1st nearest neighbors. Clearly, a new description of geometry is needed in order alleviate this issue. One possibility is incorporating long-range 3-body angular interactions along with the radial interactions. Figure 29 shows how the N-body expansion in Equation 6, using only harmonic terms, truncated up to 3-body interactions can reproduce exact 1st nearest neighbor IFCs in c-Si. The potential used in this figure is given by

$$U = \sum_{ij} k_2 (r_{ij} - r_0)^2 + \sum_{ijk} k_3 (\theta_{ijk} - \theta_0)^2 \tag{55}$$

where r_0 and θ_0 are parameters representing the equilibrium 2-body distances and angles for the 1st nearest neighbors, respectively. Parameterizing this potential using the GA yields a 2-dimensional optimization problem to solve for k_2 and k_3, the constants affecting the

strength of two and three body interactions, respectively. The only quantities included in the objective function were the 2nd order IFCs.

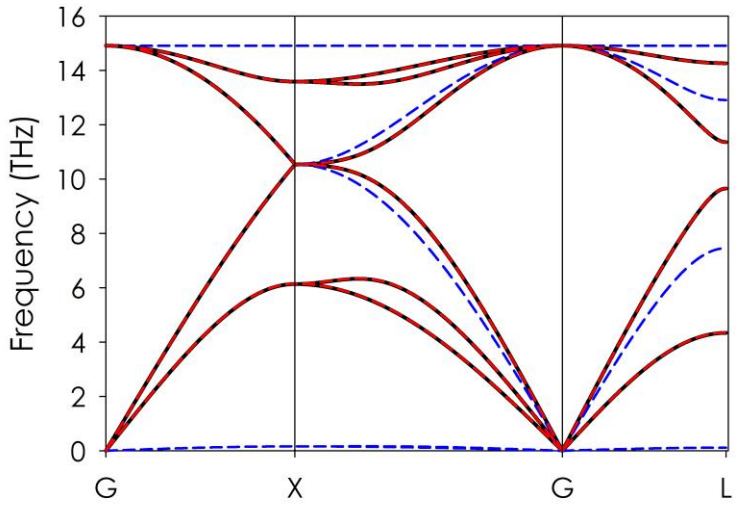

Figure 29 – Two and three body harmonic potential including first nearest neighbors of c-Si. The black line is the TEP truncated up to first nearest neighbors, the red dashed line is the two and three body harmonic potential, and the blue dashed line is just the two body harmonic potential. The 2+3 body harmonic potential can exactly reproduce first neighbor TEP results, unlike the 2-body potential alone.

The GA could exactly reproduce the 2nd order IFCs up to 1st nearest neighbor using the full expression in Equation 55. When only the two-body term was used, however, the problem turns into a simple one-dimensional optimization and there is no good solution, as shown by the disagreement of the blue dashed line in Figure 29. This shows that a Equation 55 can match results of the TEP and resolve its IFCs, but applying this potential past 1st nearest neighbors is problematic due to the need of a unique angle term for longer ranged neighbors. An easier alternative is using the TEP, which serves as the definition of the IFCs themselves in Equation 22. More importantly, the TEP describes geometry in such a way that the uniqueness of IFCs in all directions can be resolved. The convergence of TEP phonon dispersion as cutoff is increased for c-Si is shown in Figure 30.

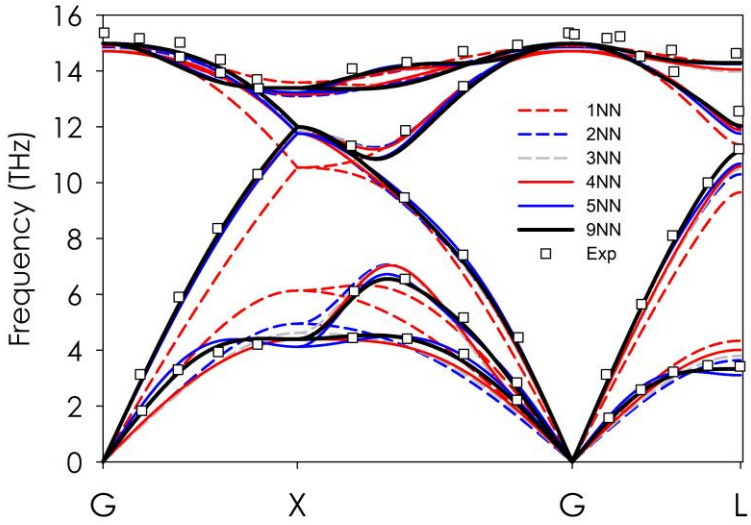

Figure 30 – 2nd order TEP phonon dispersions for various cutoffs in c-Si. The cutoffs range from values including 1st nearest neighbors (NN) up to 9th NN, for which the phonon dispersion converges almost exactly with experiment.

Figure 30 shows that as the cutoff of the TEP is increased from 1st nearest neighbour (1NN) interactions up to 9th nearest neighbors (9NN), the predicted phonon frequencies converge to experimental values. It is also seen that the long-range 2nd order TEP can reproduce the characteristic frequency flattening at the Brillouin zone boundary, unlike the long-range central potentials used in Chapter 5. The long-range 2nd order TEP exactly reproduces the correct phonon dispersion as compared to DFT, and therefore accurately describes the modal characteristics of the system. The TEP is therefore a candidate for serving as a POP functional form. While the TEP can exactly reproduce derivatives of the energy by definition, thus fully satisfying the POPs Tenet 2, its reported use in MD simulations is minimal, and the few applications of the TEP did not involve MD simulations above room temperature [210]. Thus further investigation into the use of the TEP for MD was needed.

6.2 Molecular Dynamics with the TEP

The 2nd order TEP potential will be denoted as TEP-2, expansions up to 3rd order will be denoted TEP-3, expansions up to 4th order will be denoted TEP-4, and so forth. When trying to perform MD simulations using TEP-2, c-Si was only stable up to 100 K. The system would quickly fall apart, and atoms would experience large displacements, noted by the surge in potential energy in Figure 31.

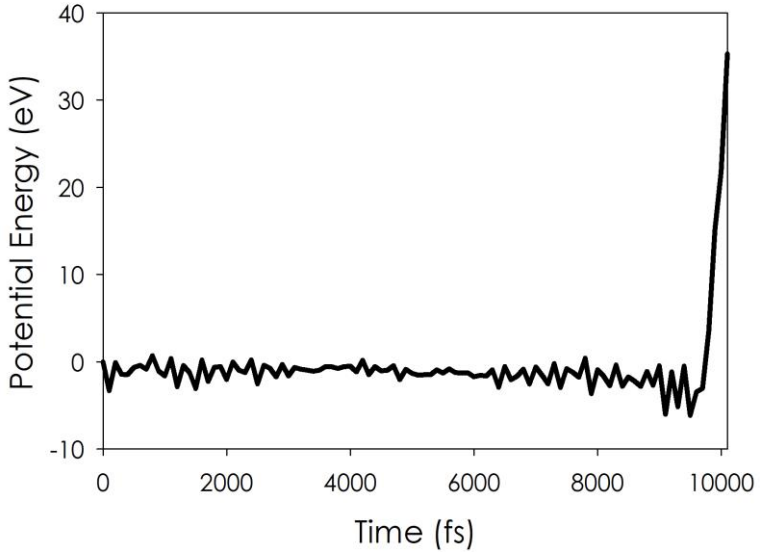

Figure 31 – TEP instability at 300 K for c-Si in a NVE ensemble. The rise in potential energy around 10 ps denotes unphysically large atomic displacements when the system collapses.

The immediate cause of this instability was unclear and raised important question; if the forces and IFCs predicted by the TEP are accurate, what causes the instability? Unlike the instabilities observed in Chapter 4 which seemed to arise from errors in pressure and stress compared to DFT, the TEP predicts accurate stresses (<10%) for randomly displaced configurations. Furthermore, it is of interest to incorporate the TEP in MD simulations of thermal transport, so we can reap the benefits that general MD methods have over the PGM, which begs a seocnd question; will eliminating the unknown cause of instability allow the

TEP to be used in MD simulations? First and foremost, the first question dealing with the underlying cause of instability must be investigated. Originally, it was hypothesized that the 2nd order interactions, which diverge to positive and negative infinity potential energy as shown by the TEP-2 PES in Figure 32, lead to unrealistically large forces and energies at high temperatures (large displacements).

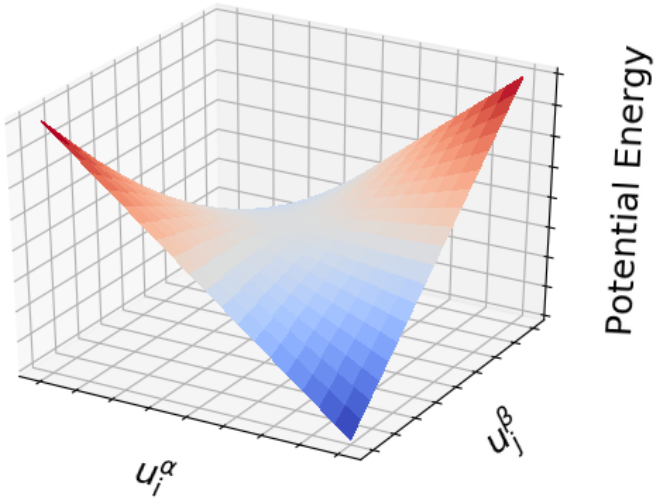

Figure 32 – TEP-2 PES for a single 2-body interaction as a function of displacements of atoms i and j. The divergence to negative infinity was the original hypothesis for instabilities at elevated temperatures corresponding to large displacements.

Potential energy for the TEP-2 in Figure 32 is plotted in terms of the TEP geometric descriptors, the displacements of atoms i and j in α and β Cartesian directions. It is evident that the slope of this PES increases linearly, and that for large displacements, the resulting forces would diverge. This led to the original hypothesis that the harmonic approximation of the TEP-2 leads to instabilities for higher temperatures, or large displacements. With this hypothesis in mind, it was of interest to investigate how the TEP PES could be modified somehow, so that these large forces no longer arise.

6.3 Enhancing TEP Stability

Attempts at enhancing stability of the TEP in MD simulations were be based on the hypothesis that large forces in the harmonic approximation are invalid, and thus cause instability. Several potential solutions were then devised to obtain more stable forces: (1) using higher order expansions in the TEP, (2) combining a long-range TEP to get correct long-range IFCs, along with traditional stable short-range potentials like Tersoff, and (3) modifying the TEP PES to smooth the divergence and large forces. Incorporating higher order expansions was the simplest of these tasks, since IFCs up to 4th order are readily calculable [116] and was thus tried first.

6.3.1 Higher Order Expansions

A previous study performed MD simulations using the TEP truncated to a 4th order expansion (TEP-4), and calculated accurate thermal conductivity up to room temperature in covalent alloys [210]. Accurate thermal conductivity in c-Si requires 3rd order IFCs up to 2nd nearest neighbors when using the BTE [116], and the 4th order terms were suggested in previous studies to ensure greater stability in MD simulations [210]. TEP-4 MD simulations were therefore tested with c-Si and were indeed more stable than TEP-2, with stability occurring up to 300 K. Higher temperatures, however, resulted in unstable dynamics and similar surges in potential energy as seen in Figure 31. It was therefore thought that 4th order terms were not sufficient for higher temperatures, but calculating 5th and 6th order terms is quite challenging [116,173]. Simple 6th order self interactions, however could readily be added in the following form:

$$U = \sum_i \lambda_i u_i^6 \tag{56}$$

where λ_i is a parameter prefactor governing the strength of the self-interaction. For large values of λ_i a potential well is created around the atoms that creates large restoring forces when the atoms move far from equilibrium. The harmonic phonon dispersion with small displacements is therefore only slightly affected, as shown via Figure 33.

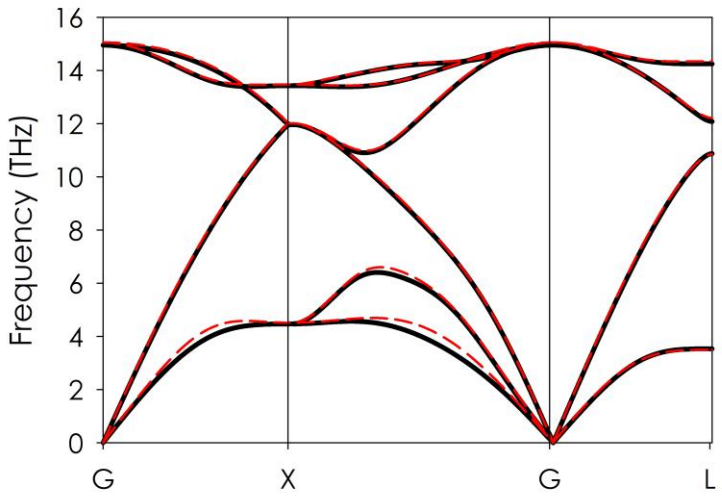

Figure 33 – Phonon dispersion for TEP + 6th order term given in Equation 56, with a prefactor value of 100 $eV / Å^6$. The black line is the original DFT TEP-2 and the red dashed line is the TEP-4 + 6th term.

Figure 33 shows how the 6th order term of Equation 56 hardly affects the phonon dispersion and 2nd order IFCs, which may be worth it for the sake of additional MD stability. It was thought that such an interaction would create a strong potential well for each atom, thus restricting them from vibrating too far away from their equilibrium positions. The MD using the 6th order TEP added to Equation 56 indeed exhibited seemingly stable dynamics up to 1000 K, but the dynamics were visually and obviously unrealistic. Atoms tended to

vibrate with a mean square displacement over an order of magnitude higher than what the originally should according to DFT-MD simulations, and the forces were more than an order of magnitude higher than what is seen during an MD simulation below 1,000 K. This suggests that the artificial well generated by Equation 56 leads to unrealistic dynamics at elevated temperatures, even though potential energy and dynamical stability are satisfied. Nevertheless, accurate dynamics and phonon transport at higher temperatures is necessary to utilize MD simulations to study such phenomena. If the 6th order term resulted in too much restriction, although it was stable, it was thought that traditional analytical potentials such as Tersoff, which are known to possess MD stability when properly parameterized [58,66], might be able to cancel out the instability of the TEP when the two potentials are combined.

6.3.2 Anharmonic Core Potentials + TEP

The addition of higher order TEP terms only seemed to increase MD stability up to room temperature, and the addition of an artificial 6th order well increased stability but again resulted in unrealistic forces and dynamics at elevated temperatures. It was therefore hypothesized that the 2nd order TEP could be used as a long-range potential along with some traditional potential, such as Tersoff or Morse, for the anharmonic first nearest neighbor interactions. The anharmonic core potential was assumed to be able to stabilize the system better than just the pure TEP, since the largest IFCs and forces stem from first nearest neighbors and decay rapidly with distance [33]. Parameterization of a Tersoff + TEP-2 using the GA in the POPS program yielded solutions that possess negligible errors in 2nd order IFCs, but the stability of these potentials was no better than the TEP expanded up to 4th order.

The attempts at stabilizing the TEP up to this point involved additions to the TEP-2 functional form in the form of higher order expansions, and short-range traditional potentials. All these attempts still resulted in unstable TEP dynamics, especially near room temperature and above. It therefore seemed at that point, that additions to the TEP would not alleviate the stability issue, and that modifications to the PES itself must be required. Observing the TEP-2 PES in Figure 32, and noting the hypothesis that the divergence of forces and potential energy at large displacements causes instability, it was therefore of interest to alleviate this divergence by modifying the TEP-2 PES. This can be achieved using cutoff functions to smooth the PES to constant potential energy at large displacements, thus resulting in zero forces at large displacements at higher temperatures.

6.3.3 TEP with Cutoff Functions

To alleviate the potential energy divergence seen in Figure 32 for the TEP-2, mathematical formulations were developed to smooth the transition such that the slope of the PES would decrease at large displacements. The goal here was to come up with mathematical formulations that smoothed the TEP-2 PES past a certain displacement. An easily visualized example of such smoothing for the TEP-2 self-interaction is shown in Figure 34.

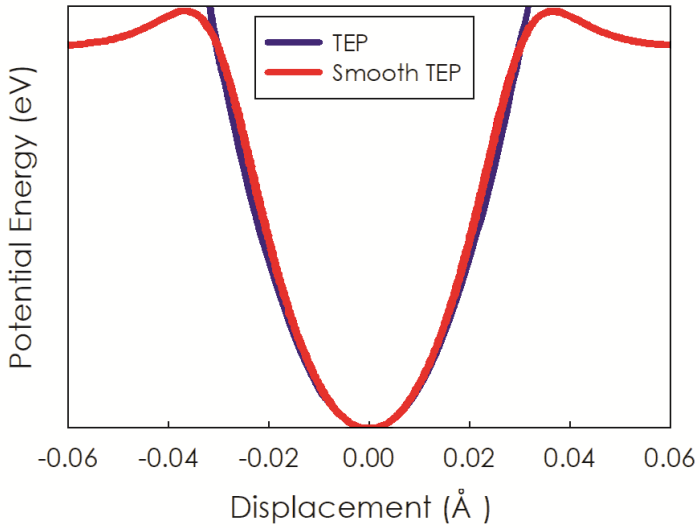

Figure 34 – Smoothing of the TEP-2 self-interaction. The blue line is the original TEP-2 and the red line incorporates a smoothing function.

Figure 34 shows the first attempt at smoothing the TEP-2 function, and this example begins smoothing around a displacement magnitude of 0.04 Å as shown in the figure. The theory built into producing Figure 34 revolved attempting to smoothly connect two functions. The procedure for the smoothing involved first choosing cutoff functions for each side of the parabolic shape, $s_1(x)$ and $s_2(x)$. The choices here were the hyperbolic tangent cutoffs $s_1(x) = 0.5 + 0.5\tanh\left(\frac{x-a}{b}\right)$ and $s_2(x) = 0.5 + 0.5\tanh\left(\frac{x+a}{b}\right)$. A function is then defined such that $h(x) = a \cdot s_1(x) + x(1 - s_1(x))$, which is the function $y(x) = x$ converging to the constant a on the right side. Another function is then defined such that $f(x) = h(x) \cdot s_1(x) - a(1 - s_2(x))$, which is $h(x)$ converging to a on the left side. Rearranging to get in a different form and factoring out an x, we have

$$f(x) = x \cdot f_c(x) = x\left[s_2(x)(1 - s_1(x)) + \frac{a}{x}\left(s_2(x)s_1(x) + s_2(x) - 1\right)\right] \tag{57}$$

For two independent variables x and y we can now write $f(x,y) = (x \cdot f_c(x))(y \cdot f_c(y))$, which is in the form of the TEP-2 multiplied by cutoff functions for each displacement. The TEP-2 with cutoff functions is therefore given by

$$U = \frac{1}{2}\sum_{ij} U_{ij} = \frac{1}{2}\sum_{ij,\alpha\beta} \Phi_{ij}^{\alpha\beta} u_i^{\alpha} u_i^{\beta} f_c\left(u_i^{\alpha}\right) f_c\left(u_i^{\beta}\right) \tag{58}$$

The parameter a in Equation 57 determines the cutoff distance and b determines the sharpness of the cutoff. Care must be taken with Equation 57 to only apply the cutoff function when the displacement is nonzero, otherwise a non-real number occurs since the independent variable appears in a denominator. A simple if-statement in the MD code prevents this, namely if the displacement is nonzero, then use Equation 58, otherwise, use the normal TEP in Equation 22.

It was hypothesized that the use of Equation 58 combined with an anharmonic first nearest neighbor potential such as Tersoff would allow for stable MD simulations. Varying values of the a and b parameters were therefore tested in MD simulations of 1 ns up to 1000 K, using a 0.5 fs timestep. While certain combinations of a and b yielded more stability at elevated temperatures than the original pure TEP, in the sense that stable MD existed for longer times, all the cases failed before 1 ns. The type of instability was different than for the pure TEP case. This was no longer a dynamical instability where the atoms vibrated out of their equilibrium sites at low temperatures. Instead, the issue now was that

the entire system of atoms would always translate in a random direction for MD simulations initialized with random velocities. Normally in MD simulations, the system center of mass remains fixed, unless an external force is applied to make the system translate [211]. Incorporating the TEP-2 with cutoff functions in 58, however, would result in translating MD simulations where the center of mass translates. The extremity of this translation is seen in Figure 35, where the center of mass deviates well over 100 Å from the original center of mass within 1 ns of simulation time.

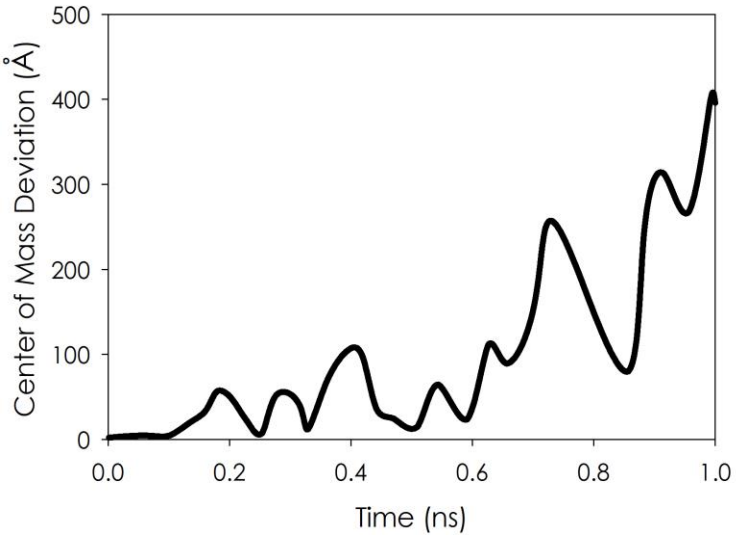

Figure 35 - Center of mass distance from the initial position as a function of time during a 300 K MD simulation of c-Si using the TEP with cutoff functions in Equation 58.

Translations involved with using the TEP with cutoff functions in Equation 58 caused the entire system to translate greatly from its initial position, thus effectively translating outside the potential well which approximates the TEP-2 in Figure 34. It is critical to note here that the TEP-2 potential well does not translate with the system, since the geometric descriptors (atomic displacements) of the TEP reference absolute Cartesian coordinates for equilibrium positions. This was problematic in terms of phonon calculations since the

system would translate outside the region described by the TEP and into the cutoff region in the flat area of the red curve in Figure 34, thus effectively shutting off the TEP forces.

In the absence of TEP forces, the system retains the intrinsic stability of the Tersoff potential, but the original problem of properly describing IFCs remains. Alleviating this translation issue was therefore of utmost importance in utilizing the cutoff TEP for MD simulations. It was originally hypothesized that this translation was due to the bump of the blue curve seen in Figure 34, but the mathematical formulation developed here did not allow for alleviation of this bump unless the function becomes less smooth, which would negatively affect stability in a different way, by introducing a discontinuity. A different formulation of the cutoff TEP was therefore be developed.

To avoid the bumps of the previously developed cutoff TEP, another functional form approximation to the TEP was sought that more smoothly approached zero slope at the cutoff distance without experiencing any bumps in the PES. This led to the development of the following hyperbolic tangent approximation to the TEP-2, given in Equation 59

$$U_{ij}^{\alpha\beta} = \Phi_{ij}^{\alpha\beta} r_c^2 \tanh\left(\frac{u_i^{\alpha}}{r_c}\right)\tanh\left(\frac{u_j^{\beta}}{r_c}\right) \tag{59}$$

where the cutoff at which the potential starts to decrease in slope is given by r_c. The PES for non-self-interactions is given by Figure 36.

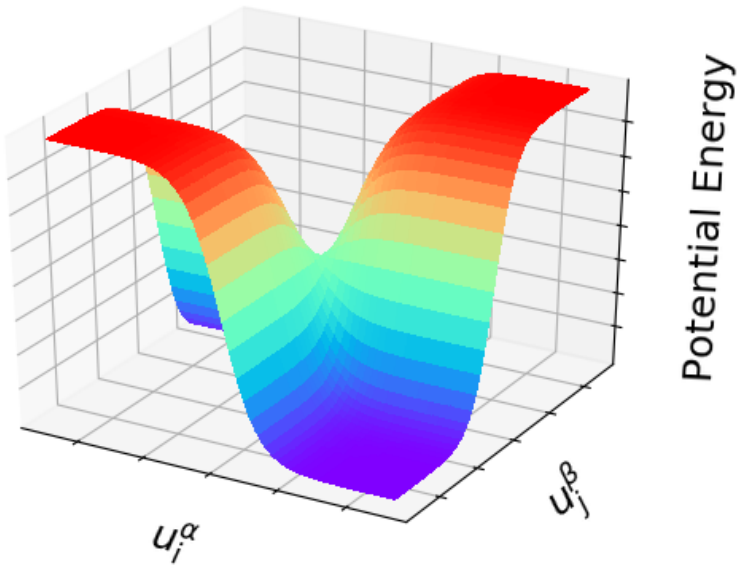

Figure 36 – PES of the hyperbolic tangent approximation to the TEP via Equation 59.

Although the hyperbolic tangent approximation to the TEP is smoother, surprisingly, the center of mass translation in MD simulations still occurred. It was hypothesized that the linear momentum could be redistributed every timestep to freeze the system from translating, thus forcing the atoms to reside in the TEP PES. While this fixed the translation issue, this caused the temperature to rise along with the original potential energy instability seen in Figure 31. This shows that even in the absence of TEP-2 forces associated with large displacements, unstable dynamics still resulted.

The original hypothesis that eliminating the larger forces for large displacements would yield stability was therefore wrong. This begged the question of when does the harmonic approximation (i.e., TEP-2) become a poor representation of the PES, namely at

what level of displacement does the anharmonicity cause a strong deviation from TEP-2? The answer to this question was probed by using DFT, specifically by displacing a single atom from equilibrium in a crystal. In this test case, the displaced atom will possess the only nonzero displacement, and will therefore it will be the only atom responsible for the forces experienced by all other atoms via the TEP-2 force equation:

$$F_i^{\alpha} = -\sum_{j,\beta} \Phi_{ij}^{\alpha\beta} u_j^{\beta} \tag{60}$$

Displacing a single atom j in the β Cartesian direction will therefore influence the force on atom i in the α direction, linearly in proportion to the 2nd order IFC $\Phi_{ij}^{\alpha\beta}$. Conceptually, one would expect the forces on all other atoms to initially be linear with respect to the one atom being displaced. This would correspond to the regime where the harmonic approximation is most applicable and TEP-2 would accurately capture the slope. However, the premise of the previous hypothesis that the forces become too large for large displacements is predicated on the notion that at some level of displacement, we would expect to see major deviations from the initial linear trend yielding much smaller forces than would be predicted by TEP-2. To test the validity of this harmonic approximation, a single atom in a c-Si crystal was incrementally displaced in the x direction up to 0.4 Å. The resulting forces on other atoms were calculated via DFT, using the same settings in Section 5.1.1. The forces on 1st NN atoms, of the displaced atom, are shown in Figure 37.

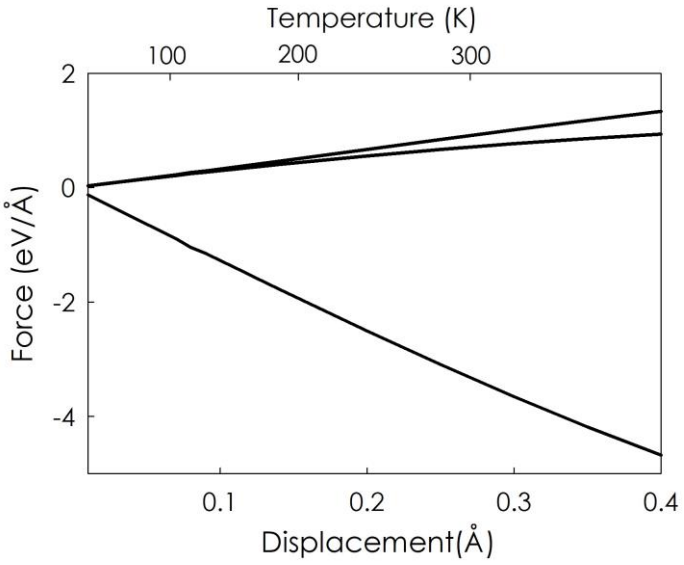

Figure 37 – Forces on 1st NN atoms of an atom that is incrementally displaced up to 0.4 Å. The temperature associated with these displacements, calculated via DFT-MD, is shown on the top axis.

Note that many forces in a crystal will be identical when a single atom is displaced, due to symmetry in the interactions [173]. It is apparent that the forces on 1st NN atoms follow a mostly linear trend as predicted by the harmonic approximation, although there is some anharmonicity apparent. However, looking a little further beyond the 1st neighbors of the displaced atom, Figure 38 shows the forces on 2nd and 3rd NN atoms.

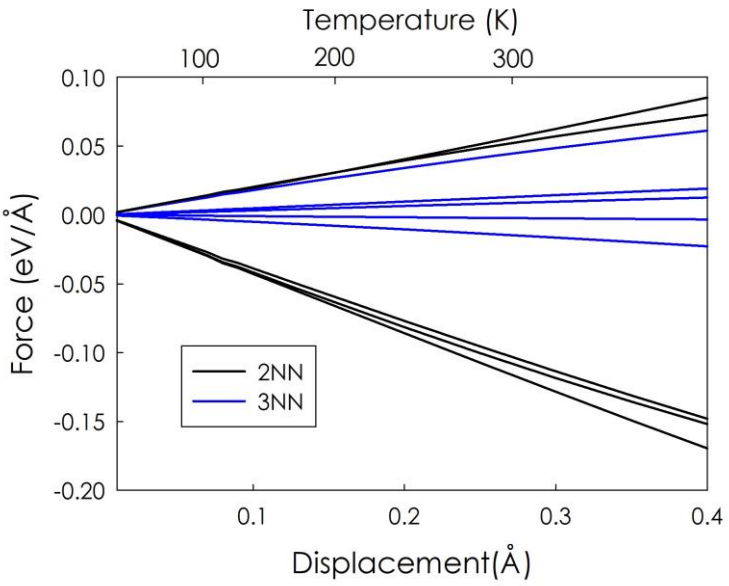

Figure 38 – Linear forces on 2nd and 3rd NN atoms of an atom that is incrementally displaced up to 0.4 Å. The temperature associated with these displacements, calculated via DFT-MD, is shown on the top axis.

As seen in Figure 38, forces on 2nd and 3rd NN atoms are also linear as a function of displacement. Figure 30 shows that phonon dispersion in c-Si begins to flatten at the Brillouin zone boundary when 5th NN interactions are included, so it is also of interest to determine whether these forces are also linear and valid under the harmonic approximation for large displacements (high temperatures). Forces on 4th and 5th NN atoms for this experiment are shown in Figure 39.

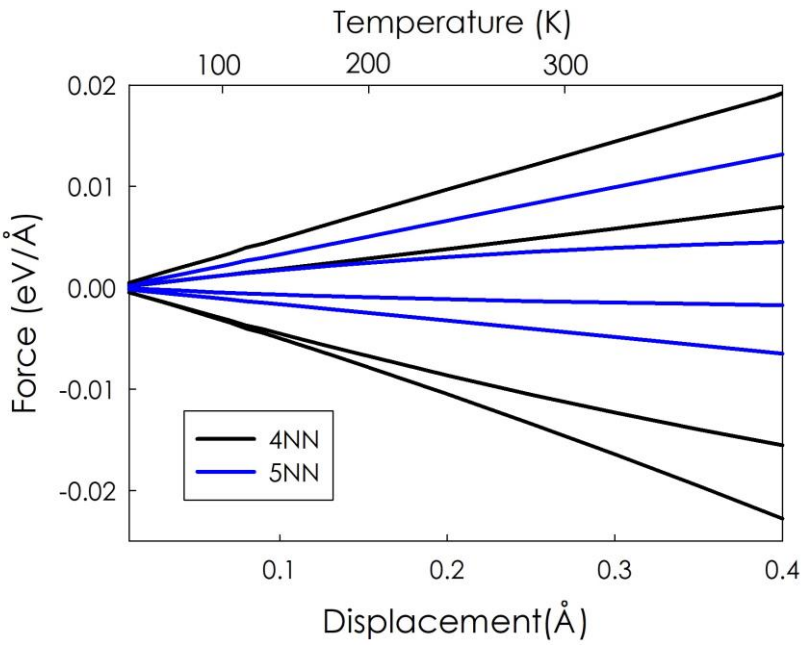

Figure 39 – Linear forces on 4th and 5th NN atoms of an atom that is incrementally displaced up to 0.4 Å. The temperature associated with these displacements, calculated via DFT-MD, is shown on the top axis.

2-body forces on the longer-range interactions, between 4th and 5th NNs, are also seen to exhibit linearity. This reveals that the original hypothesis, which suspected that divergent forces associated with the harmonic approximation lead to instabilities, was in fact wrong because the harmonic approximation for 2-body interactions seems to be valid up to displacements associated with high temperatures (> 300 K). This begged the question; if the TEP is predicting the correct behaviour of forces, what is causing its instability in MD simulations?

6.3.4 Failure of the TEP for MD

Investigating the TEP instability further, namely the instability in potential energy seen in Figure 31, the potential energy fluctuations seemed to arise from fluctuations in

total energy (kinetic plus potential). This was originally not suspected, since all MD simulations performed in these tests used the NVE ensemble, which should conserve total energy [212]. The TEP, however, seemed to experience large fluctuations in total energy regardless of using cutoff functions. Combining this lack of energy conservation with the observed translations seen with the center of mass movement in Figure 35, it was deduced that system linear momentum was not being conserved. Originally this was overlooked, but the source of the problem is the fact that the TEP geometry descriptors lack the translational and rotationally invariant features discussed in Chapter 2. Since absolute Cartesian positions are referenced in the displacement geometry descriptors of Equation 23, applying a translation operation results in a large displacement and a fictitiously large amount of energy. If the entire system translates, without changing the relative distances or displacements between atoms, the energy will therefore change; likewise, for rotation. According to Noether's theorem [126], such a system will not conserve linear or rotational momentum, which could be responsible for the observed translations seen in Figure 35. The TEP therefore does not conserve total energy, as noted in Figure 40.

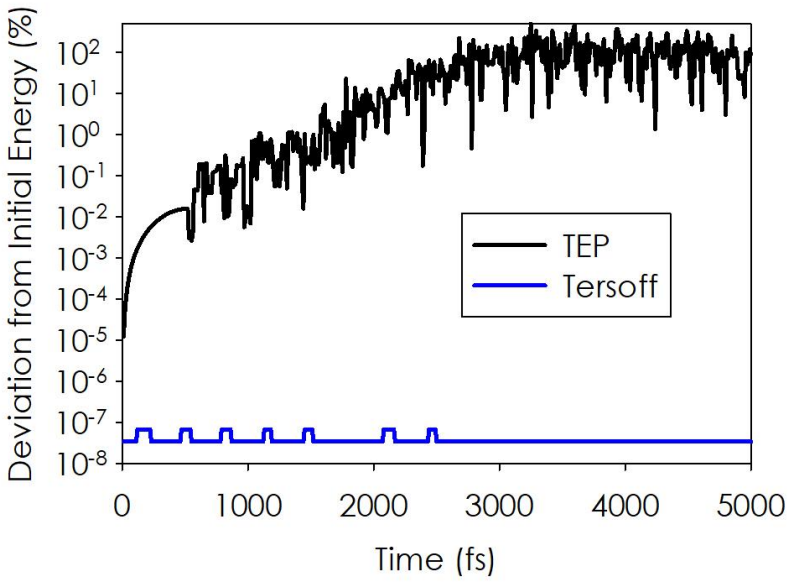

Figure 40 – Deviation of the total energy from the initial value in a 300 K c-Si MD simulation for the TEP (black line) and a Tersoff potential (blue line). The simulation was performed using the NVE ensemble.

Figure 40 shows that the percent deviation in total energy from the starting value increases up to six orders of magnitude. The Tersoff potential in Figure 40, however, possesses invariant geometric descriptors and experiences small oscillations in total energy on the order of normal numerical error for MD simulations [213]. This intrinsic and fundamental issue with the TEP renders it only useful as a LD model, as it cannot be used to perform energy-conserving MD simulations [26]. These investigations still showed what is necessary to create a potential that can exactly predict phonon frequencies, while still performing stable MD simulations. Such a potential will allow MD to be performed with more exact representations of vibrational modes in the system; this will aid in modern MD approaches to calculating modal contributions to thermal transport such as GKMA [35] and ICMA [54]. An interatomic potential that can perform this task must (1) possess invariant geometric

descriptors for stable MD, and (2) possess flexibility to describe unique IFCs in all three Cartesian directions. Development of such a potential is beyond the scope of this work, but these investigations showed what needs to be done in this regard.

CHAPTER 7. CONCLUSIONS

Important questions dealing with the development of POPs were answered in this thesis, starting with Question 1 of what fitting quantities are required to produce potentials that are guaranteed to predict phonon properties. It was shown in Chapter 4 that fitting a potential for a c-Ge system to 2nd and 3rd order IFCs yielded accurate thermal conductivity predictions. This was further confirmed for the TBC and M3BC potentials in c-Ge and c-Si in Chapter 5. Other fitting quantities, namely energy-volume curves and stresses, were necessary for stable MD simulations. Although it was originally hypothesized via Hypothesis 1 that fitting only to forces for many displacements would be sufficient, the IFCs were the main factor in obtaining potentials that accurately predicted thermal conductivity. Question 2 dealt with how closely traditional analytical functional forms could accurately match DFT forces. It was shown in Table 1 and Table 2 that it was in fact possible for DFT forces to be reproduced with less than 10% error for many of the fitting cases.

The viability of traditional analytical potentials for thermal transport was also investigated. Many traditional potentials, even for simple crystalline systems such as c-Si and c-Ge, do not accurately predict thermal conductivity as shown in Chapter 5. Since the few previous attempts by other authors to optimize potentials for thermal transport properties were unsuccessful [80,81,83,85,124], it was not known if traditional functional forms have the ability to accurately predict thermal transport properties if optimized for such a task. Hypothesis 2 posited that traditional potentials possess the flexibility to describe small forces resulting from displaced atoms about equilibrium since these quantities are

associated with thermal vibrations about equilibrium, and traditional potentials were made for seemingly more complex tasks. It was shown that Hypothesis 2 was true, since combinations of traditional potentials for c-Si and c-Ge in Chapter 5 yielded accurate thermal conductivity predictions (i.e., < 10% error) as compared to experiments and DFT.

The method in which the potentials were parameterized via random optimization with the GA confirms that many solutions may exist for traditional potentials to describe phonons. Question 3 posited whether not inferring any physical meaning to the parameters, would result in accurate fits and many new solutions. This was investigated using the GA in the POPs program to thoroughly explore the parameter search space in a stochastic manner. Hypothesis 3 suggested that this is a valid approach since traditional analytical functional forms were overdesigned for the study of simple forces associated with displacements about equilibrium positions, and should therefore possess many parameter sets that may not have physical meaning. It was found in Chapters 4 and 5, that this was indeed the case; many separate trials of GA optimizations, resulting in different parameter sets, resulted in < 10% error in forces and decent thermal conductivity prediction. By treating every parameter as a purely mathematical quantity and not restricting the parameter search ranges to what could be physically reasoned, many new and accurate solutions emerged.

A known limitation of traditional potentials for semiconductors, especially for phonons, is their absence of long-range interactions [80,83,85]. This results in accurate phonon dispersion calculations since phonon frequencies at the Brillouin zone boundaries rely on long-range interatomic interactions. Question 4 raised the question; will traditional long-range functional forms accurately capture these frequencies if parameterized to do so? It

was hypothesized that these potentials could, for the same reason that traditional long-range potentials could reproduce thermal properties. It was shown, however, that traditional long-range potentials, which are all based on 2-body radial interactions, cannot properly reproduce the phonon dispersion when parameterized to match 2nd order IFCs from DFT. In fact, Table 1 and Table 2 showed the errors in 2nd order IFCs were the highest in the fitting procedure. Despite this limitation, many solutions (i.e., different parameter sets) were found that accurately predicted thermal conductivity.

With these questions and hypotheses answered, it was of still of interest to investigate the results of Question 4, as traditional long-range potentials seemed unable to reproduce phonon frequencies at Brillouin zone boundaries. While the long-range radial descriptors lack the necessary flexibility to accomplish such a task, the TEP can exactly match the 2nd order IFCs which dictate the phonon dispersion. The TEP, however, was unstable in MD simulations, and many attempts described in Chapter 6 were unable to overcome the stability issues. It was finally realized that the core issue was the fact that in the TEP, the displacements of atoms from equilibrium are not invariant geometric descriptors. As a result, the TEP does not yield energy-conserving MD simulations with stable dynamics. This investigation showed the main requirements of a potential that can accurately predict harmonic phonon properties while performing stable MD simulations. Such a potentials must: (1) possess flexibility to uniquely describe 2nd order IFCs in all three Cartesian directions and (2) possess invariant geometric descriptors. While development of such a functional form was outside the scope of this work, it is the next logical step for future work.

The questions answered in this thesis are a first step in obtaining potentials that accurately predict phonon and thermal properties. A recipe was formulated, summarized as the POPs Tenets, and a method revolving around a powerful POPs program was developed. The POPs program alleviates three major issues known in potential development [79,123,124]: (1) it is generally applicable to a wide variety of potentials and fitting parameters due to coupling with the LAMMPS package, (2) it performs fast optimization (< 1 day) due to a massively parallel framework, and (3) it provides a user-interface to conveniently experiment with different optimization procedures for different systems and potentials. Especially when applied to the development of POPs from DFT quantities, the POPs program allows one to obtain classical analytical potentials possessing the linear computational scaling of MD with accuracy close to DFT. The findings herein therefore provide insight and methods into developing POPs, which greatly benefits the use of classical potentials in MD simulations to study thermal transport.

REFERENCES

1 Modest, M. F. *Radiative heat transfer*. (Academic press, 2013).

2 Buongiorno, J. Convective transport in nanofluids. *Journal of Heat Transfer* **128**, 240-250 (2006).

3 Makinson, R. in *Mathematical Proceedings of the Cambridge Philosophical Society*. 474-497 (Cambridge University Press).

4 Pomeranchuk, I. On the thermal conductivity of dielectrics. *Physical Review* **60**, 820 (1941).

5 Einstein, A. Planck's theory of radiation and the theory of specific heat. *Ann. Phys* **22**, 180-190 (1907).

6 Dean, P. Atomic vibrations in solids. *IMA Journal of Applied Mathematics* **3**, 98-165 (1967).

7 Klemens, P. Thermal conductivity and lattice vibrational modes. *Solid state physics* **7**, 1-98 (1958).

8 Peierls, R. On the kinetic theory of thermal conduction in crystals. *Selected Scientific Papers of Sir Rudolf Peierls, with Commentary by the Author. Edited by DALITZ RH & PEIERLS SIR RUDOLF. Published by World Scientific Publishing Co. Pte. Ltd., 1997. ISBN# 9789812795779, pp. 15-48*, 15-48 (1997).

9 Born, M. von Karman Th. *Phys. Zeit* **13**, 297 (1912).

10 Krivoglaz, M. A. THEORY OF X-RAY AND THERMAL-NEUTRON SCATTERING BY REAL CRYSTALS. (1969).

11 Brockhouse, B. & Stewart, A. Scattering of neutrons by phonons in an aluminum single crystal. *Physical Review* **100**, 756 (1955).

12 Carter, R., Palevsky, H. & Hughes, D. Inelastic Scattering of Slow Neutrons by Lattice Vibrations in Aluminum. *Physical Review* **106**, 1168 (1957).

13 Chen, G. Nanoscale energy transport and conversion. (2005).

14 Ziman, J. M. *Electrons and phonons: the theory of transport phenomena in solids*. (Oxford university press, 1960).

15 Franklin, A. D. *et al.* Sub-10 nm carbon nanotube transistor. *Nano letters* **12**, 758-762 (2012).

16 Yu, B. *et al.* in *Electron Devices Meeting, 2001. IEDM'01. Technical Digest. International.* 11.17. 11-11.17. 13 (IEEE).

17 Chang, C.-W., Okawa, D., Garcia, H., Majumdar, A. & Zettl, A. Breakdown of Fourier's law in nanotube thermal conductors. *Physical review letters* **101**, 075903 (2008).

18 Yang, N., Zhang, G. & Li, B. Violation of Fourier's law and anomalous heat diffusion in silicon nanowires. *Nano Today* **5**, 85-90 (2010).

19 Asheghi, M., Leung, Y., Wong, S. & Goodson, K. Phonon-boundary scattering in thin silicon layers. *Applied Physics Letters* **71**, 1798-1800 (1997).

20 Liu, W. & Asheghi, M. Phonon–boundary scattering in ultrathin single-crystal silicon layers. *Applied Physics Letters* **84**, 3819-3821 (2004).

21 Flik, M. & Tien, C. Size effect on the thermal conductivity of high-Tc thin-film superconductors. *Journal of heat transfer* **112**, 872-881 (1990).

22 Mitas, L., Grossman, J. C., Stich, I. & Tobik, J. Silicon clusters of intermediate size: energetics, dynamics, and thermal effects. *Physical review letters* **84**, 1479 (2000).

23 Murthy, J. Y. *et al.* Review of multiscale simulation in submicron heat transfer. *International Journal for Multiscale Computational Engineering* **3** (2005).

24 Balandin, A. & Wang, K. L. Significant decrease of the lattice thermal conductivity due to phonon confinement in a free-standing semiconductor quantum well. *Physical Review B* **58**, 1544 (1998).

25 Balandin, A. A. Nanophononics: phonon engineering in nanostructures and nanodevices. *Journal of nanoscience and nanotechnology* **5**, 1015-1022 (2005).

26 Dove, M. T. *Introduction to lattice dynamics*. Vol. 4 (Cambridge university press, 1993).

27 Peierls, R. Zur kinetischen theorie der wärmeleitung in kristallen. *Annalen der Physik* **395**, 1055-1101 (1929).

28 Zhang, Z. M. Z. M. *Nano/microscale heat transfer*. (2007).

29 Chapman, S. & Cowling, T. G. *The mathematical theory of non-uniform gases: an account of the kinetic theory of viscosity, thermal conduction and diffusion in gases*. (Cambridge university press, 1970).

30 Lindsay, L., Broido, D. & Mingo, N. Lattice thermal conductivity of single-walled carbon nanotubes: Beyond the relaxation time approximation and phonon-phonon scattering selection rules. *Physical Review B* **80**, 125407 (2009).

31 Carruthers, P. Theory of thermal conductivity of solids at low temperatures. *Reviews of Modern Physics* **33**, 92 (1961).

32 Hardy, R. J. Lowest-Order Contribution to the Lattice Thermal Conductivity. *Journal of Mathematical Physics* **6**, 1749-1761 (1965).

33 Esfarjani, K., Chen, G. & Stokes, H. T. Heat transport in silicon from first-principles calculations. *Physical Review B* **84**, 085204 (2011).

34 Broido, D., Malorny, M., Birner, G., Mingo, N. & Stewart, D. Intrinsic lattice thermal conductivity of semiconductors from first principles. *Applied Physics Letters* **91**, 231922 (2007).

35 Lv, W. & Henry, A. Direct calculation of modal contributions to thermal conductivity via Green–Kubo modal analysis. *New Journal of Physics* **18**, 013028 (2016).

36 Lv, W. & Henry, A. Examining the validity of the phonon gas model in amorphous materials. *Scientific reports* **6** (2016).

37 Lv, W. & Henry, A. Phonon transport in amorphous carbon using Green–Kubo modal analysis. *Applied Physics Letters* **108**, 181905 (2016).

38 Seyf, H. R. & Henry, A. A method for distinguishing between propagons, diffusions, and locons. *Journal of Applied Physics* **120**, 025101 (2016).

39 Allen, P. B., Feldman, J. L., Fabian, J. & Wooten, F. Diffusons, locons and propagons: Character of atomie yibrations in amorphous Si. *Philosophical Magazine B* **79**, 1715-1731 (1999).

40 Kittel, C. Interpretation of the thermal conductivity of glasses. *Physical Review* **75**, 972 (1949).

41 Müller-Plathe, F. A simple nonequilibrium molecular dynamics method for calculating the thermal conductivity. *The Journal of chemical physics* **106**, 6082-6085 (1997).

42 Ladd, A. J., Moran, B. & Hoover, W. G. Lattice thermal conductivity: A comparison of molecular dynamics and anharmonic lattice dynamics. *Physical Review B* **34**, 5058 (1986).

43 Alder, B. J. & Wainwright, T. E. Studies in molecular dynamics. I. General method. *The Journal of Chemical Physics* **31**, 459-466 (1959).

44 Kubo, R. Statistical-mechanical theory of irreversible processes. I. General theory and simple applications to magnetic and conduction problems. *Journal of the Physical Society of Japan* **12**, 570-586 (1957).

45 Verlet, L. Computer" experiments" on classical fluids. I. Thermodynamical properties of Lennard-Jones molecules. *Physical review* **159**, 98 (1967).

46 Nosé, S. A molecular dynamics method for simulations in the canonical ensemble. *Molecular physics* **52**, 255-268 (1984).

47 Gibbs, J. Elementary principles in statistical physics. *The Collected Works of JW Gibbs (Yale University, New Haven, CT, 1957)* **2** (1902).

48 Evans, D. J. & Morriss, G. The isothermal/isobaric molecular dynamics ensemble. *Physics Letters A* **98**, 433-436 (1983).

49 Andersen, H. C. Molecular dynamics simulations at constant pressure and/or temperature. *The Journal of chemical physics* **72**, 2384-2393 (1980).

50 Hardy, R. J. Energy-Flux Operator for a Lattice. *Physical Review* **132**, 168-177 (1963).

51 Brenner, D. The art and science of an analytic potential. *physica status solidi(b)* **217**, 23-40 (2000).

52 Kubo, R., Yokota, M. & Nakajima, S. Statistical-mechanical theory of irreversible processes. II. Response to thermal disturbance. *Journal of the Physical Society of Japan* **12**, 1203-1211 (1957).

53 Hansen, J.-P. & McDonald, I. R. *Theory of simple liquids*. (Elsevier, 1990).

54 Gordiz, K. & Henry, A. A formalism for calculating the modal contributions to thermal interface conductance. *New Journal of Physics* **17**, 103002 (2015).

55 Luo, T. & Chen, G. Nanoscale heat transfer–from computation to experiment. *Physical Chemistry Chemical Physics* **15**, 3389-3412 (2013).

56 Schelling, P. K., Phillpot, S. R. & Keblinski, P. Comparison of atomic-level simulation methods for computing thermal conductivity. *Physical Review B* **65**, 144306 (2002).

57 Rohskopf, A., Seyf, H. R., Gordiz, K., Tadano, T. & Henry, A. Empirical interatomic potentials optimized for phonon properties. *npj Computational Materials* **3**, 27 (2017).

58 Tersoff, J. New empirical model for the structural properties of silicon. *Physical review letters* **56**, 632 (1986).

59 Jones, J. E. in *Proceedings of the Royal Society of London A: Mathematical, Physical and Engineering Sciences.* 441-462 (The Royal Society).

60 Lennard-Jones, J. & Taylor, P. Some theoretical calculations of the physical properties of certain crystals. *Proceedings of the Royal Society of London. Series A, Containing Papers of a Mathematical and Physical Character* **109**, 476-508 (1925).

61 Morse, P. M. Diatomic molecules according to the wave mechanics. II. Vibrational levels. *Physical Review* **34**, 57 (1929).

62 Lennard-Jones, J. On the forces between atoms and ions. *Proceedings of the Royal Society of London. Series A, Containing Papers of a Mathematical and Physical Character* **109**, 584-597 (1925).

63 Girifalco, L. A. & Weizer, V. G. Application of the Morse potential function to cubic metals. *Physical Review* **114**, 687 (1959).

64 Bartlett, J. & Dienes, G. Combined pairs of vacancies in copper. *Physical Review* **89**, 848 (1953).

65 Born, M. in *Mathematical Proceedings of the Cambridge Philosophical Society.* 160-172 (Cambridge University Press).

66 Stillinger, F. H. & Weber, T. A. Computer simulation of local order in condensed phases of silicon. *Physical review B* **31**, 5262 (1985).

67 Henry, A. S. & Chen, G. Spectral phonon transport properties of silicon based on molecular dynamics simulations and lattice dynamics. *Journal of Computational and Theoretical Nanoscience* **5**, 141-152 (2008).

68 Bazant, M. Z., Kaxiras, E. & Justo, J. F. Environment-dependent interatomic potential for bulk silicon. *Physical Review B* **56**, 8542 (1997).

69 Brenner, D. W. Empirical potential for hydrocarbons for use in simulating the chemical vapor deposition of diamond films. *Physical Review B* **42**, 9458 (1990).

70 Bolding, B. C. & Andersen, H. C. Interatomic potential for silicon clusters, crystals, and surfaces. *Physical Review B* **41**, 10568 (1990).

71 Tersoff, J. Empirical interatomic potential for silicon with improved elastic properties. *Physical Review B* **38**, 9902 (1988).

72 Tersoff, J. Modeling solid-state chemistry: Interatomic potentials for multicomponent systems. *Physical Review B* **39**, 5566 (1989).

73 Volz, S. G. & Chen, G. Molecular dynamics simulation of thermal conductivity of silicon nanowires. *Applied Physics Letters* **75**, 2056-2058 (1999).

74 Berber, S., Kwon, Y.-K. & Tománek, D. Unusually high thermal conductivity of carbon nanotubes. *Physical review letters* **84**, 4613 (2000).

75 Donadio, D. & Galli, G. Thermal conductivity of isolated and interacting carbon nanotubes: comparing results from molecular dynamics and the Boltzmann transport equation. *Physical review letters* **99**, 255502 (2007).

76 Broido, D., Ward, A. & Mingo, N. Lattice thermal conductivity of silicon from empirical interatomic potentials. *Physical Review B* **72**, 014308 (2005).

77 He, Y., Savić, I., Donadio, D. & Galli, G. Lattice thermal conductivity of semiconducting bulk materials: atomistic simulations. *Physical Chemistry Chemical Physics* **14**, 16209-16222 (2012).

78 Zhang, X. *et al.* Thermal conductivity of silicene calculated using an optimized Stillinger-Weber potential. *Physical Review B* **89**, 054310 (2014).

79 Al-Derzi, A. R., Johnston, R. L., Murrell, J. N. & Rodriguez-Ruiz, J. A. Potential energy functions for atomic solids: III. Fitting phonon frequencies and elastic constants of diamond structures. *Molecular Physics* **73**, 265-282 (1991).

80 Powell, D., Migliorato, M. A. & Cullis, A. G. The Tersoff potential for phonons in GaAs. *Physica E: Low-dimensional Systems and Nanostructures* **32**, 270-272 (2006).

81 Lindsay, L. & Broido, D. Optimized Tersoff and Brenner empirical potential parameters for lattice dynamics and phonon thermal transport in carbon nanotubes and graphene. *Physical Review B* **81**, 205441 (2010).

82 Umeno, Y., Kitamura, T., Date, K., Hayashi, M. & Iwasaki, T. Optimization of interatomic potential for Si/SiO 2 system based on force matching. *Computational materials science* **25**, 447-456 (2002).

83 Powell, D. *Elasticity, lattice dynamics and parameterisation techniques for the Tersoff potential applied to elemental and type III-V semiconductors*, University of Sheffield, (2006).

84 Monteverde, U., Migliorato, M. & Powell, D. in *Journal of Physics: Conference Series*. 012015 (IOP Publishing).

85 Powell, D., Migliorato, M. & Cullis, A. Optimized Tersoff potential parameters for tetrahedrally bonded III-V semiconductors. *Physical Review B* **75**, 115202 (2007).

86 Ercolessi, F. & Adams, J. B. Interatomic potentials from first-principles calculations: the force-matching method. *EPL (Europhysics Letters)* **26**, 583 (1994).

87 Youngs, T. G., Del Pópolo, M. G. & Kohanoff, J. Development of complex classical force fields through force matching to ab initio data: Application to a room-temperature ionic liquid. *The Journal of Physical Chemistry B* **110**, 5697-5707 (2006).

88 Akin-Ojo, O., Song, Y. & Wang, F. Developing ab initio quality force fields from condensed phase quantum-mechanics/molecular-mechanics calculations through the adaptive force matching method. *The Journal of chemical physics* **129**, 064108 (2008).

89 Liu, X.-Y., Adams, J. B., Ercolessi, F. & Moriarty, J. A. EAM potential for magnesium from quantum mechanical forces. *Modelling and Simulation in Materials Science and Engineering* **4**, 293 (1996).

90 Lenosky, T. J. *et al.* Highly optimized empirical potential model of silicon. *Modelling and Simulation in Materials Science and Engineering* **8**, 825 (2000).

91 Lee, Y. & Hwang, G. S. Force-matching-based parameterization of the Stillinger-Weber potential for thermal conduction in silicon. *Physical Review B* **85**, 125204 (2012).

92 Plimpton, S. Fast parallel algorithms for short-range molecular dynamics. *Journal of computational physics* **117**, 1-19 (1995).

93 Cahill, D. G., Watson, S. K. & Pohl, R. O. Lower limit to the thermal conductivity of disordered crystals. *Physical Review B* **46**, 6131 (1992).

94 Cahill, D. G. Thermal conductivity measurement from 30 to 750 K: the 3ω method. *Review of scientific instruments* **61**, 802-808 (1990).

95 Lyeo, H.-K. & Cahill, D. G. Thermal conductance of interfaces between highly dissimilar materials. *Physical Review B* **73**, 144301 (2006).

96 Cahill, D. G. & Pohl, R. O. Thermal conductivity of amorphous solids above the plateau. *Physical review B* **35**, 4067 (1987).

97 Han, Z. & Fina, A. Thermal conductivity of carbon nanotubes and their polymer nanocomposites: a review. *Progress in polymer science* **36**, 914-944 (2011).

98 Koh, Y. K. & Cahill, D. G. Frequency dependence of the thermal conductivity of semiconductor alloys. *Physical Review B* **76**, 075207 (2007).

99 Turney, J., Landry, E., McGaughey, A. & Amon, C. Predicting phonon properties and thermal conductivity from anharmonic lattice dynamics calculations and molecular dynamics simulations. *Physical Review B* **79**, 064301 (2009).

100 Huxtable, S. T. *et al.* Interfacial heat flow in carbon nanotube suspensions. *Nature materials* **2**, 731-734 (2003).

101 Shenogin, S., Xue, L., Ozisik, R., Keblinski, P. & Cahill, D. G. Role of thermal boundary resistance on the heat flow in carbon-nanotube composites. *Journal of applied physics* **95**, 8136-8144 (2004).

102 Hsieh, W.-P. *et al.* Testing the minimum thermal conductivity model for amorphous polymers using high pressure. *Physical Review B* **83**, 174205 (2011).

103 Cahill, D. G. *et al.* Nanoscale thermal transport. *Journal of applied physics* **93**, 793-818 (2003).

104 Rodin, D. & Yee, S. K. Simultaneous measurement of in-plane and through-plane thermal conductivity using beam-offset frequency domain thermoreflectance. *Review of Scientific Instruments* **88**, 014902 (2017).

105 Volz, S. G. & Chen, G. Molecular-dynamics simulation of thermal conductivity of silicon crystals. *Physical Review B* **61**, 2651 (2000).

106 Dong, J., Sankey, O. F. & Myles, C. W. Theoretical study of the lattice thermal conductivity in Ge framework semiconductors. *Physical review letters* **86**, 2361 (2001).

107 Balamane, H., Halicioglu, T. & Tiller, W. Comparative study of silicon empirical interatomic potentials. *Physical Review B* **46**, 2250 (1992).

108 Hooke, R. De Potentia Restitutiva, or of Spring Explaining the Power of Springing Bodies, vol. 1678. *London, UK: John Martyn*, 23.

109 Parr, R. G. in *Horizons of Quantum Chemistry* 5-15 (Springer, 1980).

110 Liu, X.-Y., Ercolessi, F. & Adams, J. B. Aluminium interatomic potential from density functional theory calculations with improved stacking fault energy. *Modelling and Simulation in Materials Science and Engineering* **12**, 665 (2004).

111 Holland, D. & Marder, M. Ideal brittle fracture of silicon studied with molecular dynamics. *Physical Review Letters* **80**, 746 (1998).

112 Tersoff, J. New empirical approach for the structure and energy of covalent systems. *Physical Review B* **37**, 6991 (1988).

113 Ashurst, W.-T. & Hoover, W. Dense-fluid shear viscosity via nonequilibrium molecular dynamics. *Physical Review A* **11**, 658 (1975).

114 Karplus, M. & McCammon, J. A. Molecular dynamics simulations of biomolecules. *Nature Structural & Molecular Biology* **9**, 646-652 (2002).

115 Siegle, H. *et al.* Zone-boundary phonons in hexagonal and cubic GaN. *Physical Review B* **55**, 7000 (1997).

116 Tadano, T., Gohda, Y. & Tsuneyuki, S. Anharmonic force constants extracted from first-principles molecular dynamics: applications to heat transfer simulations. *Journal of Physics: Condensed Matter* **26**, 225402 (2014).

117 Kittel, C. *Introduction to solid state physics*. (Wiley, 2005).

118 Sokel, R. & Harrison, W. A. Long-Range Interactions in Semiconductors. *Physical Review Letters* **36**, 61 (1976).

119 Hansen, J.-P. & Verlet, L. Phase transitions of the Lennard-Jones system. *physical Review* **184**, 151 (1969).

120 Turnbull, D. & Cohen, M. H. Free-volume model of the amorphous phase: glass transition. *The Journal of chemical physics* **34**, 120-125 (1961).

121 Stewart, J. J. Optimization of parameters for semiempirical methods I. Method. *Journal of Computational Chemistry* **10**, 209-220 (1989).

122 Brommer, P. *et al.* Classical interaction potentials for diverse materials from ab initio data: a review of potfit. *Modelling and Simulation in Materials Science and Engineering* **23**, 074002 (2015).

123 Martinez, J. A., Yilmaz, D. E., Liang, T., Sinnott, S. B. & Phillpot, S. R. Fitting empirical potentials: Challenges and methodologies. *Current Opinion in Solid State and Materials Science* **17**, 263-270 (2013).

124 Brommer, P. & Gähler, F. Potfit: effective potentials from ab initio data. *Modelling and Simulation in Materials Science and Engineering* **15**, 295 (2007).

125 Bartók, A. P., Kondor, R. & Csányi, G. On representing chemical environments. *Physical Review B* **87**, 184115 (2013).

126 Noether, E. Invariante Variationsprobleme Nachr. D. König. Gesellsch. D. Wiss. Zu Göttingen, Math-phys. Klasse 1918: 235-257. *English Reprint: physics/0503066, http://dx. doi. org/10.1080/00411457108231446*, 57 (1918).

127 Thompson, A. P., Swiler, L. P., Trott, C. R., Foiles, S. M. & Tucker, G. J. Spectral neighbor analysis method for automated generation of quantum-accurate interatomic potentials. *Journal of Computational Physics* **285**, 316-330 (2015).

128 Fennell, C. J. & Gezelter, J. D. Is the Ewald summation still necessary? Pairwise alternatives to the accepted standard for long-range electrostatics. *The Journal of chemical physics* **124**, 234104 (2006).

129 Margenau, H. Van der Waals forces. *Reviews of Modern Physics* **11**, 1 (1939).

130 Tosi, M. & Fumi, F. Ionic sizes and born repulsive parameters in the NaCl-type alkali halides—II: The generalized Huggins-Mayer form. *Journal of Physics and Chemistry of Solids* **25**, 45-52 (1964).

131 Sato, S. A new method of drawing the potential energy surface. *Bulletin of the Chemical Society of Japan* **28**, 450-453 (1955).

132 Tadmor, E., Elliott, R., Sethna, J. P., Miller, R. & Becker, C. A. The potential of atomistic simulations and the knowledgebase of interatomic models. *JOM Journal of the Minerals, Metals and Materials Society* **63**, 17-17 (2011).

133 Abs da Cruz, C., Termentzidis, K., Chantrenne, P. & Kleber, X. Molecular dynamics simulations for the prediction of thermal conductivity of bulk silicon and silicon nanowires: Influence of interatomic potentials and boundary conditions. *Journal of applied physics* **110**, 034309 (2011).

134 Lindsay, L., Broido, D. & Mingo, N. Flexural phonons and thermal transport in graphene. *Physical Review B* **82**, 115427 (2010).

135 Jian, Z., Kaiming, Z. & Xide, X. Modification of stillinger-weber potentials for si and ge. *Physical Review B* **41**, 12915 (1990).

136 Osman, I. H. & Kelly, J. P. in *Meta-heuristics* 1-21 (Springer, 1996).

137 Blum, C. & Roli, A. Metaheuristics in combinatorial optimization: Overview and conceptual comparison. *ACM Computing Surveys (CSUR)* **35**, 268-308 (2003).

138 Fogel, D. B. An introduction to simulated evolutionary optimization. *IEEE transactions on neural networks* **5**, 3-14 (1994).

139 Darwin, C. On the origin of species by means of natural selection. 1859. *London: Murray Google Scholar* (1968).

140 Watson, J. D. & Crick, F. H. Genetical implications of the structure of deoxyribonucleic acid. *Nature* **171**, 964-967 (1953).

141 Simmons, R. E. & Scheepers, L. Winning by a neck: sexual selection in the evolution of giraffe. *The American Naturalist* **148**, 771-786 (1996).

142 Zitzler, E. Evolutionary algorithms for multiobjective optimization: Methods and applications. (1999).

143 Whitley, D. A genetic algorithm tutorial. *Statistics and computing* **4**, 65-85 (1994).

144 Coley, D. A. *An introduction to genetic algorithms for scientists and engineers*. (World Scientific Publishing Co Inc, 1999).

145 Črepinšek, M., Liu, S.-H. & Mernik, M. Exploration and exploitation in evolutionary algorithms: a survey. *ACM Computing Surveys (CSUR)* **45**, 35 (2013).

146 Haupt, R. L. in *Antennas and Propagation Society International Symposium, 2000. IEEE.* 1034-1037 (IEEE).

147 Curtarolo, S., Morgan, D. & Ceder, G. Accuracy of ab initio methods in predicting the crystal structures of metals: A review of 80 binary alloys. *Calphad* **29**, 163-211 (2005).

148 Scott, A. P. & Radom, L. Harmonic vibrational frequencies: an evaluation of Hartree− Fock, Møller− Plesset, quadratic configuration interaction, density functional theory, and semiempirical scale factors. *The Journal of Physical Chemistry* **100**, 16502-16513 (1996).

149 Baroni, S., De Gironcoli, S., Dal Corso, A. & Giannozzi, P. Phonons and related crystal properties from density-functional perturbation theory. *Reviews of Modern Physics* **73**, 515 (2001).

150 Scrocco, E. & Tomasi, J. Electronic molecular structure, reactivity and intermolecular forces: an euristic interpretation by means of electrostatic molecular potentials. *Advances in quantum chemistry* **11**, 115-193 (1978).

151 Feynman, R. P. Forces in molecules. *Physical Review* **56**, 340 (1939).

152 Hohenberg, P. & Kohn, W. Inhomogeneous electron gas. *Physical review* **136**, B864 (1964).

153 Kresse, G. & Hafner, J. Ab initio molecular dynamics for liquid metals. *Physical Review B* **47**, 558 (1993).

154 Giannozzi, P. *et al.* QUANTUM ESPRESSO: a modular and open-source software project for quantum simulations of materials. *Journal of physics: Condensed matter* **21**, 395502 (2009).

155 Sholl, D. & Steckel, J. A. *Density functional theory: a practical introduction*. (John Wiley & Sons, 2011).

156 Pauli, W. Über den Zusammenhang des Abschlusses der Elektronengruppen im Atom mit der Komplexstruktur der Spektren. *Zeitschrift für Physik A Hadrons and Nuclei* **31**, 765-783 (1925).

157 Zak, J. Dynamics of electrons in solids in external fields. *Physical Review* **168**, 686 (1968).

158 Born, M. & Oppenheimer, R. Zur quantentheorie der molekeln. *Annalen der Physik* **389**, 457-484 (1927).

159 Huang, K. & Yang, C. N. Quantum-mechanical many-body problem with hard-sphere interaction. *Physical review* **105**, 767 (1957).

160 Kohn, W. & Sham, L. J. Self-consistent equations including exchange and correlation effects. *Physical review* **140**, A1133 (1965).

161 Perdew, J. P. & Zunger, A. Self-interaction correction to density-functional approximations for many-electron systems. *Physical Review B* **23**, 5048 (1981).

162 Gunnarsson, O., Jonson, M. & Lundqvist, B. Descriptions of exchange and correlation effects in inhomogeneous electron systems. *Physical Review B* **20**, 3136 (1979).

163 Negele, J. W. Structure of finite nuclei in the local-density approximation. *Physical review C* **1**, 1260 (1970).

164 BRUECKNER, K. A. Correlation energy of an electron gas with a slowly varying high density. *Physical Review* **165**, 18 (1968).

165 Kresse, G. & Hafner, J. Ab initio molecular dynamics for open-shell transition metals. *Physical Review B* **48**, 13115 (1993).

166 Langreth, D. C. & Mehl, M. Beyond the local-density approximation in calculations of ground-state electronic properties. *Physical Review B* **28**, 1809 (1983).

167 Perdew, J. P. *et al.* Atoms, molecules, solids, and surfaces: Applications of the generalized gradient approximation for exchange and correlation. *Physical Review B* **46**, 6671 (1992).

168 Filippi, C., Singh, D. J. & Umrigar, C. J. All-electron local-density and generalized-gradient calculations of the structural properties of semiconductors. *Physical Review B* **50**, 14947 (1994).

169 Stampfl, C. & Van de Walle, C. Density-functional calculations for III-V nitrides using the local-density approximation and the generalized gradient approximation. *Physical Review B* **59**, 5521 (1999).

170 Dal Corso, A., Pasquarello, A., Baldereschi, A. & Car, R. Generalized-gradient approximations to density-functional theory: A comparative study for atoms and solids. *Physical Review B* **53**, 1180 (1996).

171 Burke, K., Perdew, J. P. & Wang, Y. in *Electronic Density Functional Theory* 81-111 (Springer, 1998).

172 Perdew, J. P., Burke, K. & Ernzerhof, M. Generalized gradient approximation made simple. *Physical review letters* **77**, 3865 (1996).

173 Esfarjani, K. & Stokes, H. T. Method to extract anharmonic force constants from first principles calculations. *Physical Review B* **77**, 144112 (2008).

174 Bickelhaupt, F. M. & Baerends, E. J. Kohn-Sham Density Functional Theory: Predicting and Understanding Chemistry. *Reviews in Computational Chemistry, Volume 15*, 1-86 (2007).

175 Car, R. & Parrinello, M. Unified approach for molecular dynamics and density-functional theory. *Physical review letters* **55**, 2471 (1985).

176 Goedecker, S. & Colombo, L. Efficient linear scaling algorithm for tight-binding molecular dynamics. *Physical Review Letters* **73**, 122 (1994).

177 Kadau, K., Germann, T. C. & Lomdahl, P. S. Molecular dynamics comes of age: 320 billion atom simulation on BlueGene/L. *International Journal of Modern Physics C* **17**, 1755-1761 (2006).

178 Born, M., Huang, K. & Lax, M. Dynamical theory of crystal lattices. *American Journal of Physics* **23**, 474-474 (1955).

179 Blöchl, P. E., Jepsen, O. & Andersen, O. K. Improved tetrahedron method for Brillouin-zone integrations. *Physical Review B* **49**, 16223-16233 (1994).

180 Vogelsang, R., Hoheisel, C. & Ciccotti, G. Thermal conductivity of the Lennard-Jones liquid by molecular dynamics calculations. *The Journal of chemical physics* **86**, 6371-6375 (1987).

181 Ladd, A. J. C., Moran, B. & Hoover, W. G. Lattice thermal conductivity: A comparison of molecular dynamics and anharmonic lattice dynamics. *Physical Review B* **34**, 5058-5064 (1986).

182 Gordiz, K., Singh, D. J. & Henry, A. Ensemble averaging vs. time averaging in molecular dynamics simulations of thermal conductivity. *Journal of Applied Physics* **117**, 045104 (2015).

183 Feng, T. & Ruan, X. Quantum mechanical prediction of four-phonon scattering rates and reduced thermal conductivity of solids. *Physical Review B* **93**, 045202 (2016).

184 Fox, G. C. *et al. Solving problems on concurrent processors. Vol. 1: General techniques and regular problems*. (Prentice-Hall, Inc., 1988).

185 Glassbrenner, C. & Slack, G. A. Thermal conductivity of silicon and germanium from 3 K to the melting point. *Physical Review* **134**, A1058 (1964).

186 Born, M. & Fürth, R. in *Mathematical Proceedings of the Cambridge Philosophical Society*. 454-465 (Cambridge University Press).

187 Misra, R. D. in *Mathematical Proceedings of the Cambridge Philosophical Society*. 173-182 (Cambridge University Press).

188 Born, M. & Misra, R. D. in *Mathematical Proceedings of the Cambridge Philosophical Society*. 466-478 (Cambridge University Press).

189 Thompson, A. P., Plimpton, S. J. & Mattson, W. General formulation of pressure and stress tensor for arbitrary many-body interaction potentials under periodic boundary conditions. *The Journal of chemical physics* **131**, 154107 (2009).

190 Khorshidi, A. & Peterson, A. A. Amp: a modular approach to machine learning in atomistic simulations. *Computer Physics Communications* **207**, 310-324 (2016).

191 Ozhogin, V. *et al.* Isotope effect in the thermal conductivity of germanium single crystals. *Journal of Experimental and Theoretical Physics Letters* **63**, 490-494 (1996).

192 Asen-Palmer, M. *et al.* Thermal conductivity of germanium crystals with different isotopic compositions. *Physical review B* **56**, 9431 (1997).

193 Chen, J., Zhang, G. & Li, B. How to improve the accuracy of equilibrium molecular dynamics for computation of thermal conductivity? *Physics Letters A* **374**, 2392-2396 (2010).

194 Li, Y., Siegel, D. J., Adams, J. B. & Liu, X.-Y. Embedded-atom-method tantalum potential developed by the force-matching method. *Physical Review B* **67**, 125101 (2003).

195 Blöchl, P. E. Projector augmented-wave method. *Physical review B* **50**, 17953 (1994).

196 Monkhorst, H. J. & Pack, J. D. Special points for Brillouin-zone integrations. *Physical review B* **13**, 5188 (1976).

197 Birch, F. Finite elastic strain of cubic crystals. *Physical Review* **71**, 809 (1947).

198 Okada, Y. & Tokumaru, Y. Precise determination of lattice parameter and thermal expansion coefficient of silicon between 300 and 1500 K. *Journal of applied physics* **56**, 314-320 (1984).

199 Buschert, R., Merlini, A., Pace, S., Rodriguez, S. & Grimsditch, M. Effect of isotope concentration on the lattice parameter of germanium perfect crystals. *Physical Review B* **38**, 5219 (1988).

200 Qiu, B., Bao, H., Zhang, G., Wu, Y. & Ruan, X. Molecular dynamics simulations of lattice thermal conductivity and spectral phonon mean free path of PbTe: Bulk and nanostructures. *Computational Materials Science* **53**, 278-285 (2012).

201 McGaughey, A. J. & Kaviany, M. Quantitative validation of the Boltzmann transport equation phonon thermal conductivity model under the single-mode relaxation time approximation. *Physical Review B* **69**, 094303 (2004).

202 Inyushkin, A., Taldenkov, A., Gibin, A., Gusev, A. & Pohl, H. J. On the isotope effect in thermal conductivity of silicon. *physica status solidi (c)* **1**, 2995-2998 (2004).

203 Weber, W. Adiabatic bond charge model for the phonons in diamond, Si, Ge, and α− Sn. *Physical Review B* **15**, 4789 (1977).

204 Nilsson, G. & Nelin, G. Phonon dispersion relations in Ge at 80 K. *Physical Review B* **3**, 364 (1971).

205 Sokel, R. & Harrison, W. A. Long-Range Interactions in Semiconductors. *Physical Review Letters* **36**, 61-64 (1976).

206 Weber, W. New bond-charge model for the lattice dynamics of diamond-type semiconductors. *Physical Review Letters* **33**, 371 (1974).

207 Chaplot, S. Interatomic potential, phonon spectrum, and molecular-dynamics simulation up to 1300 K in YBa 2 Cu 3 O 7− δ. *Physical Review B* **42**, 2149 (1990).

208 Munetoh, S., Motooka, T., Moriguchi, K. & Shintani, A. Interatomic potential for Si–O systems using Tersoff parameterization. *Computational Materials Science* **39**, 334-339 (2007).

209 Pascual-Gutiérrez, J. A., Murthy, J. Y. & Viskanta, R. Thermal conductivity and phonon transport properties of silicon using perturbation theory and the environment-dependent interatomic potential. *Journal of Applied Physics* **106**, 063532 (2009).

210 Murakami, T., Shiga, T., Hori, T., Esfarjani, K. & Shiomi, J. Importance of local force fields on lattice thermal conductivity reduction in PbTe1− xSex alloys. *EPL (Europhysics Letters)* **102**, 46002 (2013).

211 Harvey, S. C., Tan, R. K. Z. & Cheatham, T. E. The flying ice cube: velocity rescaling in molecular dynamics leads to violation of energy equipartition. *Journal of Computational Chemistry* **19**, 726-740 (1998).

212 Nosé, S. A unified formulation of the constant temperature molecular dynamics methods. *The Journal of chemical physics* **81**, 511-519 (1984).

213 Ryckaert, J.-P., Ciccotti, G. & Berendsen, H. J. Numerical integration of the cartesian equations of motion of a system with constraints: molecular dynamics of n-alkanes. *Journal of Computational Physics* **23**, 327-341 (1977).